COMBINATORICS AND DYNAMICS IN POLYMER KNOTS

CHRISTIAN MATTHIAS ROHWER

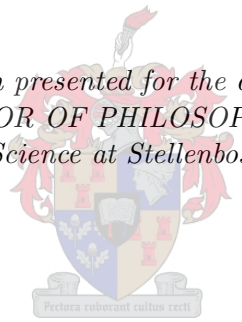

Dissertation presented for the degree of
DOCTOR OF PHILOSOPHY
in the Faculty of Science at Stellenbosch University.

Supervisor : Professor Kristian K. Müller-Nedebock

Co-supervisor : Professor Frederik G. Scholtz

April 2014

DECLARATION

By submitting this thesis electronically, I declare that the entirety of the work contained therein is my own, original work, that I am the sole author thereof (save to the extent explicitly otherwise stated), that reproduction and publication thereof by Stellenbosch University will not infringe any third party rights and that I have not previously in its entirety or in part submitted it for obtaining any qualification.

April 2014

Abstract

In this dissertation we address the conservation of topological states in polymer knots. Topological constraints are frequently included into theoretical descriptions of polymer systems through invariants such as winding numbers and linking numbers of polynomial invariants. In contrast, our approach is based on sequences of manipulations of knots that maintain a given knot's topology; these are known as Reidemeister moves. We begin by discussing basic properties of knots and their representations. In particular, we show how the Reidemeister moves may be viewed as rules for dynamics of crossings in planar projections of knots. Thereafter we consider various combinatoric enumeration procedures for knot configurations that are equivalent under chosen topological constraints. Firstly, we study a reduced system where only the zeroth and first Reidemeister moves are allowed, and present a diagrammatic summation of all contributions to the associated partition function. The partition function is then calculated under basic simplifying assumptions for the Boltzmann weights associated with various configurations. Secondly, we present a combinatoric scheme for enumerating all topologically equivalent configurations of a polymer strand that is wound around a rod and closed. This system has the constraint of a fixed winding number, which may be viewed in terms of manipulations that obey a Reidemeister move of the second kind of the polymer relative to the rod. Again configurations are coupled to relevant statistical weights, and the partition function is approximated. This result is used to calculate various physical quantities for confined geometries. The work in that chapter is based on a recent publication, ***"Conservation of polymer winding states: a combinatoric approach"*, C.M. Rohwer, K.K. Müller-Nedebock, and F.-E. Mpiana Mulamba, J. Phys. A: Math. Theor. 47 (2014) 065001**. The remainder of the dissertation is concerned with a dynamical description of the Reidemeister moves. We show how the rules for crossing dynamics may be addressed in an operator formalism for stochastic dynamics. Differential equations for densities and correlators for crossings on strands are calculated for some of the Reidemeister moves. These quantities are shown to encode the relevant dynamical constraints. Lastly we sketch some suggestions for the incorporation of themes in this dissertation into an algorithm for the simulated annealing of knots.

Opsomming

In hierdie tesis ondersoek ons die behoud van topologiese toestande in knope. Topologiese dwangvoorwaardes word dikwels d.m.v. invariante soos windingsgetalle, skakelgetalle en polinomiese invariante in die teoretiese beskrywings van polimere ingebou. In teenstelling hiermee is ons benadering gebaseer op reekse knoopmanipulasies wat die topologie van 'n gegewe knoop behou — die sogenaamde Reidemeisterskuiwe. Ons begin met 'n bespreking van die basiese eienskappe van knope en hul daarstellings. Spesifiek toon ons dat die Reidemeisterskuiwe beskryf kan word i.t.v. reëls vir die dinamika van kruisings in planêre knoopprojeksies. Daarna beskou ons verskeie kombinatoriese prosedures om ekwivalente knoopkonfigurasies te genereer onderhewig aan gegewe topologiese dwangvoorwaardes. Eerstens bestudeer ons 'n vereenvoudigde sisteem waar slegs die nulde en eerste Reidemeisterskuiwe toegelaat word, en lei dan 'n diagrammatiese sommasie van alle bydraes tot die geassosieerde toestandsfunksie af. Die partisiefunksie word dan bereken onderhewig aan sekere vereenvoudigende aannames vir die Boltzmanngewigte wat met die verskeie konfigurasies geassosieer is. Tweedens stel ons 'n kombinatoriese skema voor om ekwivalente konfigurasies te genereer vir 'n polimeer wat om 'n staaf gedraai word. Die beperking tot 'n vaste windingsgetal in hierdie sisteem kan daargestel word i.t.v. 'n Reidemeister skuif van die polimeer t.o.v. die staaf. Weereens word konfigurasies gekoppel aan relevante statistiese gewigte en die partisiefunksie word benader. Verskeie fisiese hoeveelhede word dan bereken vir beperkte geometrieë. Die werk in dié hoofstuk is gebaseer op 'n onlangse publikasie, ***"Conservation of polymer winding states: a combinatoric approach"*, C.M. Rohwer, K.K. Müller-Nedebock, and F.-E. Mpiana Mulamba, J. Phys. A: Math. Theor. 47 (2014) 065001**. Die res van die tesis handel oor 'n dinamiese beskrywing van die Reidemeisterskuiwe. Ons toon hoe die reëls vir kruisingsdinamika beskryf kan word i.t.v. 'n operatorformalisme vir stochastiese dinamika. Differensiaalvergelykings vir digthede en korrelatore vir kruisings op stringe word bereken vir sekere Reidemeisterskuiwe. Daar word getoon dat hierdie hoeveelhede die relevante dinamiese beperkings respekteer. Laastens maak ons 'n paar voorstelle vir hoe idees uit hierdie tesis geïnkorporeer kan word in 'n algoritme vir die gesimuleerde vereenvoudiging van knope.

Acknowledgements

I would like to express my sincerest thanks to my supervisor, Professor K.K. Müller-Nedebock, for his patient and supportive guidance. I am also grateful to my co-supervisor, Professor F.G. Scholtz, for his input and suggestions.

The Wilhelm Frank Bursary Trust provided financial support for my studies, not only during my Ph.D., but also during my B.Sc., B.Sc. Hons. and M.Sc. degrees. This aid was instrumental in allowing me to focus on academic priorities and I am incredibly thankful for the privilege of having received it.

The Department of Physics at Stellenbosch University has been my academic home during the past nine years. I thank Professor E.G. Rohwer and the administrative staff for all assistance and support during this time.

A great word of thanks is due to Dr. J.N. Kriel for many helpful discussions.

For their hospitality at the Leibnitz Institute for Polymer Research, Dresden, and at the Max Planck Institute for Polymer Research, Mainz, I am most grateful to Professors G. Heinrich and J.-U. Sommer, and Dr. V. Rostiashvili, respectively. The visit to Germany during 2013 provided a valued forum for exchanging ideas and identifying interesting problems for future work.

Lastly, and perhaps most importantly, I would like to thank my family and friends for their encouragement and backing.

CONTENTS

LIST OF FIGURES

CHAPTER 1
INTRODUCTION AND OUTLINE

In this dissertation we shall be concerned with topological constraints related to entanglements. Entanglements occur naturally in the setting of polymers. Physically, entanglements clearly impose constraints on the conformational freedom of polymer systems. Several factors contribute to (and impose) topological constraints. Firstly, strands physically cannot move through each other. This self-exclusion property is not trivial to incorporate into mathematical polymer descriptions. In path integral formulations of excluded volume interactions, for instance, a perturbation expansion in terms of the excluded volume parameter diverges when treated in less than four spatial dimensions [1, 2]. The underlying divergence occurs since monomer contacts for random walks are unlikely for dimensions above four, but grow as a function of polymer length for dimensions below four [1, 2]. However, other descriptions of self-avoiding walks (SAWs) exist. Simple examples include Flory's basic scaling arguments for the entropy and energy of SAWs [2], and mapping the excluded volume interaction onto the $n \to 0$ limit of n-component spin model [3].

Secondly, we need to consider how boundary conditions on polymer strands affect the nature of topological constraints. Closed polymer loops have certain "frozen in" topological constraints that are absent in systems of open strands. To illustrate this, one may contrast a system comprised of open strands (i.e., strands that are not closed on themselves) with one of closed polymer loops. Under the condition that strands cannot move through each other, it is clear that the topological constraints of these two types of systems are very different. In the first system, one may ask whether the strands are anchored or not, what their lengths are, or what their spatial separation is. The relative entanglement of the strands is, however, not a fixed property of a particular configuration of this system since the strands may slide along each other until entanglements disappear. In contrast, the conformational freedom in the second system with closed loops depends greatly on whether the loops are interlocking or not. Individual closed loops also have frozen-in topological constraints that are absent for open strands.

Other polymer systems that feature frozen in topological states include cross-linked polymer networks [4, 5]. In this dissertation, however, we shall consider individual closed

polymer loops, which may be viewed mathematically as knots. (Collections of knots that do not intersect but may be linked together are known as links.) It should be noted that there exist several biological systems where closed polymer loops occur naturally. A suited example is that of ring closure observed in DNA molecules, which has been the subject of much theoretical and experimental study; see, for instance [6], where it was concluded that "short DNA fragments are surprisingly flexible" and that "covalent joining of the ends of linear DNAs by ligase to form closed circular molecules is a fast reaction". Indeed, enzymatic reactions in biological systems have been studied with topological approaches [7]. Enzymes known as topoisomerases act on DNA to alter its topological states [8]. Furthermore, the syndissertation and topological properties of molecular knots are a subject of active study [9].

Historically, topological constraints on closed polymers have typically been addressed mathematically in the context of knot theory, where the goal is to classify knots which possess some or other common topological property or knot invariant. (We shall define knots more carefully in the following chapter; for now an intuitive idea suffices.) Knot invariants are quantities that are used to make some statements regarding topological equivalence of knots. Suppose we have two knots, K_1 and K_2, and some knot invariant $I(K)$ (usually a mathematical function of the knot or even a yes / no question) which may be calculated for any knot K. The purpose here is that if I evaluates to the same result for both knots, i.e., $I(K_1) = I(K_2)$, this should allow for some conclusions about the topological equivalence of K_1 and K_2. Several knot invariants (which have varying degrees of complexity and applicability) have been defined on knot diagrams (planar projections of knots) — see, for instance, [10, 11, 12]. Examples include simple numbers like winding or linking numbers, and polynomial invariants like the Jones and Alexander polynomials. Polynomial invariants are algebraic expressions calculated from planar knot projections. As stated, invariants are used in an attempt to classify topologically equivalent knots. However, as yet it is uncertain whether any invariant provides a complete classification scheme for knots. Alexander polynomials, for instance, do not distinguish between all types of knots. Jones and Kauffman polynomials provide a more powerful classification scheme, but do not distinguish all knot types either [13]. Stated differently, as yet there is no known invariant I which guarantees that if $I(K_1) = I(K_2)$, then K_1 is topologically totally equivalent to K_2.

Since any system with topological constraints is limited in the conformational changes that it may undergo (i.e., only changes subject to these constraints are allowed), it is not surprising that the tools formulated in the context of knot theory are frequently applied to the matter of topological constraints in polymers. However, this task poses many mathematical challenges. Usually some knot invariant is included into path integrals through a delta functional which is then exponentiated through the Fourier representation. In this way some aspects of topology conservation are captured by restricting the conformations that are summed over in the path integral. An extensive review article by Kholodenko and Vilgis [14] elucidates how entangled polymers may be described by such constrained path integrals which can ultimately be mapped onto Chern-Simons theories. As one may suspect, these mathematical descriptions are complicated. Indeed, even using but the simplest knot invariants to determine the partition function of a constrained polymer system, is a non-trivial matter — see, for instance, the article by Edwards [15], where a closed polymer wound around a rod is investigated through the use of winding numbers as a knot invariant. (This problem will be revisited later in this work.)

In this dissertation we shall take a slightly different approach: instead of asking whether K_1 and K_2 have a common knot invariant, we shall ask whether it is possible for K_1 to be *manipulated* to look like K_2 (or vice-versa) through some series of moves. The aim is not to find a comparative schema (through knot invariants) for knot classification, but rather to create a formalism that will allow us to generate all knots that are topologically equivalent to a given knot. To this end, we shall make use of the Reidemeister moves, which are a fundamental concept in knot theory [16]. These moves provide a necessary and sufficient recipe for manipulating knot diagrams in a way that leaves the knots' topology unchanged. Two knots that are related by any sequence of these moves are generally referred to as being "regularly isotopic". This is sufficient where we consider topology *conservation* and no further classification scheme is needed.

This dissertation is organised as follows. In Chapter 2 we set out basic definitions of knots and describe how they may be represented in terms of planar projections. We address there the Reidemeister moves and their implications for topological equivalence. In particular, these topology-conserving knot manipulations are translated into rules on the manipulations of crossings on knot diagrams. Several representations of knots, crossings and the Reidemeister moves will be discussed. The remainder of the dissertation is then

concerned with investigations and applications of these concepts. In Chapters 3 and 4 we shall address "equilibrium-type" questions. Both chapters are concerned with the generation of all topologically equivalent contributions to the partition function of a given knot, subject to particular topological constraints. Chapter 3 deals with equivalence under the zeroth and first Reidemeister moves only. This is a very limited description, but serves as an introduction to some fundamental ideas. A partition function is calculated and physical quantities are studied. The work in Chapter 4 is based on a recent submission [17] and deals with topology conservation under the second Reidemeister move. This is discussed in the setting of winding a polymer around a rod, and a detailed enumeration scheme for equivalent configurations is discussed. For certain confined geometries the partition function is approximated and physical quantities are calculated. In Chapter 5 we then turn to a dynamical description. The rules for topology-conserving crossing dynamics (from Chapter 2) are encoded into an operator formalism for stochastic dynamics. The aim is to consider *purely topological* stochastic dynamics that generate (or evolve) equivalent knot configurations. This formalism allows for the derivation of differential equations for various densities and correlators. The zeroth and first Reidemeister moves are discussed in detail, and densities and correlators of crossings on arc-segments are shown to encode the underlying topological constraints. Chapter 6 contains some suggestions toward an algorithm for simulated annealing of knots, based on the work of previous chapters. Lastly, conclusions and future ideas are set out in Chapter 7.

CHAPTER 2
SOME BASICS: KNOTS, CROSSINGS AND REPRESENTATIONS

As set out in the previous chapter, several motivations from biological, chemical and polymer systems exist to incorporate knot theory into theoretical polymer descriptions. Indeed, a closed, self-entangled polymer loop could be viewed as a knot. In this chapter we shall discuss various aspects of knots and their representations. We further address the Reidemeister moves — local manipulations on planar knot diagrams that conserve the knot topology. In particular, we show how these moves may be translated into rules for dynamics of the crossings of knot diagrams.

2.1 What is a knot?

A classical knot is an embedding of a circle in three-dimensional Euclidean space. There exist more abstract, so-called "virtual" knots, which are a generalisation of standard knots [18]; we shall not deal with these here. Physically such embeddings could be realised by taking an open piece of string (i.e., a one-dimensional object in three dimensional space), entangling it with itself in some chosen way, and closing the piece of string on itself. The closing of the string captures (freezes) some aspects of the particular entanglement. Clearly different knots may be topologically distinct, i.e., one cannot be deformed into the other.

The shadow of a knot is defined as the two-dimensional (i.e., planar) projection of the knot. We assume that we are dealing with regular projections, for which the shadow is a regular graph with vertices that all have a degree of four. A knot diagram is a shadow where some line-segments are deleted at the crossings to indicate over- or undercrossings; examples are shown in Figure 2.1.

Prime knots are knots that cannot be reduced or decomposed to simpler knots through manipulations that do not break strands — this notion will be expanded on in the following section. They are classified according to the number of crossings they contain. (In Section 2.8 we shall make these notions more explicit.) The knots 3_1 and 4_1 in Figure 2.1 are prime knots; they are essentially in their "simplest form" in that the number of their crossings cannot be reduced through topology-conserving manipulations. Clearly these knots are topologically distinct: one cannot be deformed into the other without breaking a

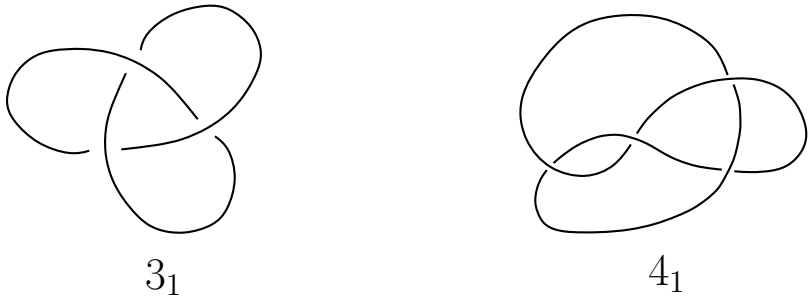

Figure 2.1: Knot diagrams depicting the knots 3_1 (trefoil knot) and 4_1, as found in any table of prime knots.

strand of the knot somewhere. The question arises how topologically distinct knots may be classified. To this end many knot invariants (functions to distinguish different knots) have been defined. As stated, examples include winding numbers, linking numbers and several polynomial invariants; see, for instance [10, 11]. Alternatively one may ask what relates two knots that are topologically equivalent. Indeed, it is this question that is of interest for the subject matter of this dissertation. With that goal we turn to a set of rules — the Reidemeister moves.

2.2 Reidemeister moves and knot equivalence

As set out in [16], the only manipulations that may be performed on a knot so that it retains its topology are the three Reidemeister moves, denoted as **R1**, **R2** and **R3**. These three moves involve the local manipulation of strands on a knot diagram (such as those in Figure 2.1). A fourth move (labelled **R0**) involves basic topological deformations of planar curves that do not alter the crossing structure of the knot. This move is topologically trivial, and may be viewed as stretching and pulling a knot without affecting its crossing structure [10]. We illustrate the Reidemeister moves in Figure 2.2.

The move **R0** is shown in the first line of Figure 2.2. In the sections that follow, however, we shall use the label **R0** for the topologically trivial move that alters the relative lengths of different segments between crossings by sliding strands across each other at a crossing in such a manner that no crossings disappear and no new crossings are introduced. (This is set out in section 2.6.1.) **R1** involves the removal of a single loop from a strand that is crossing with itself (or the addition of such a loop to a naked strand). **R2** entails the separation of two strands that cross each other in two places (or moving two separate strands so that

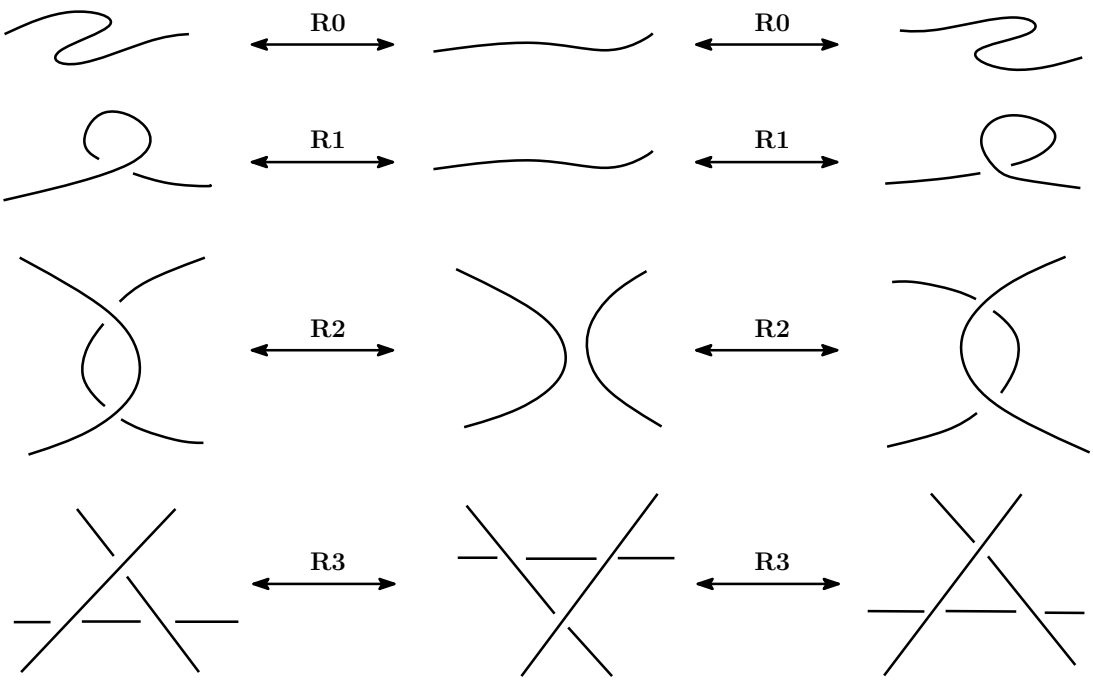

Figure 2.2: The Reidemeister moves, illustrated on strand segments that form part of some (unspecified) knot.

they cross each other). Finally, **R3** involves moving one strand across a single crossing of two other strands. Naturally all three of these moves are reversible. It is also clear that none of the moves forces strands to intersect each other.

In his famous theorem, Reidemeister established that two knots are equivalent if and only if there exists some sequence of the Reidemeister moves that relates them [16]. (This relation is also known as isotopy [10].) Henceforth, this will be used as the definition of topological equivalence in knots. Note that the orientations of the various strands in Figure 2.2 have not been specified. In the remainder of this chapter we shall present a scheme for representing knots according to their crossings. This scheme will be used to derive rules on crossings of knots that encode the topology conservation captured by the Reidemeister moves. To this end we shall outline conventions and labelling schemes in the next subsections.

2.3 Crossings: allocation of signs and representation on a plot

In order to specify positions on a polymer knot of length L, we introduce an "arc length" parameter $s \in [0, L]$, which describes the position relative to an arbitrary "starting point"

where $s = 0$ (and/or where $s = L$, since the knot consists of an unbroken strand and is periodic). The 3-dimensional position vector from some origin to the knot at a given value of s is now denoted by $\vec{r}(s) = (r_x(s), r_y(s), r_z(s))$. The corresponding 3-dimensional tangent vector is $\vec{t}(s) = \partial\vec{r}(s)/\partial s$. (Naturally we assume that $\vec{r}(s)$ is suitably smooth.)

Suppose we look at a projection of a 3-dimensional knot onto a 2-dimensional plane (for convenience, we choose this to be the xy-plane, i.e. we project out the z-axis). As mentioned earlier, this projection is simply a knot diagram such as Figure 2.1. A crossing occurs when the components parallel to this plane of two position vectors on the knot are equal. More specifically, define

$$\vec{r}_{\parallel}(s) \equiv (r_x(s), r_y(s), 0) \quad \text{and} \quad \vec{r}_{\perp}(s) \equiv (0, 0, r_z(s))\,. \tag{2.1}$$

A crossing of two parts of the knot (at points labeled by s_1 and s_2, respectively) would occur when

$$\vec{r}_{\parallel}(s_1) = \vec{r}_{\parallel}(s_2), \quad s_1 \neq s_2. \tag{2.2}$$

We now wish to define signs of crossings. In Figure 2.3 the strand containing s_1 lies above the one containing s_2. (Note that we shall indicate the upper strand with a red dot, and the lower strand with a blue dot. These dots should, of course, be on top of each other, but will be drawn in this offset manner to indicate the spatial sequence of the strands along the projected z-axis.) We assign a "+" to the crossing on the upper strand at s_1 and a "−" to the lower strand at s_2. In terms of the position and tangent vectors, the sign of a crossing between the strands at s_1 and s_2 is given by

$$\begin{aligned} \text{sign}(s_1, s_2) &= \text{sgn}\Big[\hat{z} \cdot \big(\vec{r}(s_1) - \vec{r}(s_2)\big)\Big] \frac{\vec{t}_{\parallel}(s_1) \times \vec{t}_{\parallel}(s_2)}{\big|\vec{t}_{\parallel}(s_1) \times \vec{t}_{\parallel}(s_2)\big|} \cdot \frac{\vec{r}(s_1) - \vec{r}(s_2)}{|\vec{r}(s_1) - \vec{r}(s_2)|} \\ &= \text{sgn}\Big[\hat{z} \cdot \big(\vec{r}_{\perp}(s_1) - \vec{r}_{\perp}(s_2)\big)\Big] \frac{\vec{t}_{\parallel}(s_1) \times \vec{t}_{\parallel}(s_2)}{\big|\vec{t}_{\parallel}(s_1) \times \vec{t}_{\parallel}(s_2)\big|} \cdot \frac{\vec{r}_{\perp}(s_1) - \vec{r}_{\perp}(s_2)}{|\vec{r}_{\perp}(s_1) - \vec{r}_{\perp}(s_2)|}. \end{aligned} \tag{2.3}$$

It is clear that if we continue moving along the knot until we come to the same crossing along the other strand, then

$$\text{sign}(s_1, s_2) = -\text{sign}(s_2, s_1). \tag{2.4}$$

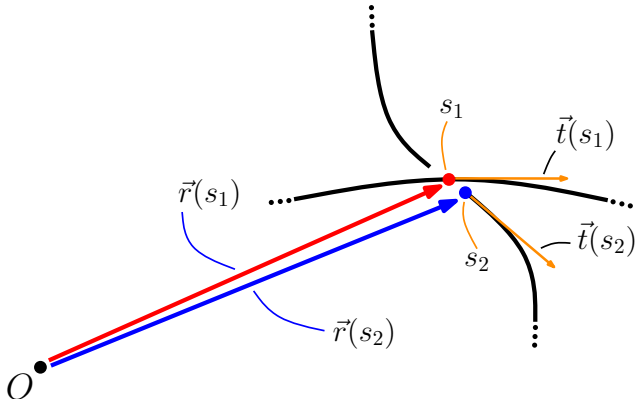

Figure 2.3: A crossing of two strands of a knot (the rest of the knot is not shown). Shown here are the origin (O), the two arc-length co-ordinates at the crossing (s_1 and s_2) and the corresponding position vectors ($\vec{r}$) and tangent vectors ($\vec{t}$).

We wish to represent the crossing structure of a given knot in a graphic manner in order to capture information regarding the signs of the crossings. To this end, an algorithmic procedure may be followed:

- Choose a reference point on the knot to be labelled as $s = 0$, and choose an orientation for the knot (arbitrary).
- Begin moving along the knot. Suppose a crossing occurs when the point s_1 is reached. Note the sign of this crossing, and the position on the other strand involved with the crossing, say s_2.
- Use a set of axes labelled by s (the current location on the knot) and s' (the other location on the knot involved in a particular crossing) – see Figure 2.4. Enter the sign of aforementioned crossing at co-ordinate (s_1, s_2) on this plot.
- Continue in this manner until the reference point is reached again, i.e. until $s = L$.
- It is implicitly assumed that the projection is such that at most two strands lie above each other at a given crossing. This is a standard assumption for knot diagrams [10].

Diagrams generated in this manner will henceforth be referred to as $s-s'$ plots. To illustrate these ideas, we consider a simple figure-of-eight with a single crossing in Figure 2.4. (It is

clear through a simple application of **R1** that this configuration is equivalent to the unknot, i.e., a closed loop with no crossings.)

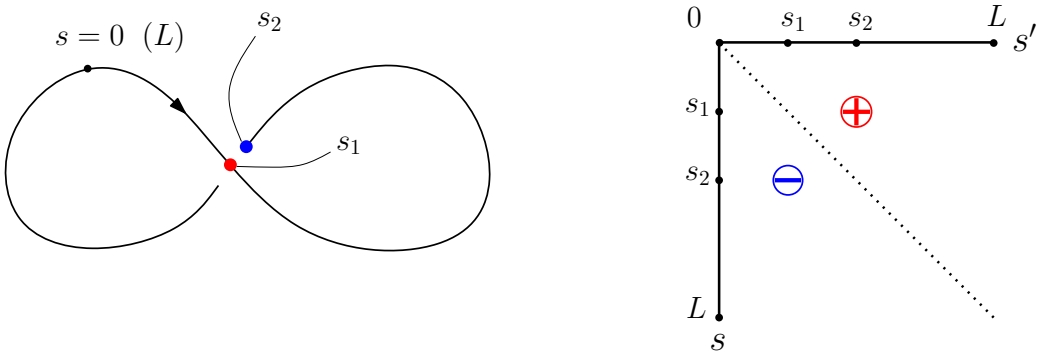

Figure 2.4: Plot of s against s' for a simple knot with one crossing.

As a consequence of equation (2.4), it is clear that the resulting plot of signs on the s vs. s'-axes will always be anti-symmetric (with respect to signs) about the diagonal (indicated in Figure 2.4 by a dotted line). Naturally such a plot with two "species" reminds us of particles on a lattice. Indeed, we shall use the terms "sign" and "particle" interchangeably henceforth. The arc-length parameter could be discretised or continuous — which of these choices is implied will be clear from the context in sections to follow.

2.4 Boundary conditions on $s - s'$ plots

As stated, the closed knots considered here are labelled with an arbitrary beginning (end) arc-length co-ordinate where $s = 0$ (L). This co-ordinate is thus periodic in the length of the knot L. Looking at Figure 2.4 we observe that this plot thus obeys toroidal boundary conditions; this is illustrated in Figure 2.5.

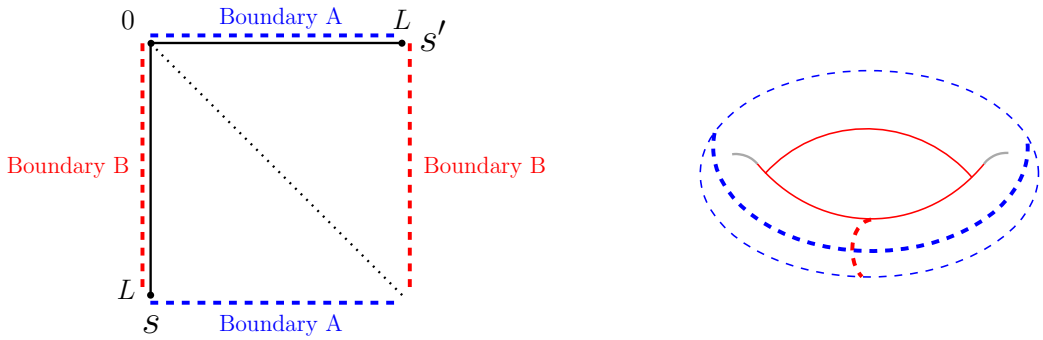

Figure 2.5: Illustration of the toroidal boundary conditions on an $s - s'$ plots. (One dimension has been rescaled on the right.)

We conclude that if a particle / sign were to move horizontally out of the lower triangle across boundary B it would enter the top triangle at the same height across the boundary. (A similar statement applies, of course, to a sign / particle moving vertically across boundary A.) Since the $s - s'$ plot is anti-symmetric, however, one may also view this as follows: if a particle leaves the lower triangle at co-ordinate $(s, 0)$ across boundary B it is clear that a particle *of the opposite sign* must leave the upper triangle across boundary A at co-ordinate $(0, s)$. (It is implied throughout that any such process occurs together with the corresponding process for the anti-symmetric counterpart sign in the $s - s'$ plot.) The periodic boundary conditions may also be viewed such that a particle leaving the lower triangle at co-ordinate $(s, 0)$ across boundary B re-enters the *same triangle* across Boundary A at co-ordinate (L, s) as a particle *of the opposite sign*.

Clearly it is sufficient to investigate only one triangle in a given $s - s'$ plot, since we may reconstruct the content of the other triangle from the boundary conditions and anti-symmetry. The convention of choice henceforth will be to consider the lower triangle.

2.5 $s - s'$ plots and the Gauss code of a knot

Our $s - s'$ plot representation of crossings of knots is very similar to one known as the "Gauss code". We shall describe the Gauss code briefly, following the discussions of Kauffman *et al.* [18, 19].

2.5.1 The Gauss code

Not unlike our $s - s'$ plots, the Gauss code is a sequence of labels for the crossings of a knot. Each label (crossing) is repeated twice, since each crossing would be encountered twice while walking once along the entire length of any unbroken knot. In addition to the crossing sequence, a Gauss code records whether a particular strand segment is at the top or bottom of a given crossing. In Figure 2.6 we show a trefoil knot and its corresponding $s - s'$ plot. The Gauss code corresponding to this trefoil is

$$g_{\text{tref.}} = O1U2O3U1O2U3, \tag{2.5}$$

where O and U refer to "over" and "under", respectively. Comparing this sequence to the $s - s'$ plot in Figure 2.6, we note that the same information is contained in the $s - s'$ plot: we simply follow the s axis from the origin ($s = 0$) and observe that the signs encountered are analogous to the sequence of Os and Us. The $s - s'$ plots, however, further record the distance between consecutive crossings and not only their order.

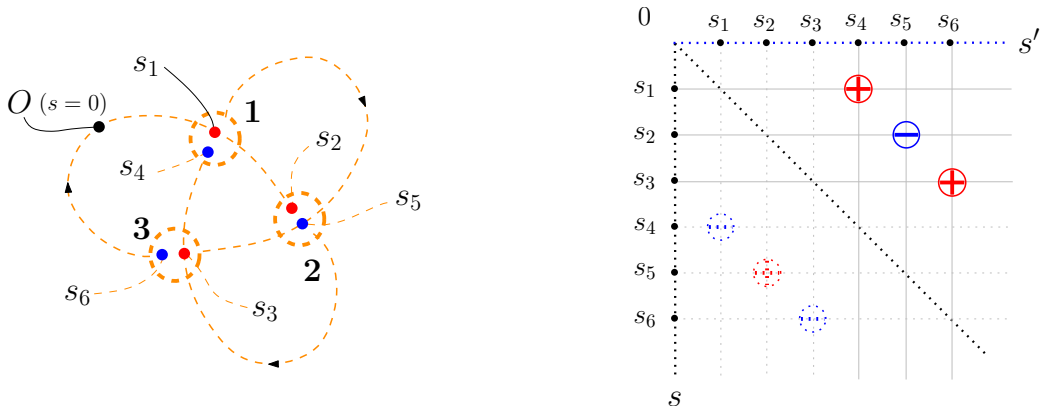

Figure 2.6: The trefoil knot is shown on the left. An origin and an orientation have been chosen and the three crossings (circled in red) have been numbered. The s co-ordinate of each strand at the crossings is indicated by s_i, $i = 1, 2, \ldots, 6$ (not to scale). On the right the corresponding $s - s'$ plot is shown.

An extension of the standard Gauss code is the signed Gauss code, which further records the orientation of each crossing, as defined in Figure 2.7. This orientation is denoted as $+$ if a crossing is "right-handed" and as $-$ if it is "left-handed".

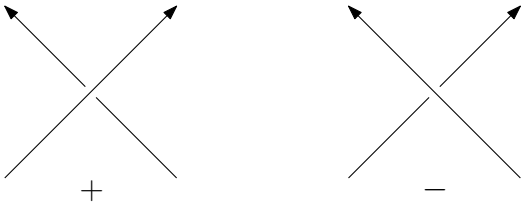

Figure 2.7: Standard knot theory convention for assigning orientation to a crossing according to its "handedness".

The signed Gauss code for the trefoil knot in Figure 2.6 is

$$g^{(s)}_{\text{tref.}} = O1 + U2 + O3 + U1 - O2 - U3 - . \tag{2.6}$$

Note that this is *not* the same convention chosen to allocate signs to crossings in our $s - s'$ plots. Indeed, the $+$ and $-$ signs in our $s - s'$ plots denote the information contained in the Os and Us of a Gauss code, i.e., about the order of strands along the projection axis. By implication, an $s - s'$ plot does not capture the orientation of crossings as defined in Figure 2.7.

2.5.2 Reconstructing knots from an $s - s'$ plot: is it possible?

As set out in [19], there exists an algorithm for reconstructing a knot shadow from a particular Gauss code (this code need not be be signed). The one proviso here is that the Gauss code underlying the construction be "reconstructible", i.e., that there is no need to introduce virtual crossings during the reconstruction of the planar shadow [18, 19]. (Knot diagrams with virtual crossings do not have physical realisations as embeddings in three-dimensional space.) Since we are considering classical (read "non-virtual") knots, this requirement is trivially satisfied: we work with Gauss codes that were generated from a real knot. For such Gauss codes, the reconstruction process is possible up to isotopy [20]. During reconstruction one initial choice in crossing orientation is arbitrary, but the orientation of the remaining crossings is fixed using the aforementioned algorithm [19], i.e., the reconstructed knot could be the mirror image of the projection used to generate the Gauss code initially. For our purposes, a knot and its mirror image are topologically trivially related. (Some knots are chiral, and cannot be deformed into their mirror images [12].)

In the previous section we showed that an $s - s'$ plot contains the same information as a Gauss code. By implication one may reconstruct the knot shadow from a given $s - s'$ plot. This is crucial to our discussion, as we wish to concern ourselves with the rules that relate topologically equivalent knots. We shall omit the explicit discussion of this reconstruction algorithm since we wish to focus on the representation of these *rules* — the Reidemeister moves — on $s - s'$ plots.

It should be noted that the manipulation of Gauss codes according to the Reidemeister moves has been studied; see, for instance, the appendices of Kauffman's book [12].

2.6 Representations of the Reidemeister moves on $s - s'$ plots

We now have a recipe to illustrate the crossing structure of a given knot. The next step is to see how the Reidemeister moves would look on such a plot. In essence, this implies that the Reidemeister moves define / determine what dynamics are allowed for the signs on a plot of the type in Figure 2.4. The aim is to produce the $s - s'$ plot for a given knot, and then to treat the $+$ and $-$ signs therein as dynamical objects, which "diffuse" around on the plot like particles on a lattice as various crossings "slide" around in the planar projection. The Reidemeister moves then determine the interaction rules.

To proceed we discretise the axes of the $s - s'$ plots, so that $s_i = i\epsilon$ where $\epsilon = \frac{L}{N}$ would be a minimal length-scale / Kuhn length of the strands. We shall now consider each Reidemeister move individually, as seen on segments of a knot in Figure 2.2. Since we only consider the segments of the knot which are close to the crossings involved, the orientations of line segments will be chosen arbitrarily. In practice, these orientations would naturally be determined by the specifics of the remainder of the knot in question. This will prove to be of particular importance for the representations of **R2** and **R3**, the implications of which will be discussed later.

2.6.1 The move R0

Contrary to what is shown in Figure 2.2, we shall describe by **R0** the (topologically trivial) move that alters the relative lengths of different segments in the strand, as shown in Figure 2.8. This translates to "diffusion" of the signs in $s - s'$ plots which leaves the number of crossings unchanged. Of course this happens in such a way that the structure of the plot is still anti-symmetric. In our projection we require that at most two strands

ever cross each other. This translates into the requirement that any row or column in the $s - s'$ plot contains at most one sign at any given time. Naturally this constrains the aforementioned diffusion of the signs.

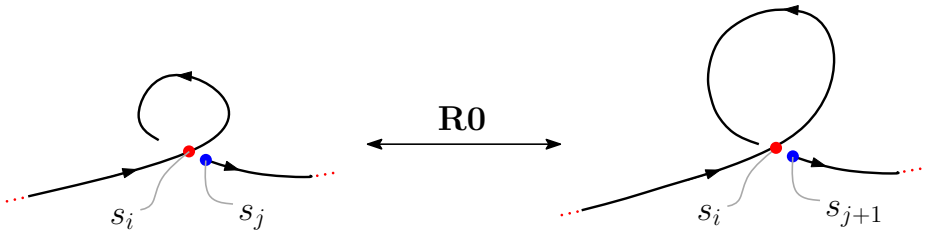

Figure 2.8: The move **R0**

Figure 2.9 shows the $s - s'$ plot corresponding to the scenario in Figure 2.8.

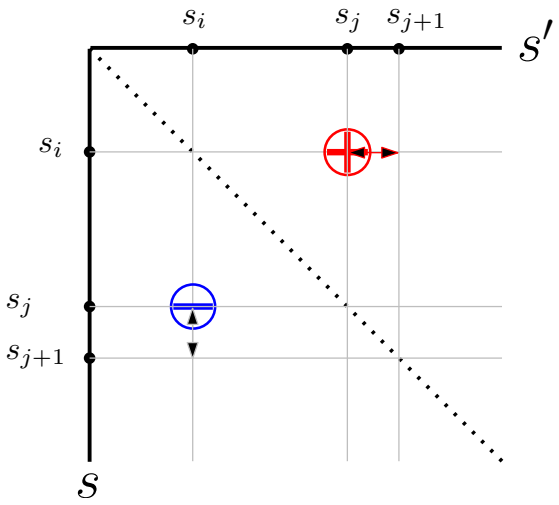

Figure 2.9: Plot of s vs s' for the move **R0**.

Similarly, the process can happen for the co-ordinate s_i, which would involve diffusion of the particles in a perpendicular direction on the $s - s'$ plot.

2.6.2 The move R1

We now consider the move **R1** in Figure 2.2. Adding an orientation (arbitrarily chosen) and site labels to the loop involved in this move, we may represent **R1** as follows:

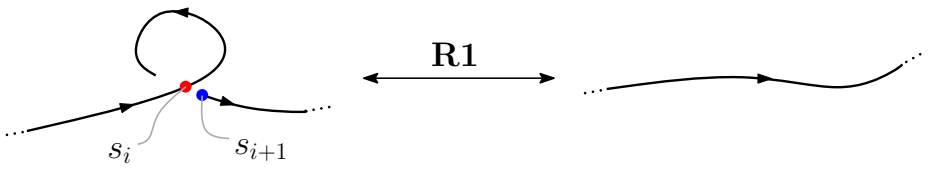

Figure 2.10: The move **R1**.

The corresponding $s - s'$ plot (in the vein of Figure 2.4) would look like this,

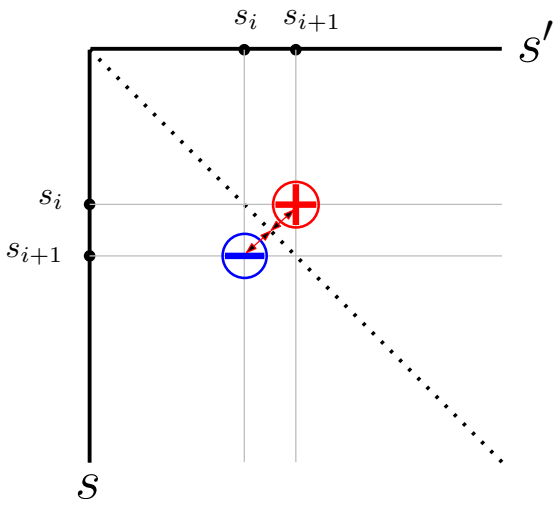

Figure 2.11: Plot of s vs s' for the move **R1**.

Suppose we consider the forward direction in Figure 2.10. As the loop is shortened, the signs in Figure 2.11 approach the diagonal, where they are "annihilated" as soon as the loop is totally removed from the strand. Note that the signs in Figure 2.11 would be exchanged if the orientation of the loop was reversed or if the loop was such that s_{i+1} lay beneath s_i.

If we were to consider the reverse direction in Figure 2.10, i.e., if a crossing were created in a strand that was previously crossing-free, the corresponding process on Figure 2.11 would be the "creation" of two particles on opposite sides of the diagonal dotted line. Again, the specific signs would be exchanged if the orientation of the strand were reversed, or if the twist was created in the other direction so that s_{i+1} lay beneath s_i.

2.6.3 The move R2

Next we consider the move **R2** in Figure 2.2. For this move, the relative orientation of the two strands involved will prove to be of importance. For that reason we will consider two separate cases.

Strands with parallel orientation

Let us consider the case where the two strands have parallel orientation, and label the sites of the crossings involved:

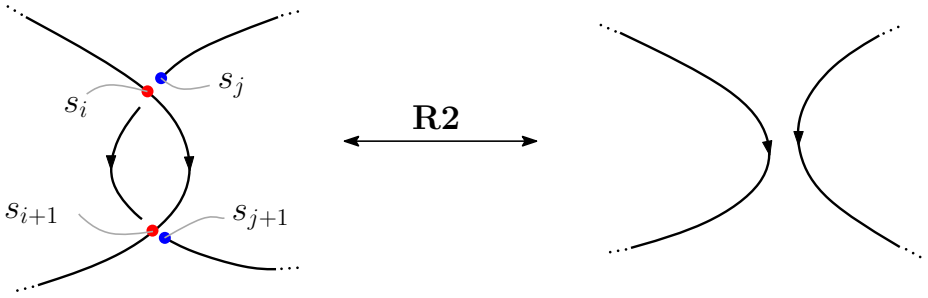

Figure 2.12: The move **R2**.

The corresponding $s - s'$ plot would look as follows:

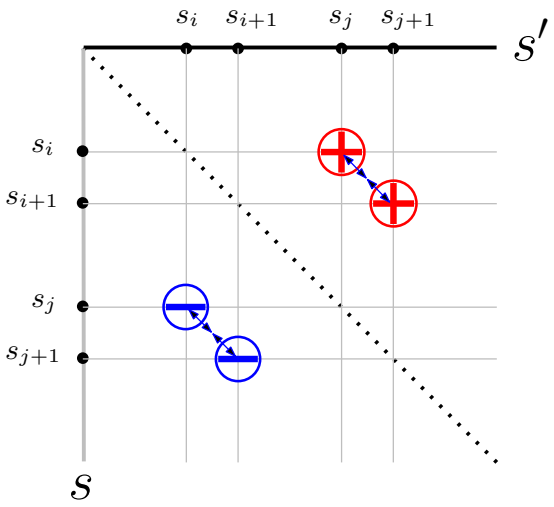

Figure 2.13: Plot of s vs s' for the move **R2**.

The execution of the forward move **R2** in Figure 2.12 involves two pairs of signs (++ and

$--$, respectively) approaching each other in Figure 2.13 on opposite sides of the diagonal. As the two strands are totally pulled apart in Figure 2.12, the two pairs annihilate each other. The execution of the reverse move in Figure 2.12 would simply result in the creation of the above sign pairs in Figure 2.13.

It should be noted that if the other strand were on top (i.e., s_j and s_{j+1} were above s_i and s_{i+1}, respectively), then the $++$ and $--$ pairs would simply be exchanged in 2.13. Furthermore, the distance between points s_{i+1} and s_j depends on the rest of the knot, which is not shown here. This distance is not important for any part of this discussion, since we are considering the crossings in isolation.

Strands with anti-parallel orientation

Let us reverse the orientation of one of the strands in Figure 2.12 (for instance by exchanging the labels s_j and s_{j+1}).

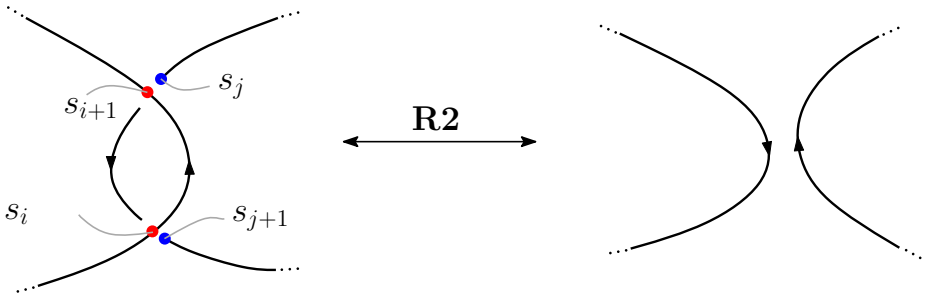

Figure 2.14: The move **R2** with anti-parallel strands.

It is clear that in this case the orientation of the $++$ (respectively $--$) pair would be rotated, as is seen here:

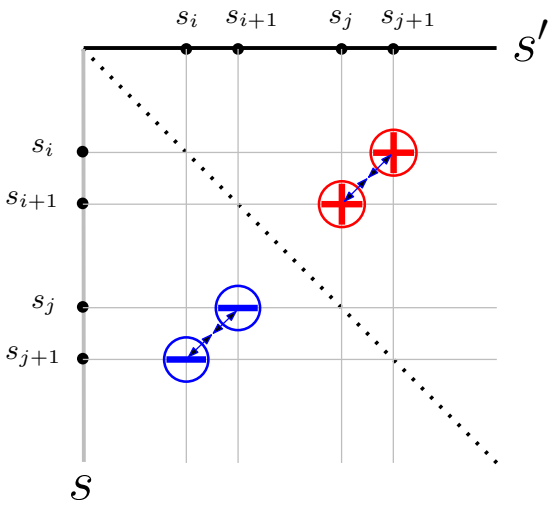

Figure 2.15: Plot of s vs s' for the move **R2** with anti-parallel strands.

Again, changing which of the strands is on top would simply exchange the $++$ and $--$ pairs. It is, however, clear from Figures 2.13 and 2.15 that we need know the orientation of the two strands involved in order to specify along which direction the signs approach each other (or move apart). In the following section we shall provide an algorithm for finding this relative orientation of the strands.

2.6.4 Finding the relative orientation of two strands involved in an R2 move

Consider Figure 2.16, where we have two such strands, and where the remaining parts of the knots (which connect the two strands) have been condensed into a "blob". The difference between parallel and anti-parallel orientations involves one more crossing between the strands.

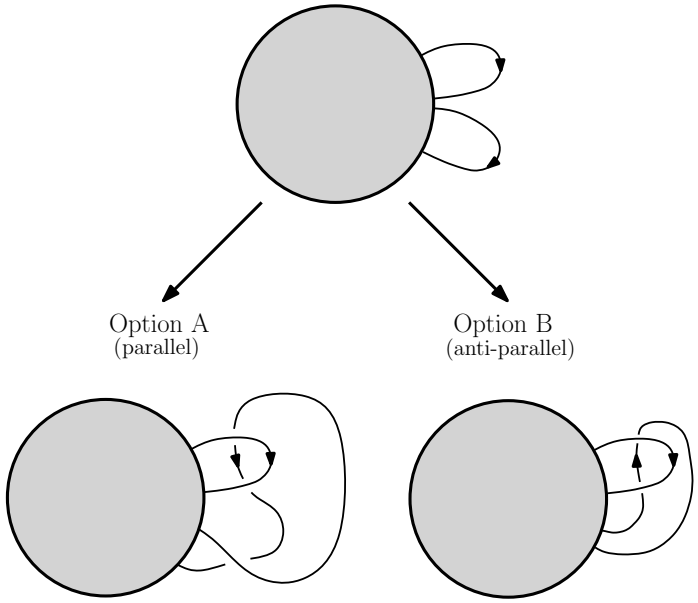

Figure 2.16: Relative orientations of strands involved in the move **R2**.

To illustrate this feature more specifically, we look at the creation of an **R2** move for a specific knot in Figure 2.17. We note that there is a fundamental difference between creating an **R2** move by overlapping points A and B and by overlapping points B and D. In the case of Option 1, we encounter two signs when following the strand between the involved $++$ pair at (s_i, s_{j+1}) and (s_{i+1}, s_j) and the $--$ pair at (s_{j+1}, s_i) and (s_j, s_{i+1}). The crossing between s_T and s_B is traversed *twice*, and the relative orientation of the strands is *anti-parallel*. In the case of Option 2, however, there is only one sign change between the $++$ pair at (s_i, s_j) and (s_{i+1}, s_{j+1}) and the $--$ pair at (s_j, s_i) and (s_{j+1}, s_{i+1}), since the crossing between s_T and s_B is only traversed *once*. Here the relative orientation of the strands is *parallel*.

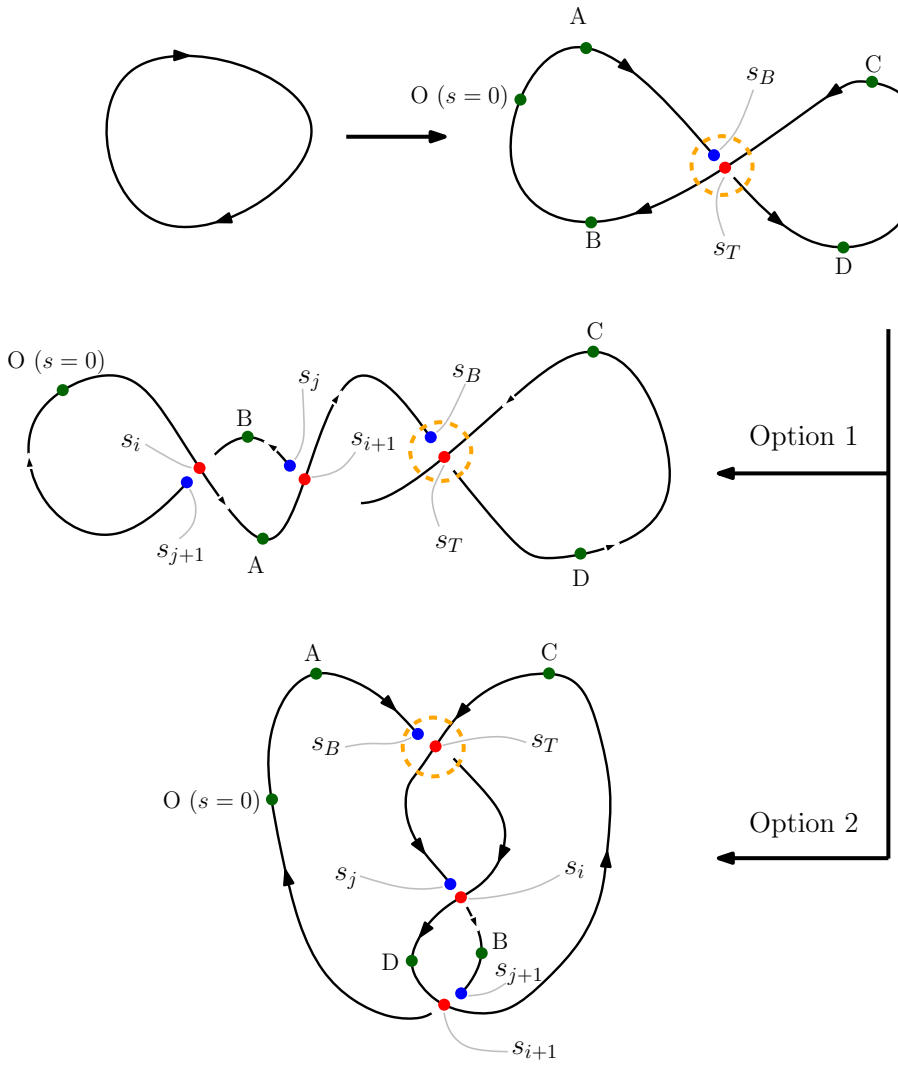

Figure 2.17: Possible ways to execute an **R2** creation move.

Suppose we want to create an **R2** move between two strands. To find the relative orientation of the strand containing the two + signs and that containing the two − signs, we derive the following rule from Figures 2.16 and 2.17: suppose the co-ordinates are ordered $s_i < s_{i+1} < s_j < s_{j+1}$. To check the relative orientations of the strands, simply move along the s axis from point s_{i+1} to point s_j. If an even number of signs is encountered, the orientation of the strands must be anti-parallel, and the pairs will be created as in Figure 2.15. If, however, an odd number of signs is encountered, the strands will be parallel in orientation and the signs will be created as in Figure 2.13.

It is clear that the check required for the creation of an **R2** move is *non-local*: information about the rest of the knot (and not only the involved crossings) is needed to determine the orientation of the strands.

2.6.5 The move R3

Finally we take a look at the last Reidemeister move. As before, orientations of strands were chosen arbitrarily, and points were labeled as follows in Figure 2.18.

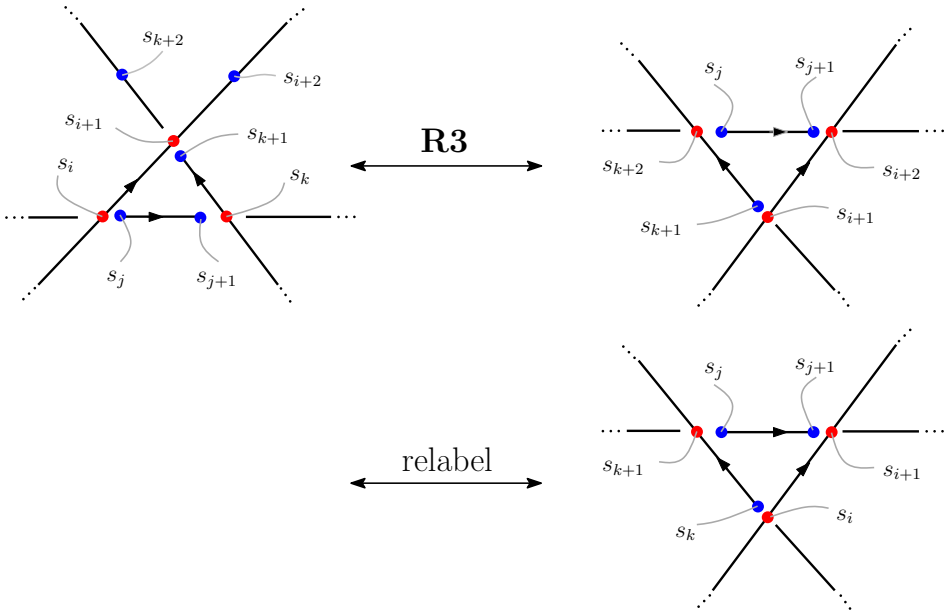

Figure 2.18: The move **R3**.

This figure shows the move being applied to the strands in two parts: the strand containing points s_j and s_{j+1} is moved past the crossing of the other two, and then the other two strands are shifted along to return to a convenient configuration for labelling. (This is technically a combination of **R0** and **R3**, but is absorbed into our definition of the latter move.) It should be noted that the move **R3** can only be executed when one of the three strands has a $+$ and a $-$, and the remaining two strands either have two $+$ signs or two $-$ signs. If we consider, for instance, the case where all three strands have a $+$ and a $-$ sign, it would be impossible to move one of the strand past the crossing of the other two.

The $s - s'$ plot for the move performed in Figure 2.18 would be

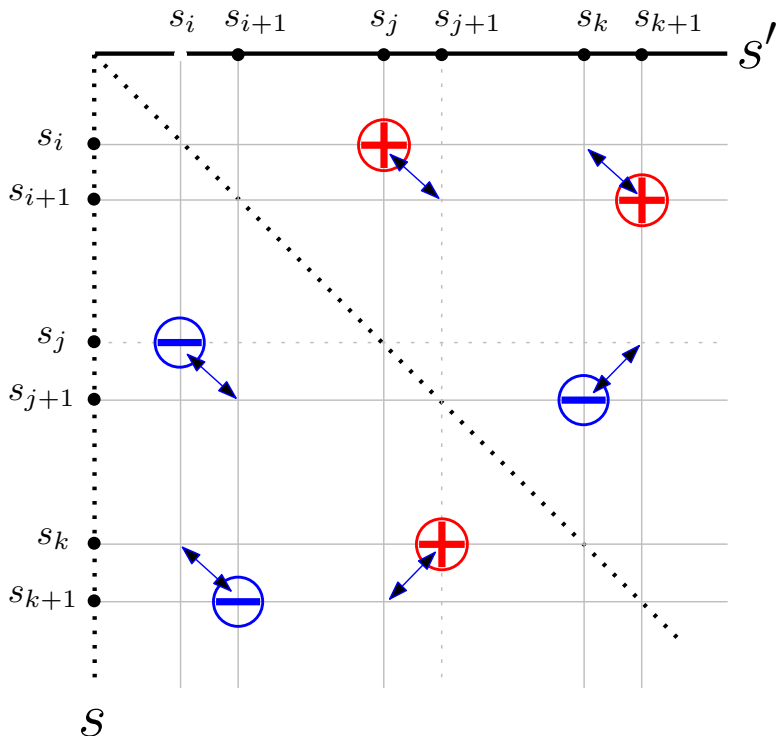

Figure 2.19: Plot of s vs s' for the move **R3**.

The arrows represent the execution of the move **R3**. Again the distances between the crossings depend on specifics of other parts of the knot, and are not relevant for this process. We see clearly, that at the instant where the cross-over occurs, the signs in each triangular half of Figure 2.19 arrange in a right-angled triangle before exchanging rows and columns (as indicated by the arrows). The constraint that was noted on the previous page (regarding the signs on each strand involved) is clearly satisfied: if we consider the sequence of signs along the s axis, namely $++--+-$, we note that there are two strands with equal signs ($++$ and $--$) and one strand with opposite signs ($+-$) as is required. Indeed, there are $2^3 = 8$ possible ways to arrange + and - signs in a triangle in the bottom triangular half of the $s - s'$ plot, as shown in Figure 2.20.

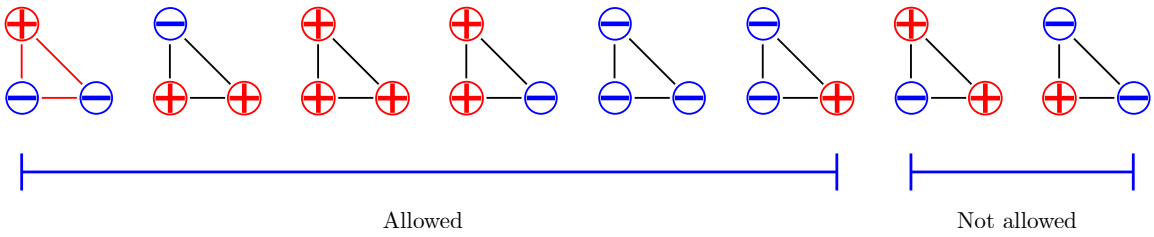

Figure 2.20: The eight possible arrangements of signs in a triangle.

Naturally, the anti-symmetric equivalent would occur in the upper triangle of the lattice. The constraint on which strands are allowed in this move translates into the following statement: only the first 6 of these are allowed for the execution of **R3**. The two last triangles in Figure 2.20 represent strands that are tangled in such a way that they cannot pass each other. This scenario is illustrated in Figure 2.21.

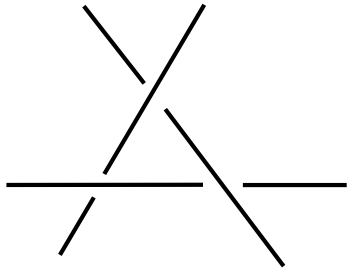

Figure 2.21: In this configurations it is impossible for one strand to move past the crossing of the two remaining strands.

Lastly we consider the specific arrangement of signs at the vertices of the right-angled triangle. In Figure 2.22 we label these three vertices as A, B and C, respectively. Each vertex has four sites where a sign could be. As stated, there may be at most one particle per row and column in an $s - s'$ plot. By implication there are eight possible ways to occupy these vertices. Beginning with vertex A there are four available sites. Choosing one implies that there are two sites remaining at vertex B for the next sign. Choosing one of these leaves only one site remaining at vertex C. The eight choices here correspond to the 2^3 possible choices in orientation for the three strands. As stated, all rows and columns passing through A, B and C are then exchanged upon execution of **R3**.

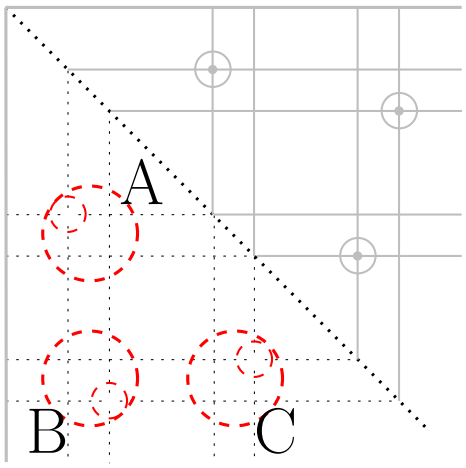

Figure 2.22: The vertices of the right-angled triangle involved in **R3**, circled in red and labelled A, B and C. Due to the restriction that there may be at most one particle per row and column in the $s - s'$ plot, there are 8 ways to arrange the three signs at the vertices. The top half of the $s - s'$ plot is included in grey to make this clear.

2.6.6 Summary of allowed "dynamics" on $s - s'$ plots

- Only one sign is allowed per row and column, since at most two strands may cross each other in the projection.
- Signs "diffuse" on the (anti-symmetric) $s - s'$ plot. This may only occur if target rows / columns are unoccupied. Two signs "collide" if they are in adjacent rows / columns. If such a "collision" occurs, the signs may not move past each other. This process corresponds to lengthening / shortening of loops in the projection, as governed by **R0**. See Section 2.6.1 for more details.
- The particles / signs on $s - s'$ plots "interact" according to the remaining Reidemeister moves:
  - **R1**: two single (opposite) signs are created or annihilated at the diagonal of the $s - s'$ plot, one in the top triangle and the other in the bottom triangle. This introduces new single loops into the knot projection. See Section 2.6.2 for more details.

- **R2**: equal sign pairs are created or annihilated (diagonally, anywhere on plot). This moves two strands across each other or separates them.
- **R3**: given that one of the correct right-angled triangle configurations exists, exchange of rows and columns may occur as described earlier. See Section 2.6.3 for more details.
- Importantly, ONLY **R3** allows signs to exchange rows or columns. **Without this move, the particles cannot move past each other in rows and columns on the $s - s'$ plot**. See Section 2.6.5 for more details.

2.7 Bow diagrams from $s - s'$ plots

As stated previously, the $s - s'$ plots are anti-symmetric, so it is sufficient to consider the lower triangle of such a plot. Instead of labelling the positions of signs on the s and s' axes, we now project these co-ordinates onto the diagonal of the plot. Note that this information suffices if we wish to reconstruct the corresponding $s - s'$ plot. This labelling scheme is illustrated for a few examples in Figure 2.23. The resulting diagrams in these figures may also be viewed as "contact-point diagrams" of the knot shadow. We comment on this explicitly in Section 2.9.

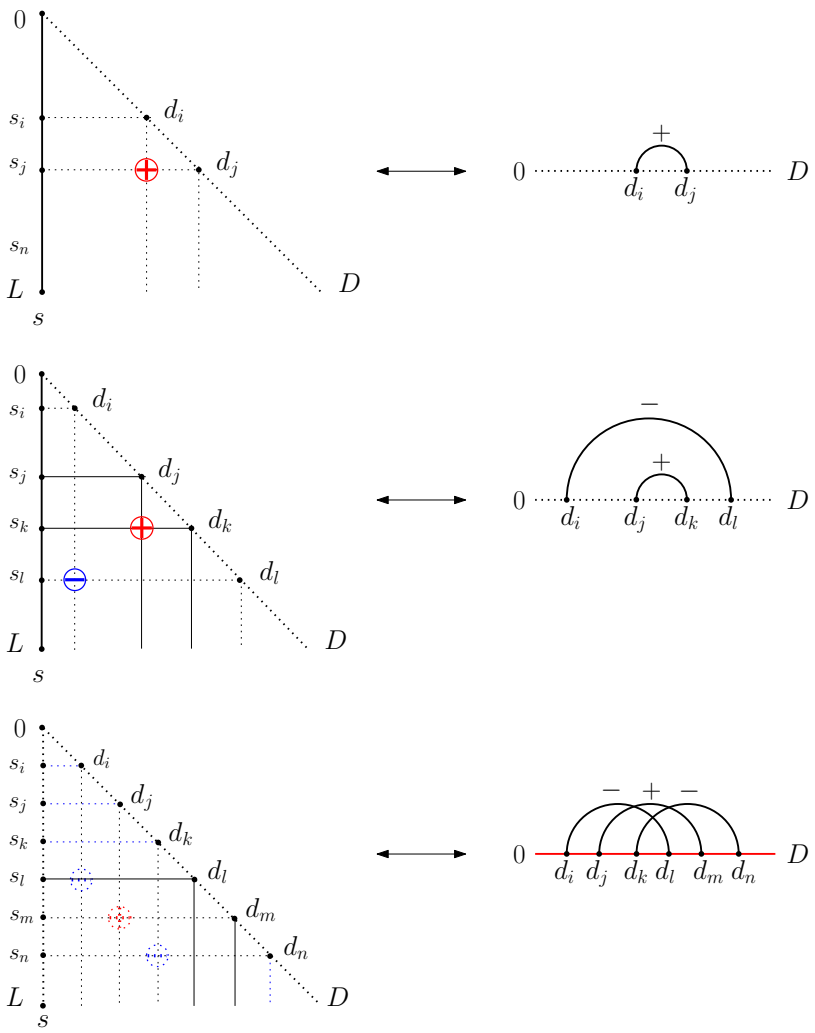

Figure 2.23: New labelling scheme: projection of co-ordinates onto the diagonal. Three examples of $s - s'$ plots are shown together with the corresponding bow diagrams.

For $s - s'$ plots we had the requirement that there be at most one sign per row and column. This condition translates into a much simpler condition on bow diagrams: each site on the line of a bow diagram may be occupied by *at most one single bow foot*. Further we recall the toroidal boundary conditions on $s - s'$ plots, as set out in Section 2.4. The corresponding boundary condition on bow diagrams is that if one foot of a bow diffuses off one side of the line it re-enters the line at the other side while the sign of the bow changes. Naturally one may view this as a circular boundary condition with a sign-change boundary. This is illustrated in Figure 2.24.

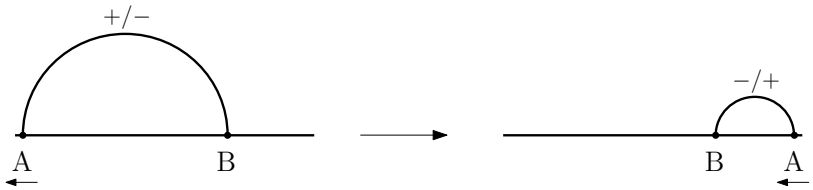

Figure 2.24: Boundary conditions on bow diagrams: diffusion of bow foot A off the left end of the line is associated with a sign change of the bow, and with bow foot A re-entering the other side of the line. (This is obviously reversible.)

2.7.1 The move R0 on bow diagrams

We shall now illustrate the representation of **R0**, as set out in Section 2.6.1, on bow diagrams. The "free diffusion" of signs on $s - s'$ plots translates to nearest neighbour hopping of bow feet on a bow diagram, subject to the boundary conditions and occupancy restrictions set out above. This is illustrated in Figure 2.25.

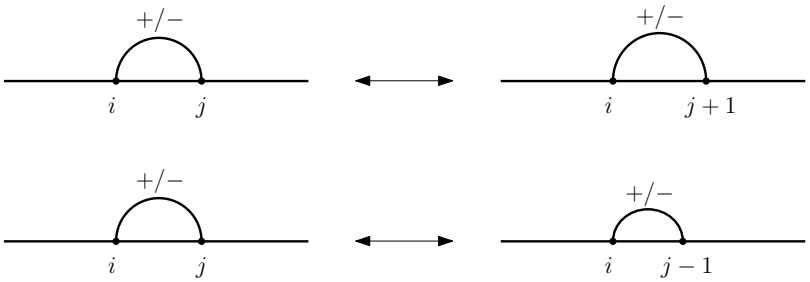

Figure 2.25: The move **R0** on a bow diagram. One bow foot "diffuses" to an adjacent site on the line, provided that this site is empty. A corresponding scenario where the left foot (labelled i) diffuses is not shown here.

2.7.2 The move R1 on bow diagrams

The move **R0** involves the creation / annihilation of a single sign on an $s - s'$ plot, as explained in Section 2.6.2. The corresponding process on a bow diagram is the creation / annihilation of a single bow at two adjacent sites on the line. The creation process may only happen if the two sites are unoccupied. This is shown in figure 2.26.

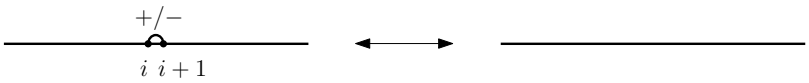

Figure 2.26: **R1** on a bow diagram: creation / annihilation of a single bow (of any sign) at neighbouring sites on the line.

2.7.3 The move R2 on bow diagrams

During this move an equal-sign pair is created / annihilated on an $s - s'$ plot, as shown in Section 2.6.3. On a bow diagram this is represented by the creation / annihilation of a bow pair, where the left feet of both bows are adjacent and the right feet of both bows are adjacent. We recall from Section 2.6.3 that the relative orientation of the two strands is unimportant for the annihilation process. This means that the forward processes shown in Figure 2.27 can both happen assuming that two bows *of equal sign* are in the correct configuration. For the **R2** annihilation process on a bow diagram it is thus unimportant whether the two bows cross each other (top of Figure 2.27) or whether they are "nested" (bottom of Figure 2.27).

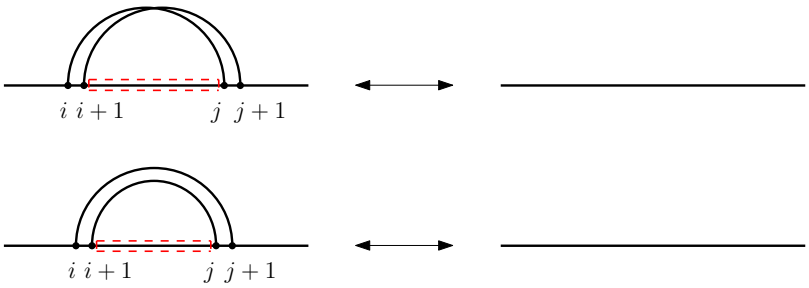

Figure 2.27: **R2** on a bow diagram: creation / annihilation of an equal-sign bow pair. It is required that the left feet and right feet of both bows be nearest neighbours on the line.

For the **R2** creation process (i.e., the reverse processes in Figure 2.27), however, care must be taken with the relative orientations of the two strands. In Section 2.6.4 it was explained how the relative orientation of two strands on an $s - s'$ plot may be found (this involved counting the number of signs along the strand between the two crossing points). On a bow diagram we simply need to count the number of bow feet encountered between the two pairs of neighbouring sites — this region is indicated in red in Figure 2.27. For the creation of an **R2** pair on *parallel strands* (compare to Figures 2.12 and 2.13) this region

would contain an odd number of bow feet. In this case the reverse process at the top of Figure 2.27 would occur. For the creation of an **R2** pair on *anti-parallel strands* (compare to Figures 2.14 and 2.15) the red region would contain an even number of bow feet. In this case the reverse process at the bottom of Figure 2.27 would occur.

2.7.4 The move R3 on bow diagrams

In Section 2.6.5 a right-angled triangle in the $s - s'$ plots was shown to be associated with the move **R3**. In Figure 2.20 the allowed sign combinations are shown, and in Figure 2.22 the arrangement of the signs at the vertices of the triangle is explained. Execution of the move results in the exchange of adjacent rows and columns at the vertices.

We now represent this information in terms of bow diagrams. To each sign in the $s - s'$ plot we associate a corresponding (labelled) bow. Execution of **R3** translates into three pairwise exchanges of the positions of neighbouring bow feet. An example of this is shown in Figure 2.28.

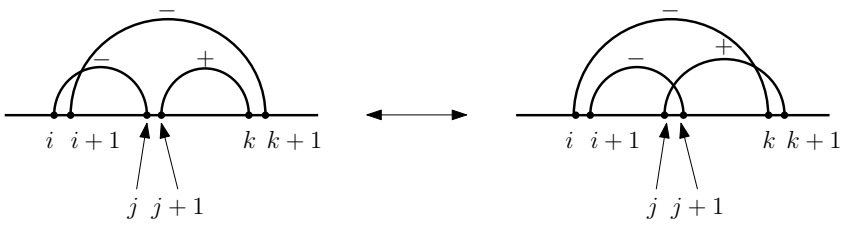

Figure 2.28: **R3** on a bow diagram. This particular arrangement of signs corresponds to the $s - s'$ plot from Figure 2.19. Execution of the move results in exchange of positions of nearest neighbour bow feet.

Naturally the restrictions on valid combinations of signs and their arrangement at the vertices (again, see Section 2.6.5 and Figures 2.20 and 2.22) still apply to bow diagrams. The implications thereof are easy to translate.

2.7.5 $s - s'$ plot and bow diagrams: ease of use

In $s-s'$ plots we record signs that each have a horizontal and a vertical positional degree of freedom. This provides a clear visual aid to represent knots, and facilitates, in particular, clear labelling of the valid configurations for **R3**. In this setting, however, the occupancy restriction (at most one sign per row and column) is somewhat tedious: the check is non-

local, since we need to check each site in every row and column. Furthermore, checking for the right-angled configurations as shown in Figure 2.22 is difficult: to see whether two neighbouring columns of an $s - s'$ plot contain the required signs, it is necessary to check each site in both columns.

In bow diagrams we record bows that each have two positional degrees of freedom, *viz.* the position of the two bow-feet. Here the occupancy restriction reduces to a simple *one-dimensional* check. The nearest-neighbour checks for the various Reidemeister moves are also significantly easier than in the $s - s'$ plot geometry.

If the aim is to describe crossing dynamics in terms of hopping rules on a lattice, it is clear that the description of bow diagrams provides a suitable framework with simple occupancy and neighbouring tests.

2.8 Prime knots and their representation

As alluded to earlier, prime knots are the "simplest" knots in that they cannot be reduced to knots with fewer crossings through some sequence of Reidemeister moves. A theorem by Schubert [21] states that any knot may be expressed uniquely as the connected sum of prime knots. (This can be viewed as cutting prime knots open and splicing them together.) In this sense prime knots provide a categorisation scheme for fundamental (i.e., undecomposeable) knots according to the number of crossings they have. Some examples were mentioned in Section 2.1, but more extensive tables of prime knots are readily available — see, for instance, [22].

Prime knots will be particularly relevant for the remainder of the dissertation. Consequently it is important that our labelling schemes and representations of the Reidemeister moves do indeed distinguish between different prime knots with the same number of crossings, and that this minimal number of crossings cannot be altered for a given prime knot. In Figure 2.29 two prime knots with 5 crossings are shown. Clearly one cannot be deformed into the other — they are topologically distinct objects. It is clear that our labelling scheme captures this feature — the associated bow diagrams are not equal. Furthermore it is easy to verify that none of the Reidemeister moves on bow diagrams (as set out in Section 2.7) can reduce the number of bows (i.e., crossings) for these examples: the minimal number of crossings of prime knots is maintained, as required. For the bow diagrams of Figure 2.29 no crossings can be removed through **R1** or **R2**. Furthermore, no triplet of bows exists

that allows the execution of **R3**; see Figure 2.20 and Figure 2.28

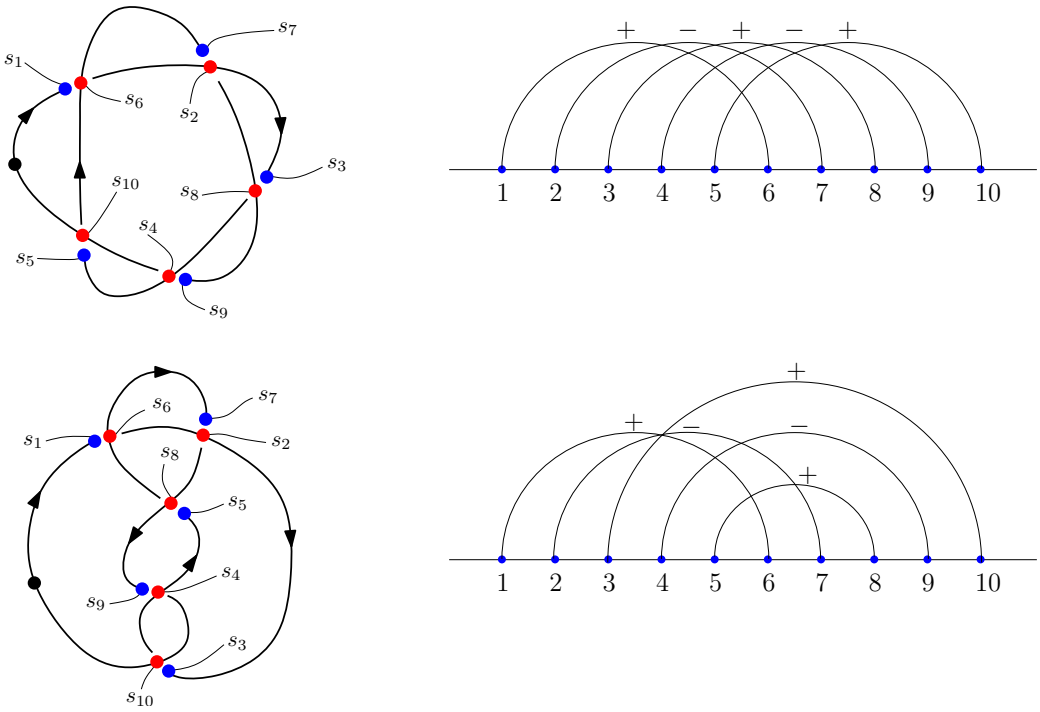

Figure 2.29: The two prime knots 5_1 (top) and 5_2 (bottom) and their associated bow diagrams. These knots both have five crossings, but they are topologically distinct. Distances between bow feet have been rescaled. The corresponding $s - s'$ plots are not shown since they may easily be reconstructed from the bow diagrams.

Indeed, it is an interesting question to ask what is the prime knot underlying some randomly generated knot which is not in its simplest form (i.e., the form with the least number of crossings). In Chapter 6 we shall present some ideas on how the representation of bow diagrams could perhaps be used in the setting of a Monte Carlo type simulation to address such matters.

2.9 Bow diagrams as contact point diagrams

From Figure 2.29 we see clearly that the bow diagram is also a list of the contact points of the knot shadow. If we walk along the base of a bow diagram, we simply find the sequence of numbers of the crossings that are encountered while following the strand of the knot in projection. The bows then simply indicate what two points of the strand are on top of each

other in the projection. Whether we view a given bow diagram as the projection of crossings on an $s - s'$ plot or as a "contact point diagram" simply involves a re-scaling of lengths. The former view point, however, makes the rules for Reidemeister-type manipulations very explicit.

A much-studied problem in polymer physics is the diagrammatic expansion associated with the path integral of a self-avoiding random walk. Self-avoidance is typically encoded through a delta-function interaction that ensures exclusion of two parts of the walk at the same place. It is not surprising, then, that a diagrammatic expansion of this interaction involves diagrams that look very similar to our bow diagrams; see, for instance, [23, 24, 25]. It should be noted, however, that the length-scale parameter in our diagrams is the arc-length of the projected knot, whereas that in the aforementioned references is the actual real-space contour length of the random walk.

(In the setting of critical dense polymers, similar diagrams arise, albeit in the unrelated context of algebraic properties of volume-filling planar walks [26]).

2.10 Summary and outlook

We have demonstrated how the Reidemeister moves may be viewed in terms of rules for dynamics of crossings. Various representations were considered, including the Gauss code, $s - s'$ plots and bow diagrams.

In Chapter 3 we shall now consider all bow diagrams that may be generated for an empty strand that is allowed to undergo **R0** and **R1**. The partition function for a full prime knot with c crossings, subject to these constraints, is approximated. A similar scenario is considered in Chapter 4 for **R2**. The latter is presented in the context of winding a polymer around a rod, since this process involves an **R2** move of the polymer relative to the rod. The remaining chapters then address a dynamical description of the rules from this chapter in terms of an operator formalism and suggestions towards an algorithm for simulated annealing of knots.

CHAPTER 3
REIDEMEISTER MOVES OF THE ZEROTH AND FIRST TYPE

In this chapter we shall consider the scenario where we allow only the zeroth and first Reidemeister moves to take place. Interesting biological systems exist where different topological configurations are related through some sequence of these moves. These motivations will be discussed in the next section. Thereafter we set out a procedure for enumerating all bow diagrams for an empty polymer arc subject to **R0** and **R1**, and use this to approximate the corresponding partition function for a full prime knot with several crossings. Various quantities are investigated in dependence on polymer length and crossing number.

3.1 Motivations from biological systems

Several DNA based systems exhibit a phenomenon known as supercoiling, which may be visualised as follows: if we hold a shoe lace by its end, stretch it and then begin twisting it, torsion builds up in the string. As soon as the tension is released, a supercoil is formed (assuming that sufficient torsion is present) — this is known as the buckling transition. Such supercoils (also known as plectonemes) are a familiar annoyance to any user of garden hoses or telephones with cords. On a more microscopic level, the existence of supercoiled DNA molecules was established by electron microscopy and sedimentation studies as early as 1965 [27]. Theoretical descriptions of this phenomenon have been studied extensively; a brief background follows.

Closed loops of DNA exhibit supercoiled states, consisting of solenoidal or plectonemic superhelices. The conserved quantity of interest during a buckling transition is the linking number, a topological invariant that counts the number of times two curves are wound around each other. Closed supercoil conformations are thus subject to linking number constraints. This topological invariant has been incorporated into statistical mechanical descriptions, see, for instance, [28], where the entropic contributions of supercoils are shown to compete with the energy contributions induced for a given torsion / writhe. This allows for the identification of various coiling regimes. Thermal fluctuations are shown to be of particular importance in this context. In a more sophisticated model [29] formulated in terms of arc length parameters and tangent vectors, the elastic energy and electrostatic

interactions are combined with topological aspects of supercoils to obtain an equation of state. Similar energy vs. entropy models have been constructed for linear DNA molecules [30], and the torque dependence on the extension force has been studied [31].

A point of some contention has been whether such systems are preferentially in single-plectoneme or multi-plectoneme states, and what length of the DNA molecule is found inside supercoils. This question was recently addressed theoretically [32] and experimentally [33]. In the latter reference, the dynamics of DNA supercoils are investigated through temporally resolved experiments using fluorescent marking of a DNA strand attached to a magnetic bead that is twisted. Multi-plectoneme phases are observed, and dynamics are shown to have a slow plectoneme diffusion component and fast plectoneme hopping component. This multi-plectoneme phase for DNA under torsion was discussed extensively in a very recent article [34] where a theoretical models based on worm-like chain is shown to agree with the experimental observations in [33].

Returning to notions of topological equivalence, we note that several supercoiling states may be arrived at through a repeated repetition of the first Reidemeister move. This serves as a motivation for the discussions in the following section, where we consider a very simple and restricted model. The focus there is on generating equivalent configurations under a topological constraint.

3.2 Knots in "minimal projection"

Following the motivations from the previous section, we now restrict ourselves to a strongly simplified system where we only allow the zeroth and first Reidemeister moves to take place in an $s - s'$ plot or bow diagram of a given knot. We recall that the zeroth move entails relative lengthening and shortening of particular loops in the projection, whereas the first move involves creation and annihilation of single loops or twists on an arc-segment in the projection, as set out in Section 2.6. We shall assume that the projection we begin with is that of some prime knot, i.e., it contains the minimum number of crossings (c) obtainable by suitable application of the Reidemeister moves. As stated in Section 2.8, an example of a prime knot is the trefoil knot with three crossings. We shall consider a particular arc-segment between two crossings in this projection, as indicated by the blue arrow in Figure 3.1. Such arc-segments in the projection of a prime knot will henceforth be referred to as *minimal arc-segments*.

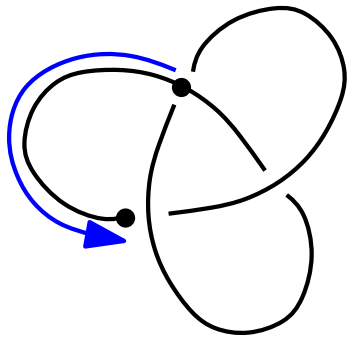

Figure 3.1: The trefoil knot (a prime knot) with $c = 3$. A minimal arc-segment is indicated by the blue arrow.

The $s - s'$ plot of a given minimal arc-segment would as yet still be empty (since there are no crossings). Suppose we dress this single arc-segment by introducing a single loop through **R1**. This would imply the creation of a single sign on each side of the diagonal of the $s - s'$ plot, as set out in Section 2.6.2. Correspondingly the bow diagram of the minimal arc-segment would initially contain no bows, and the creation of a single **R1** loop would create a single bow; see Section 2.7.2. Clearly, in this labelling scheme the addition of more signs (i.e., allowing more loops to form along the minimal strand – we will use these terms interchangeably) through **R1** would result in the addition of more bows. An example is shown in the second illustration in Figure 2.23. Note, however, that the third configuration in Figure 2.23 *cannot* be achieved through **R1**. Indeed, the addition of more loops through the first Reidemeister move can be performed in two ways,

1. stacking bows above each other ("nested insertion of loops"), and

2. adding bows next to each other ("sequential insertion of loops").

The plectonemic states alluded to in the previous sections are examples of states arising from the nested insertion of loops.

For this restricted model it further follows that the bows created on a minimal arc-segment under **R1** cannot cross each other in a general diagram, since we are not allowing **R3** to occur here. Executing **R0** on such a diagram also cannot exchange rows or columns in the $s - s'$ plot , i.e., this move can also not cause bows to cross. Additionally the diagrams are subject to the constraint that there may be at most one sign per row or column, or at most one bow-foot per co-ordinate on the bow diagram. Some examples of diagrams

resulting from various applications of **R1** to the minimal arc-segment are shown in Figure 3.2.

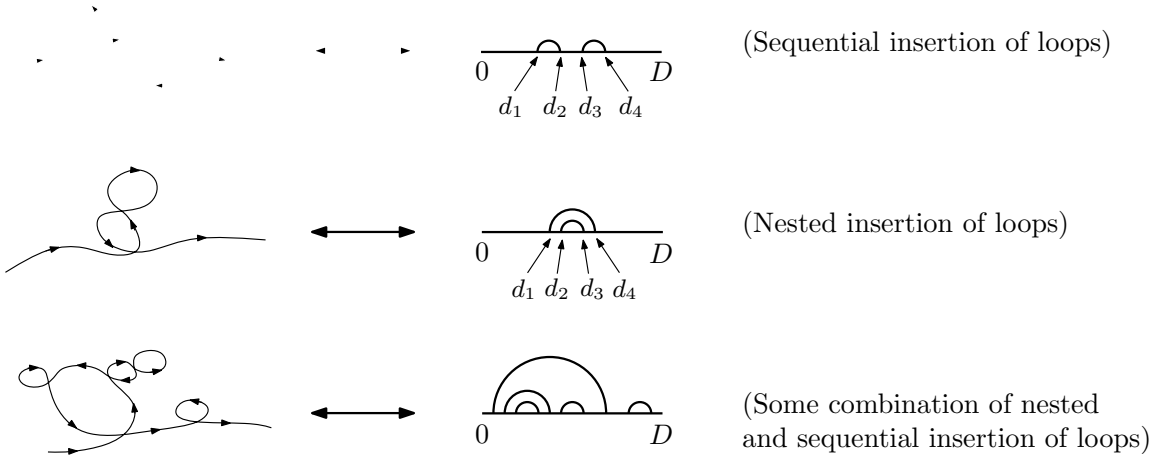

Figure 3.2: Some examples of application of some sequences of **R1** moves in the new diagrammatic representation. The signs of the bows have been omitted.

Our aim is to find the partition function of a minimal arc-segment by finding all possible configurations obtainable through applications of **R0** and **R1**, as illustrated in Figure 3.2. To this end we shall construct a series containing all these diagrams, and then assign a particular Boltzmann weight to each diagram; the summation of these weights then yields the partition function. We draw on notions regarding a similar diagrammatic expansion for the terms contributing to the propagator for the rod-coil transition in polymers as set out in [35], where the summation is written as a recursive diagrammatic expansion. This allows for the construction of a Dyson-like equation for the propagator / partition function. In Figure 3.3 we show this series for our minimal arc-segment (having omitted the signs of each bow), and illustrate the corresponding recursive form thereof.

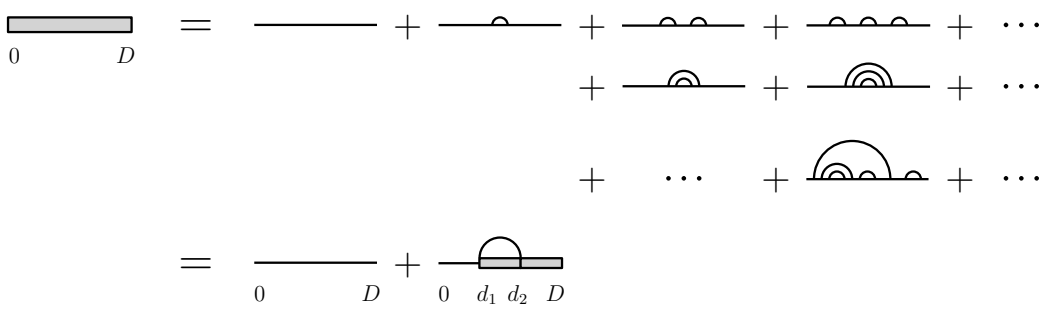

Figure 3.3: A diagrammatic series of all possible diagrams obtainable by the application of **R1** to a minimal arc-segment. Through **R0** the position of the bow-feet may be changed, but bows cannot cross each other. The solid bar represents the entire summation and the final step shows the recursive form of the expansion. Again, signs of bows have been omitted here.

The proof that the series may be written recursively as in the last step of this figure is simple, and is outlined in Appendix A.2. Note that the solid line symbol

represents the sum of all possible diagrams. As yet we have neglected that there are indeed two species of bows, namely + and −. This simply introduces a factor of two in the diagrammatic expansion above, as shown in Figure 3.4.

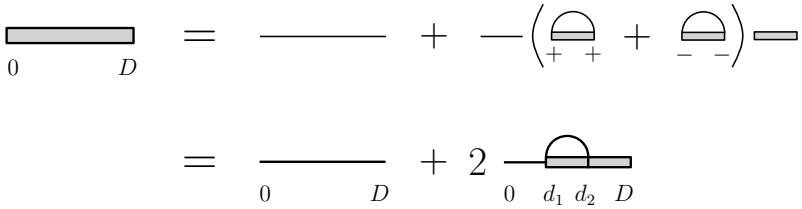

Figure 3.4: Diagrammatic series where we allow two species, + and −.

In the last step in Figure 3.4 the equality holds on the level of statistical weighting. To explain that statement, we shall now discuss how to translate the recursive diagrammatic expansion above into an integral equation for the partition function.

3.3 Partition function of a minimal arc-segment subject to R0 and R1

In order to write down a partition function, it is necessary to attach a particular statistical weight to each possible diagram in the series in terms of Boltzmann weights. The sum of these weights is the partition function of the minimal strand subject to **R0** and **R1**. It would be reasonable to assume that the Boltzmann weight B associated with any arc-segment, is a function of the length of the segment. The bows on bow diagrams (see, for instance Figure 3.2) act as partitions of the arc-segment of length D. Since the crossings may "diffuse" around the corresponding $s - s'$ plots under **R0** until they encounter other crossings. On the bow diagram this translates to changes in the relative spacing of bow-feet (see Section 2.7.1). If we now partition the arc-segment according to positions of the bow feet, we will need to integrate over the partition co-ordinates d_i of the bow feet when we write down the partition function for the minimal strand as a function of D. Note that we assume these co-ordinates to be continuous here, departing from the discrete notation of earlier sections. For a single loop (see the first illustration in Figure 2.23) we obtain

$$Z_{\text{single}}(D) = \int_{d_1} \int_{d_2} B(d_1 - 0)\, B(d_2 - d_1)\, B(D - d_2), \quad \text{with } 0 \leq d_1 \leq d_2 \leq D. \tag{3.1}$$

What happens when we add more loops (crossings)? We turn to the first diagram in Figure 3.2. Introducing a second loop *sequentially* into the minimal strand (i.e., of a second bow into the diagram) further partitions the line of the bow diagram. The corresponding partition function for this diagram (with two sequential loops) would be

$$Z_{\text{seq.}}(D) = \int_{d_1} \int_{d_2} \int_{d_3} \int_{d_4} B(d_1 - 0)\, B(d_2 - d_1)\, B(d_3 - d_2)\, B(d_4 - d_3) B(D - d_4), \tag{3.2}$$

where we have the constraint $0 \leq d_1 \leq d_2 \leq d_3 \leq d_4 \leq D$. It is clear from the second diagram in Figure 3.2 that adding loops in a *nested* manner also introduces more partitions, but it does so in a different order. The partition function for this diagram (with two nested loops) is

$$Z_{\text{nest.}}(D) = \int_{d_1} \int_{d_2} \int_{d_3} \int_{d_4} B(d_1 - 0)\, B(d_4 - d_1)\, B(d_3 - d_2)\, B(D - d_4), \tag{3.3}$$

again with $0 \leq d_1 \leq d_2 \leq d_3 \leq d_4 \leq D$. Equation (3.2) would be greatly simplified by a transformation to co-ordinates $\Delta_i = d_i - d_{i-1}$, whereas this is not the case for equation (3.3).

Consequently we will proceed with the approximation that the first two diagrams in Figure 3.2 carry the same statistical weight, i.e., that equation (3.2) also describes the partition function for the second diagram in this figure. The implication of this assumption is that we don't distinguish between open and closed polymer loops in the projection, thereby essentially neglecting some local correlations of actual polymer strand. Instead of viewing the two nested loops as one primary loop (described by A and C in Figure 3.5 below) upon which we create a secondary, nested loop (described by B in Figure 3.5), we view the loops in three separate segments (A, B and C in Figure 3.5).

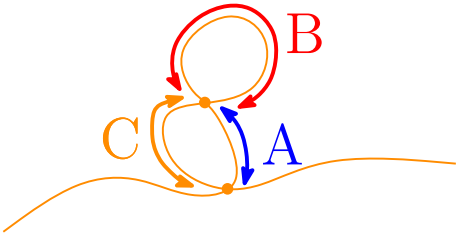

Figure 3.5: Contributions of nested insertion of loops.

Under this assumption, the recursive diagrammatic expansion from Figure 3.4 translates into a Dyson-like integral equation,

$$Z(D) = B(D) + 2\int_{d_1}\int_{d_2} B(d_1 - 0)\, Z(d_2 - d_1)\, Z(D - d_2), \quad \text{with } 0 \leq d_1 \leq d_2 \leq D. \tag{3.4}$$

At this point it should be noted that we have neglected the continuity of the tangent vectors to the polymer strand. Such details could be included into a discussion entailing semi-flexible polymer models in this setting. We re-iterate here the simplifications of this model. Indeed, the actual real-space position dependence is neglected in the choice of Boltzmann weight (we only include arc-dependence), as are torsional effects. The focus of this section was on enumerating topologically equivalent configurations in a diagrammatic expansion. We shall now turn to solution techniques for the partition function of a single minimal arc under the aforementioned simplifying assumptions. The construction of the partition function for the full knot is addressed in Section 3.5.

3.4 Laplace transformation for solving the integral equation for a single minimal arc-segment

If we denote $d_0 = 0$ and $d_3 = D$, the integral on the right of equation (3.4) can be transformed to relative co-ordinates

$$\Delta_i = d_i - d_{i-1}, \quad i \in \{1, 2, 3\}, \tag{3.5}$$

under the constraint $\sum_{i=1}^{3} \Delta_i = D$. In doing so we obtain

$$Z(D) = B(D) + 2 \int_0^\infty d\Delta_1 \int_0^\infty d\Delta_2 \int_0^\infty d\Delta_3 \;\; B(\Delta_1) Z(\Delta_2) Z(\Delta_3) \;\; \delta\left(\sum_{i=1}^{3} \Delta_i - D \right). \tag{3.6}$$

We denote the Laplace transformation of any function $f(D)$ as

$$\tilde{f}(t) = \int dD \;\; e^{-tD} f(D). \tag{3.7}$$

It becomes clear immediately that this transformation diagonalises the integrals on the right of equation (3.6). The result is an algebraic equation for the Laplace transformation $\tilde{Z}(t)$ of the partition function $Z(D)$,

$$\tilde{Z}(t) = \tilde{B}(t) + 2\, \tilde{B}(t)\, \tilde{Z}^2(t). \tag{3.8}$$

Here $\tilde{B}(t)$ is the Laplace transform of the Boltzmann weight $B(D)$. Naturally equation (3.8) would have two solutions. However, since $Z(D)$ and $B(D)$ are positive functions, their Laplace transformations should be monotonically decreasing. This precludes one solution, and we obtain

$$\tilde{Z}(t) = \frac{1 - \sqrt{1 - 8\tilde{B}^2(t)}}{4\tilde{B}(t)}. \tag{3.9}$$

Furthermore, we note that

$$|\tilde{B}(t)| \leq \sqrt{\frac{1}{8}} \tag{3.10}$$

is required for the reality of the $\tilde{Z}$. For a particular choice of Boltzmann weight this may impose restrictions on certain ranges of the Laplace parameter t. In later sections we shall consider an example where $\tilde{B}(t)$ is a monotonically decreasing function. In this case

equation (3.10) implies the necessity for a critical (minimal) Laplace parameter t_c, so that

$$t \in (t_c, \infty), \quad t_c > 0. \tag{3.11}$$

This may be viewed from a physical perspective: since t is essentially a "chemical potential" that determines the energy contributions of increasing the length of the minimal arc-segment, t_c is essentially a critical (minimal) chemical potential. These notions are clarified in later sections where a particular choice for the Boltzmann weight $B(D)$ is made.

3.5 From a minimal arc-segment to the full prime knot: the complete partition function

Thus far we have only considered one minimal arc-segment and its various "embellishments" through addition of loops. In order to find the partition function of the full prime knot (which has c crossings), we note that every crossing connects exactly two minimal arc-segments. Since the knot diagram is a closed diagram, there are $2c$ minimal arc-segments. (As stated, knot diagrams are regular graphs with functionality four. The latter statement follows trivially from this.) This implies that, since the integral equation for the minimal arc-segment factorises algebraically (see equation 3.8), the Laplace transformation of the partition function of the full prime knot is simply

$$\tilde{Z}_c = \left[\tilde{Z}(t)\right]^{2c}. \tag{3.12}$$

It should be noted, that (3.12) implies that any two prime knots with equal numbers of crossings (e.g., the knots 5_1 and 5_2 from Figure 2.29) would have the same partition function in this scheme. The procedure of dealing with minimal arc-segments as set out here thus does not distinguish between topologically distinct prime knots with equal c. Although the crossing number is a weak invariant in this sense, such an approach is not unusual; see, for instance, [36] where similar arguments are employed when considering the static and dynamic effects of knots in polymers.

3.6 The Laplace transformation as a generating function for expectation values

Let us rewrite the Laplace parameter in equation (3.11) so that

$$t = t_c + t', \quad \text{where } t' \in (0, \infty). \tag{3.13}$$

For a single minimal arc-segment, we may now find the average of D through differentiation,

$$\langle D \rangle(t) = -\frac{\partial}{\partial t_c} \ln(\tilde{Z}(t_c, t')). \tag{3.14}$$

Naturally this quantity will change for a knot with c minimal crossings, whose Laplace transformed partition function is given by equation (3.12). Indeed, it is clear that for such a knot the quantity above is simply multiplied by $2c$, as is expected: since $2c$ minimal arc-segments are being considered we anticipate that the average length of the whole knot grows proportionally. The fluctuations of D (as a function of the Laplace parameter) can also be calculated according to

$$\langle (\delta D)^2 \rangle(t) = \frac{\partial^2}{\partial t_c^2} \ln(\tilde{Z}(t_c, t')). \tag{3.15}$$

It would also be interesting to ask what the average number of crossings $\langle N \rangle$ would be for a minimal arc-segment, given a particular choice of Boltzmann weight. To this end we include a source term to count the number of crossings in each term of the diagrammatic expansion (recall Figure 3.4) by assigning a factor of e^{nb} to a diagram with n bows. Differentiating with respect to b and subsequently setting $b = 0$ allows us to count the number of crossings for the diagram since each bow represents a crossing. Extending this to the algebraic equation (3.8) yields

$$\tilde{Z}(t) = e^0 \tilde{B}(t) + 2\, e^b \tilde{B}(t)\, \tilde{Z}^2(t), \tag{3.16}$$

thereby allowing us to solve

$$\tilde{Z}^{(b)}(t) = \frac{1 - \sqrt{1 - 8e^b \tilde{B}^2(t)}}{4e^b \tilde{B}(t)}. \tag{3.17}$$

After relabeling t according to equation (3.13), we may now calculate the average number of crossings as

$$\langle N\rangle(t) = \left[\frac{\partial}{\partial b}\ln(\tilde{Z}^{(b)}(t_c,t'))\right]_{b=0}. \tag{3.18}$$

It is clear from equation (3.12) that this quantity would also scale linearly by a factor of $2c$ for a knot with c crossings, as expected.

3.7 Specific model: a particular choice of Boltzmann weight

Thus far the only assumption made regarding the Boltzmann weights is that they are functions of the distance between crossings. We note that the bending energy of a polymer strand that is described by a position vector $\vec{r}(s)$ (with $s \in [0, L]$) is defined as

$$E_{\text{bend}} = \frac{k}{2}\int_0^L ds\ \left(\frac{\partial^2\vec{r}(s)}{\partial s^2}\right)^2, \tag{3.19}$$

where k is some stiffness constant for the polymer. For a circular polymer in the xy-plane with circumference $L = 2\pi R$, for instance, the position vector would be

$$\vec{r}(s) = \frac{L}{2\pi}\left[\cos(\frac{2\pi s}{L})\hat{i} + \sin(\frac{2\pi s}{L})\hat{j}\right], \tag{3.20}$$

and the corresponding bending energy would simply be

$$E_{\odot} = 2\pi^2 k(\frac{1}{L}) \sim \frac{1}{L}. \tag{3.21}$$

Suppose we consider instead a circular spiral (with a single turn) whose total arc-length is $\tilde{L}$, and that is lying along the z-axis. Viewed in projection along the z-axis the spiral looks like a circle with a circumference $L = 2\pi R$, say. (Here R is the radius of the spiral / circle, and $L \leq \tilde{L}$.) The position vector describing such a spiral is

$$\vec{r}(s) = \frac{L}{2\pi}\left[\cos(\frac{2\pi s}{\tilde{L}})\hat{i} + \sin(\frac{2\pi s}{\tilde{L}})\hat{j}\right] + \frac{\alpha}{\tilde{L}}s\hat{k}, \quad \text{with } s \in [0, \tilde{L}]. \tag{3.22}$$

Here α is simply the length of the spiral along the z axis. It is easy to verify that the corresponding bending energy is

$$E_{\text{spiral}} = 2\pi^2 k\left(\frac{L^2}{\tilde{L}^3}\right) \sim \frac{1}{L} \tag{3.23}$$

since $\tilde{L} \propto L$. We conclude that both a spiral and its two dimensional projection (a circle) have bending energies that scale according to

$$E \sim \frac{1}{L}. \tag{3.24}$$

(Naturally equality between the two energies is reached if $\alpha = 0$, i.e., $\tilde{L} = L$, i.e., the length of the spiral along the projected dimension is zero). We use this to motivate a choice for the Boltzmann weight in equations (3.4) and (3.6) that captures this scaling behaviour, namely

$$B(D) = e^{-k/D}, \tag{3.25}$$

where k is the stiffness constant[1]. It is clear that k simply sets a fundamental length-scale for the system, and may thus be absorbed without loss of generality by setting $k = 1$ (this amounts to making a particular choice for the stiffness of the strands involved). The Laplace transformation of the Boltzmann weight (3.25) with $k = 1$ is

$$\tilde{B}(t) = \frac{2}{\sqrt{t}} K_1(2\sqrt{t}), \tag{3.26}$$

where $K_n(x)$ are modified Bessel functions of the second kind. We find the solution for the Laplace transformation of the partition function from (3.9), namely

$$\tilde{Z}(t) = \frac{\sqrt{t} - \sqrt{t - 32K_1(2\sqrt{t})^2}}{8K_1(2\sqrt{t})}. \tag{3.27}$$

Equation (3.10) implies the requirement

$$2\sqrt{t}\, K_1(2\sqrt{t}) \leq \sqrt{\frac{1}{8}}. \tag{3.28}$$

Numerically we obtain an allowed range for the Laplace parameter,

$$t \geq t_c \approx 0.876952. \tag{3.29}$$

[1] We identify the typical form of the Boltzmann weight $e^{-\beta E}$ (here $\beta = \frac{1}{k_B T}$) for a configuration with energy E with $e^{-k/D}$. The stiffness k thus plays the usual role analogous to that of inverse temperature.

Since the Laplace parameter has the dimension of inverse length, the existence of the minimal cutoff t_c may be viewed as a minimal chemical potential through which larger loops in the strand are penalised energetically. (The association of a type of "inverse length" to the Laplace parameter is natural, since the Laplace transform weights large values of D more at small t, and vice versa. Of course this is not a direct inverse proportionality.) We proceed by transforming the Laplace parameter as in equation (3.13), with t_c as above. According to equation (3.14), we find

$$\begin{aligned} \langle D \rangle(t) &= -\frac{\partial}{\partial t_c} \ln(\tilde{Z}(t_c, t')) \\ &= \frac{K_2(2\sqrt{t_c + t'})}{K_1(2\sqrt{t_c + t'})\sqrt{t_c + t' - 32K_1(2\sqrt{t_c + t'})^2}}. \end{aligned} \tag{3.30}$$

A plot of this result is shown in Figure 3.6. This plot supports the notion that the Laplace parameter may be viewed as a chemical potential: for large t' small polymer lengths carry a larger weight in the partition function.

Figure 3.6: Average length of minimal arc-segment as function of Laplace parameter.

We may further calculate the fluctuations in D according to equation (3.15). This quantity is plotted below.

Figure 3.7: Fluctuations in length of minimal arc-segment as function of Laplace parameter.

For large values of the Laplace parameter, Figure 3.6 could thus be used as a type of "lookup table" to express functions in terms of D rather than t, since the fluctuations decay rapidly.

To aid us with the interpretation of the plots above, we proceed by calculating the average number of crossings for a minimal arc-segment according to equation (3.18),

$$\langle N\rangle(t) = \frac{t_c + t' - 16K_1\left(2\sqrt{t_c+t'}\right)^2 - \sqrt{t_c+t'}\sqrt{t_c+t'-32K_1\left(2\sqrt{t_c+t'}\right)^2}}{8K_1\left(2\sqrt{t_c+t'}\right)\sqrt{t_c+t'-32K_1\left(2\sqrt{t_c+t'}\right)^2}}. \tag{3.31}$$

This result may also be plotted, yielding

Figure 3.8: Average number of crossing on minimal arc-segment as function of Laplace parameter.

This plot also makes sense in the context of viewing the Laplace parameter as a chemical potential. As we see from Figure 3.6, longer minimal arc lengths are more likely at smaller values of t'. It is to be expected, then, that the number of crossings should grow as the average minimal arc length grows. To make this more explicit, we make a parametric plot of $\langle N \rangle$ against $\langle D \rangle$ in Figure 3.9. We observe that for large values of $\langle D \rangle$ there seems to be a linear relation to $\langle N \rangle$. The interpretation is clear: the longer the minimal arc-segment becomes, the more "space" there is for crossings on the strand, and one would expect this type of proportionality. The initial slow growth of $\langle N \rangle$ is indicative of the fact that crossings are strongly suppressed for short lengths due to the choice of Boltzmann weight.

In principle it would be useful to invert the Laplace transformation of the partition function $\tilde{Z}(t_c, t')$ in order to find an analytical form for $Z(D)$. Since it is not possible to perform this inversion analytically in this case, we turn our attention once more to the Laplace transform. In Appendix A.1, we argue that simple assumption

$$\tilde{Z}(t_c, t') \sim e^{-\sqrt{at'+b}}, \tag{3.32}$$

with fitting parameters a and b, is a good approximation to the actual Laplace transform

Figure 3.9: Parametric plot of average number of crossing vs. average minimal arc length.

$\tilde{Z}(t_c, t')$. The inverse Laplace transformation of this "guess" function gives

$$Z(D) \sim \frac{e^{Dt_c - \frac{1}{4D}}}{2\sqrt{\pi} D^{3/2}}. \tag{3.33}$$

Identifying the free energy F of the system with the negative logarithm of $Z(D)$, one finds in this approximation that

$$F \sim -Dt_c + \frac{1}{4D} + \frac{3\log(D)}{2}. \tag{3.34}$$

For large D the leading term in this expression linear in D, i.e., the free energy is extensive, as expected. Furthermore we are able to minimise the free energy and for t_c,

$$t_c \sim \frac{3}{2D} - \frac{1}{4D^2}. \tag{3.35}$$

For large D it is clear that t_c is inversely proportional to the length of the strand, as one may anticipate.

3.8 Summary and outlook

In this chapter we considered a restricted system subject to only the zeroth and first Reidemeister moves. A diagrammatic expansion was derived to enumerate all topologically equivalent configurations for a strand subject to these constraints. An approximate partition function was then derived under simplifying assumptions using a Laplace transformation, and physical quantities were calculated for a particular simple choice of Boltzmann weight. For this choice, an approximation to the inverse Laplace transformation was also suggested.

From Figures 3.2 and 3.3 we also see that plectoneme-like configurations form a subseries of our complete diagrammatic expansion. These configurations would have further constraints involving the sequence of signs introduced through **R1**. For instance, a stack of bows corresponding to a single plectoneme would consist of alternating + and − signs; this would constitute a simple modification of the expansion. For a complete description of such configurations one could further incorporate torsion and tension as aspects of a more detailed partition function.

In the next chapter we turn to the second Reidemeister move, and present a similar (albeit much more extensive) enumeration scheme for equivalent configurations. This is presented in the setting of a polymer that is wound around a rod.

CHAPTER 4
REIDEMEISTER MOVES OF THE SECOND TYPE

The work in this chapter is inspired by a classical problem: the statistical physical properties of a closed polymer loop that is wound around a rod. Historically the preserved topology of this system has been addressed through identification of similarities with magnetic systems. We present a brief overview of such strategies, as usually addressed in setting of constrained path integrals.

Here we depart slightly from the explicit representations of knots addressed in earlier chapters, and focus on the applicability of the second Reidemeister move to this physical problem. In our approach the topological invariance is treated in terms of a set of rules that describe all augmentations by additional arcs of some fundamental basic loop of a given winding number. These augmentations satisfy the **R2** move, relevant for the polymer with respect to the rod. We shall construct the topologically constrained partition function using the combinatorics of allowed arc additions and their appropriate statistical weights. We illustrate how, for winding number 1, we can formally derive expressions for lower and upper bounds on the partition function. Using the lower bound approximation we investigate a flexible polymer loop wound between two slits, calculating the force on the slit as well as the average numbers of arc types in dependence of slit width and separation.

The results here may be extended to higher winding numbers. Further, the intuitive nature of this combinatoric scheme allows the development of a variety of approximations and generalisations.

The work in this chapter was recently published in *Journal of Physics A: Mathematical and Theoretical* [17].

4.1 Introduction

As has been argued, entanglements occur naturally in polymer systems, and are related to topological constraints. Indeed, the fact that different polymer strands cannot pass through each other is manifest in two observations: a) there exists an excluded volume interaction in real polymers that leads to self-avoidance, and b) for closed loops topological states must be conserved. We will focus on the latter statement, and concern ourselves with

the associated configurational constraints. Such constraints determine which configurations of the polymer system are topologically equivalent to each other, and thus restrict the polymer configurations over which we must sum to calculate the partition function for a given topological state. Mathematically the notion of topological equivalence may be captured (at least partially) by topological invariants. The role of topological constraints in polymers remains an important issue in various systems (see reviews by Kholodenko and Vilgis[14], and, more recently, [37, 38, 39]). Entanglement of synthetic or biological macromolecule loops continues to be treated in analytical and computational modelling (for example, in [40, 41, 42]) and is deemed to be particularly relevant for localisation of DNA in cells [43]. Although computer simulations have driven results strongly, there is still a need in expanding the range of analytical tools to deal with entangled chains.

As early as 1961, Frisch and Wasserman [44] considered topological isomerism in chemical systems, investigating knotted and unknotted links, loops and rings that occur in certain chemical molecules. Soon thereafter (1967), Edwards [15] explicitly pointed out the importance of topological constraints to polymer systems, and that such constraints need to be included into the statistical mechanics of polymers. In that article, the specific example of a polymer wound around a rod is considered, and the winding number is identified as a suitable topological invariant that categorises topologically distinct configurations. The winding number simply represents the number of times the polymer winds around the rod before closing on itself. Viewing this problem in a projection along the rod, one may capture the planar winding number (angle) of the polymer around a fixed point (i.e., the projection of the rod) through the integral

$$\oint \frac{x\dot{y} - y\dot{x}}{x^2 + y^2}\, ds, \tag{4.1}$$

where s is the arc-length parameter of the strand, and $\dot{x} \equiv \frac{\partial x}{\partial s}$ etc. Naturally this winding number cannot be altered once the polymer loop has been wound around the rod and closed. In [15] this constraint is included into the path integral partition function (probability distribution) of the polymer inside a delta function that is exponentiated through the introduction of auxiliary fields. The resulting action is related to that of a magnetic system, and is treated under certain approximations. In the same year as Edwards, the same physical system was investigated by Prager and Frisch [45]. This problem can also be addressed through the introduction of a tailored potential that approximates an interaction

at short distances with the rod, and is included in the path integral through an additional Boltzmann factor [46]. We shall, however, focus on topological invariance as the basis of our approach.

A further simple invariant is the linking number, which tells us how many times two distinct loops a and b are wound around each other. The linking number is given by the Gauss integral

$$\oint_a \oint_b \left(\dot{\vec{r}}_a(s_a) \times \dot{\vec{r}}_b(s_b)\right) \cdot \frac{\vec{r}_a - \vec{r}_b}{|\vec{r}_a - \vec{r}_b|^3}\, ds_a\, ds_b, \tag{4.2}$$

where the position vectors $\vec{r}$ and their derivatives $\dot{\vec{r}}$ are parametrised by the arc-lengths s_a and s_b. This invariant may also be included as a constraint in the polymer path integral (see, for instance, [14, 15, 47, 48, 49]).

Winding and linking numbers (and other basic invariants) do not capture all topological constraints in polymer systems. More complex higher order invariants (which may represent more detailed topological information) exist and may, in principle, also be included as constraints in path integrals. Indeed, the field theories that thus arise from topologically constrained polymer systems have been studied extensively [14, 47, 48, 49]. There is also a deep connection between polynomial knot invariants and quantum field theories. The reader is referred to the seminal work by Witten [50] where Jones polynomials are investigated in the setting of Yang-Mills theory. This work opened the door to subsequent extensions such as perturbative approaches – see, for instance, [51].

Typically, however, simple invariants such as winding numbers and linking numbers have been considered in the context of polymer path integrals since more complex invariants become mathematically tedious to handle. The conservation of these topological invariants has been shown to relate to symmetry transformations that ultimately manifest in local gauge invariance in such field theories [47, 48].

In this chapter we shall address the often studied problem of a polymer wound around an infinitely long obstacle in a plane. In doing so, we shall not consider any self-entanglements of the loop, but simply concern ourselves with the topology of the loop *relative to the rod*. Consequently the mathematical intricacies of higher order invariants will not be of bearing here: we need look no further than winding numbers to address this physical system. Perhaps it is (in part) for this reason that the "polymer wound around a rod" has been studied so extensively. More recently (in 2003) Grosberg and Frisch [52] presented

various modifications and extensions of Edwards' original results, both in the quenched (constrained partition sum) and the annealed (probability distributions of winding angles) settings. These include confining the polymer-and-rod system to a cavity, and winding the polymer around a disc. Our aim in this chapter is similar that of [15] and [45]: we wish to find the partition function of a polymer wound around an obstacle. Our partition function, obtained through a different calculational approach, is then used to study physical quantities for various geometries.

We employ a strategy that differs significantly from the path integral schemes cited above, namely to evaluate invariant knots by a combinatoric scheme. This may be done in terms of enumerations of braids, as shown by Nechaev and co-workers [53, 54]. We also develop a combinatoric scheme, and use this for enumerating configurations subject to a winding number constraint in particular. We then couple the combinatorics to polymer degrees of freedom. This is presented in two parts. Firstly we outline how configurations may be labelled according to piercings that the strand makes through a plane—similar to braids. Then, as in [53, 54], one needs to generate all appropriate unique but topologically equivalent configurations. We construct the partition function as sums of products of polymer arc probability distributions. This enables us to find upper and lower bounds for the free energy. In principle, this formalism allows for the description of various types of polymer chains, e.g., Gaussian or semi-flexible. Since we do not calculate the probability of winding numbers, but enforce the winding number constraint on the partition function, we are considering the quenched setting. Secondly, we illustrate the calculation of the partition function and related averages for various winding scenarios, e.g., winding between two slits. We are able to calculate forces and ratios of arc types for confining geometries. To this end we consider Gaussian chains and their associated probability distributions, and calculate statistical quantities of interest.

4.2 Winding a polymer around a rod

The basis of our problem is a topological obstacle around which a polymer strand is wound. We start by presenting some simple examples of loops wound around a rod and then illustrate different configurational modifications / augmentations that do not alter the topology of these basic loops. Such procedures are essentially braid manipulations on two strands which may be represented in terms of braid groups — see, for instance [12, 55]. Since

we immediately couple the configurations of this quenched scenario to polymer degrees of freedom, however, the braid group relations alone are not sufficient for our enumeration procedure. This is discussed in detail in B.1, in reference to [53, 54].

4.2.1 Example of the basic loop, winding number $w = 1$

Consider an infinitely long rod that is placed along the y axis of a system of axes in $\mathbb{R}^3$. Suppose now that an open polymer strand is wound around this rod and then closed on itself to form a closed loop. The first natural question to ask is *how often* the polymer is wound around the rod. Indeed, this number distinguishes topologically distinct configurations of the polymer, and is appropriately known as the winding number, w. For the remainder of the chapter, the scenario in Figure 4.1 with the minimal number of arcs will be referred to as the *basic loop*. If we take this configuration with $w = 1$ (the simplest case where strand is wrapped around the rod only once) we cannot deform or alter this configuration to obtain one where $w \neq 1$ without physically breaking the polymer strand. In this sense the winding number is a topological invariant of the particular configuration created when closing the open strand after w windings.

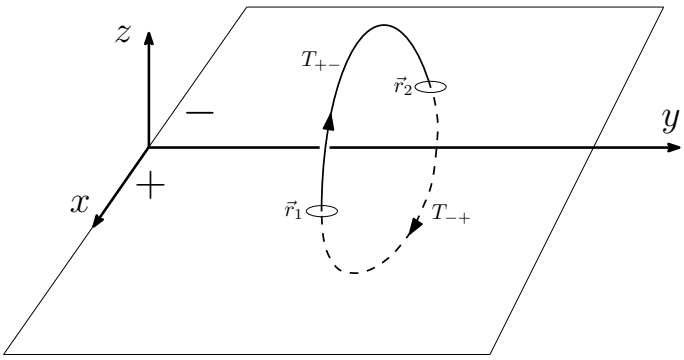

Figure 4.1: Closed polymer loop, $w = 1$.

Let us divide the complete polymer loop into sub-arcs, the division occurring whenever the xy-plane is pierced by the polymer. For the example in Figure 4.1 the entire polymer loop may be viewed as consisting of a "sequence" of two polymer arcs, each constrained by the xy-plane to a half-space w.r.t. the positive / negative z axis. In this figure we have labelled each of these arc-segments with a T whose subscript is $+-$ if the arc begins in the $x > 0$ half-plane $\{(x, y) : x > 0, y \in \mathbb{R}\}$ and ends in the $x < 0$ half-plane $\{(x, y) :$

$x < 0$, $y \in \mathbb{R}\}$. The subscript $-+$ applies to the opposite case. The Ts themselves will later represent the probability distributions for the half-space restricted sub-arcs. They are functions of the (planar) beginning and end co-ordinates of the respective polymer segments and of the arc-lengths of the segments. For now we will simply use this notation to represent sequences of such sub-arcs, and demonstrate how we may capture the topology of any polymer loop as a composition / sequence of such Ts. In this spirit, we represent the simple closed loop of Figure 4.1 symbolically by the sequence $T_{+-}T_{-+}$ (or alternatively by the cyclic permutation $T_{-+}T_{+-}$). Essentially the sequence of subscripts indicates how one would follow the polymer strand around the rod from one piercing of the plane to another. An orientation convention (indicated by the arrows in Figure 4.1) is chosen without loss of generality. The partition function corresponding to Figure 4.1 in less compact notation would be

$$Z = \int_{\mathcal{D}} T_{+-}(\vec{r}_1, \vec{r}_2)\, T_{-+}(\vec{r}_2, \vec{r}_1) = \int_{\mathcal{D}} T_{-+}(\vec{r}_2, \vec{r}_1)\, T_{+-}(\vec{r}_1, \vec{r}_2), \tag{4.3}$$

where the position vectors label the piercings of the xy-plane and integration is over the relevant domain

$$\mathcal{D} = \{x_1 \in (0, \infty);\ x_2 \in (0, -\infty);\ y_1, y_2 \in (-\infty, \infty)\}. \tag{4.4}$$

Each $T(\vec{r}_i, \vec{r}_j)$ represents the statistical weight of a polymer arc restricted to half-space with appropriate initial and final positions in the plane. T depends on the nature of the specific polymer. In principle the methods shown here can be applied to Gaussian as well as semiflexible polymers, etc. The symbolic sequence $T_{+-}T_{-+}$ thus represents the integrand of the partition function for the basic loop. This notion will be clarified in Section 4.3. We shall now extend this picture (and the symbolic notation) to higher winding numbers.

4.2.2 Higher winding numbers: $w > 1$

Figure 4.2 shows a polymer strand with winding number $w = 2$.

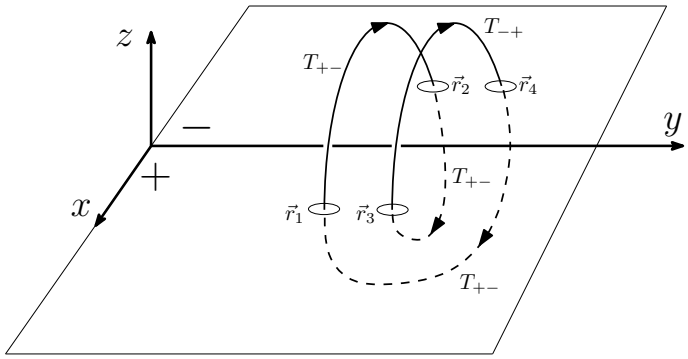

Figure 4.2: Closed polymer loop, $w = 2$.

Again the complete polymer strand may be decomposed into a sequence of confined sub-arcs, each living in either the $z > 0$ or the $z < 0$ half-space. Following the notation above, the case $w = 2$ can thus be described symbolically by the sequence $T_{+-}T_{-+}T_{+-}T_{-+}$ (or any cyclic permutation thereof, depending on the choice of reference point for labeling). The partition function for Figure 4.2 would be

$$\begin{aligned} Z &= \int_{\mathcal{D}} T_{+-}(\vec{r}_1,\vec{r}_2)\, T_{-+}(\vec{r}_2,\vec{r}_3)\, T_{+-}(\vec{r}_3,\vec{r}_4)\, T_{-+}(\vec{r}_4,\vec{r}_1) \\ &= \int_{\mathcal{D}} T_{-+}(\vec{r}_2,\vec{r}_3)\, T_{+-}(\vec{r}_3,\vec{r}_4)\, T_{-+}(\vec{r}_4,\vec{r}_1)\, T_{+-}(\vec{r}_1,\vec{r}_2) \quad \text{etc.} \end{aligned} \tag{4.5}$$

Clearly Z is invariant under cyclic permutation of the factors in the integrand in equation (4.5). Consequently one could just as well label Figure 4.2 with any cyclic permutation of $T_{+-}T_{-+}T_{+-}T_{-+}$. The order of the Ts does, however, matter, since the arguments of consecutive Ts (i.e., $\vec{r}_i$, $\vec{r}_{i+1}$ etc.) must match up. This may be viewed in analogy to operator multiplication.

The strategy in Section 4.3 will be to "diagonalise" the integral above, so that we may write symbolically $T_{+-}T_{-+}T_{+-}T_{-+} = (T_{+-}T_{-+})^2$. Analogously loops wound w times are expressed as $(T_{+-}T_{-+})^w$ in this compact notation.

The examples considered thus far only show limited configurations associated with specific winding numbers, since they are composed of sub-arcs that cross from one side of the rod to the other. Other permissible configurations (that maintain the winding number) can include sub-arcs that remain on one side of the rod. In the next section we illustrate how simple loops such as those in Figures 4.1 and 4.2 may be augmented in this way.

Some combinatoric rules will be established on the symbolic level of sequences of Ts. The connection of these combinatoric sequences to a complete partition function will be made in Section 4.3. We shall now focus on the case of $w = 1$, since the partition functions for higher winding numbers are generated from powers of the basic loop.

4.2.3 Augmenting the basic loop: insertion of sub-arcs

Let us return to the basic loop from Figure 4.1 with $w = 1$. We note that it is possible to augment or "decorate" this simple loop with more half-space constrained sub-arc segments. This process is subject to a Reidemeister move of the second type (see Figure 4.3) of the polymer strand relative to the rod, viewed in a side-on projection along the x axis.

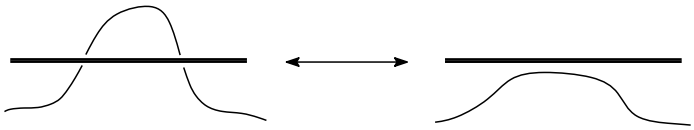

Figure 4.3: Type two Reidemeister move of the polymer (thin) relative to the rod (thick).

Since the Reidemeister moves do not alter a particular topological state for closed strands [16], this augmentation does not alter the winding number but simply introduces more piercings of the xy-plane. Clearly the number of Ts equals the number of piercings for a particular configuration. Introducing additional piercings / arc-segments may be done in two ways:

1. We may insert two more sub-arcs, each beginning and ending in the half-plane $\{(x, y) : x > 0,\ y \in \mathbb{R}\}$, one living in half-space $z < 0$ and the other in $z > 0$:

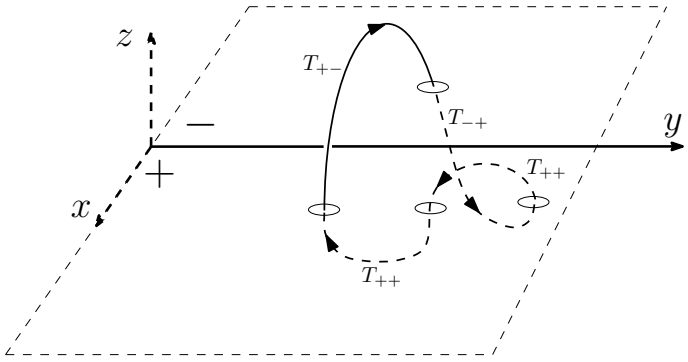

Figure 4.4: Closed polymer loop, $w = 1$, additional constrained arc-segments.

We describe the sequence of arcs in Figure 4.4 with the symbolic sequence $T_{+-}T_{-+}T_{++}T_{++}$ (or any cyclic permutation). Here the subscript $++$ indicates a sub-arc beginning and ending in the half-plane $\{(x, y) : x > 0, y \in \mathbb{R}\}$.

2. Given Figure 4.4 we observe that we could also take one of the T_{++} sub-strands and "pull it across" the rod, as follows:

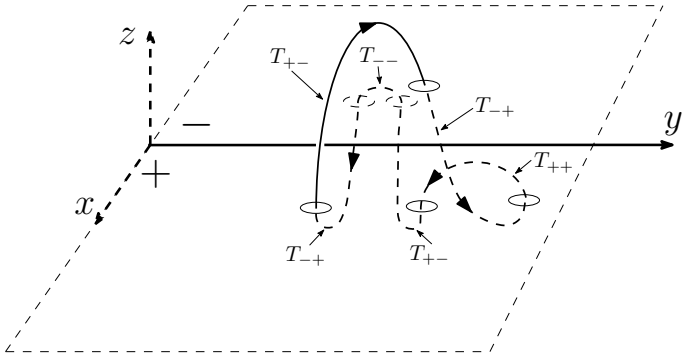

Figure 4.5: Closed polymer loop, $w = 1$, a further augmentation.

The diagram shown here could be described by the sequence $T_{+-}T_{-+}T_{++}T_{+-}T_{--}T_{-+}$ (or any cyclic permutation thereof).

These two augmentation procedures form the basis for a set of combinatoric rules that govern what sequences are derivable from the basic loop with $w = 1$. Let us return once more to said basic loop in Figure 4.1. From the examples above it is clear that this is the simplest loop for two reasons: (i) it has the smallest possible winding number $w = 1$, and (ii) it has the smallest number of piercings of the xy-plane. Clearly the two examples in Figures 4.4 and 4.5 are topologically equivalent to that in Figure 4.1: they have the same winding number. However, they have more piercings of the xy-plane because more sub-arcs were inserted. The inclusion of these augmenting sub-arcs was topologically consistent: the winding number was not altered and the strand was not broken. We continue now by stating concretely what rules govern the augmentation of basic loops through insertion of sub-arcs in such a way that the basic topology (i.e., their winding numbers) are conserved.

4.2.4 Condensed notation

The statistical weights of the sub-arcs considered here are symmetric around $z = 0$. It is, however, important to distinguish between Ts that cross the rod and those whose two piercings of the plane are on the same side of the rod. We introduce the following shorthand,

$$T_{+-}, T_{-+} \to T_c \tag{4.6}$$

and

$$T_{++}, T_{--} \to T_s, \tag{4.7}$$

where the subscripts c and s refer to "crossing" and "same side", respectively. For Figure 4.5, for example, we may write

$$T_{+-}T_{-+}T_{++}T_{+-}T_{--}T_{-+} \;=\; T_cT_cT_sT_cT_sT_c. \tag{4.8}$$

Of course it is implicit that a string be uninterrupted in its subscripts: two consecutive Ts of the form

$$T_{\alpha\beta}T_{\gamma\delta} \quad \text{with} \quad \alpha, \beta, \gamma, \delta \in \{+, -\} \tag{4.9}$$

must be such that $\beta = \gamma$. If this were not the case one would have a broken strand since consecutive sub-arcs in different half-planes cannot be connected due to the rod which separates the two half-planes.

4.2.5 Augmentation rules: maintaining $w = 1$

It should be noted that the condition of continuity in subscripts between consecutive Ts (as set out in section 4.2.4) is not sufficient to ensure that any polymer loop described by a string of Ts with this unbroken property need be topologically equivalent to the basic loop with $w = 1$. This is easily seen from the string $(T_cT_c)^w$, $w > 1$, which is clearly unbroken, but is not topologically equivalent to the case $w = 1$. Indeed, only strings that are derived from each other in very specific ways represent the same topology. To illustrate this, we now summarise some elementary inferences derived from the examples above:

1. A closed loop with $w = 1$ in its simplest form (i.e., with the minimal number of

piercings of the $z = 0$ plane) is represented by the sequence

$$T_c T_c. \tag{4.10}$$

2. A closed loop with $w > 1$ in its simplest form (i.e., with the minimal number of piercings of the $z = 0$ plane) is represented by the sequence

$$(T_c T_c)^w. \tag{4.11}$$

3. The basic sequence $T_c T_c$ can be augmented ("dressed") as in Figure 4.4 according to the lengthening rule

$$T_c \longrightarrow T_c T_s T_s. \tag{4.12}$$

4. A further augmentation procedure, as shown in Figure 4.5 is described by the replacement rule

$$T_s \longrightarrow T_c T_s T_c. \tag{4.13}$$

It is clear that compound rules arise, namely

$$T_x \longrightarrow T_x T_s T_s \tag{4.14}$$

and

$$T_s \longrightarrow (T_c)^n T_s (T_c)^n. \tag{4.15}$$

We note here that (4.14) and (4.15) essentially encode group relations of the braid group B_2 – see B.1. Any other alteration of the polymer strand through insertion / alteration of Ts that is *not* of type (4.12) or (4.13) (or equivalently (4.14) or (4.15)) would necessarily either break the strand (see previous section) or increase the winding number (see (4.11)). This implies that the two rules (4.14) and (4.15) above capture all possible ways of generating loops that are topologically equivalent to the basic loop shown in Figure 4.1. As in sections 4.2.1 and 4.2.2, calculation of the partition function requires integration over various degrees of freedom.

4.2.6 What sequences are valid for $w = 1$?

Valid sequences generated from the simplest form T_cT_c ($w = 1$) according to Section 4.2.5 must have the following properties:

1. in order for the loop to be closed, the first and last index must be equal (where cyclic permutations of sequences are equivalent) - see equation (4.8) as an example,
2. for the same reason, the second index of any T in the sequence must equal the first index of the next T,
3. the total number of Ts in the sequence must be even (since the basic undecorated closed loop has two terms, and both augmentation rules keep the total number even),
4. the number of T_cs must be even,
5. the number of T_ss must be even,
6. the string must be algorithmically reducible (this is defined in the next section).

4.2.7 Algorithmic reducibility of valid strings for $w = 1$

Let us define the sets of generic functional units / substrings counting either even (G) or odd (U) sequences of T_s:

$$G_n = T_c(T_s)^{2n}, \quad n = 0, 1, 2, \ldots \tag{4.16}$$

and

$$U_n = T_c(T_s)^{2n+1}, \quad n = 0, 1, 2, \ldots. \tag{4.17}$$

Any string of Ts could now be rewritten as a string of Gs and Us. For the basic unit for $w = 1$ we may write $T_cT_c = G_0G_0$, with another example being $T_cT_cT_sT_sT_sT_cT_sT_cT_sT_s = G_0U_1U_0G_1$. Since the substring T_sT_s may be trivially inserted or removed in any sequence (see (4.14)), it is clear that

$$G_n \leftrightarrow G_0 \tag{4.18}$$

and

$$U_n \leftrightarrow U_0. \tag{4.19}$$

We further infer from (4.14) and (4.15) that

$$X\,U_0^{2n}\,Y \leftrightarrow XY \quad (n = 1, 2, \ldots) \quad \forall \text{ substrings } X, Y \tag{4.20}$$

and

$$G_0^m\,U_0\,G_0^m \leftrightarrow U_0 \quad (m = 1, 2, \ldots). \tag{4.21}$$

We define a given string to be algorithmically reducible if the following procedure is possible:

1. apply (4.18) and (4.19) to simplify the string wherever possible,
2. apply (4.20) to simplify the string wherever possible,
3. now apply (4.21) to simplify the string wherever possible,
4. repeat until only the functional unit G_0G_0 remains.

Strings that are algorithmically reducible in this manner are topologically equivalent to the basic unit T_cT_c which represents $w = 1$. For $w > 1$ the string $(G_0)^{2w}$ would remain in step 4 after complete application of this procedure.

4.3 Partition function

The full partition function for a given winding number is now given by the integrals over the sums of all the configurations that are compatible with the winding number.

4.3.1 Summing over diagrams

The rules by which moves are produced do lead to all possible configurations permissible as described in Section 4.2. The corresponding sequence of Ts represents the statistical weight for each configuration. In order to enumerate the valid sequences correctly, each distinct configuration needs to occur exactly once in the partition function. (Alternatively one needs to be able to determine the correct multiplicity for the crossings in order to sum the appropriate terms in the partition function correctly.)

For completeness we state here once more the rules from equations (4.14) and (4.15),

(i) $T_x \to T_xT_sT_s$ and

(ii) $T_s \to T_cT_sT_c$.

The first rule adds loops of the type T_s in *even multiples* and the second rule is responsible for the addition of new terms in T_c. It is simple to see that different sequences of applying the rules (i) and (ii) above, on different elements, can lead to configurations that are identical. This has obvious implications in writing expressions for the sum in the partition function. Here we investigate a scheme by which enumeration or an approximate enumeration are possible. (The explicit procedure can be compared to the configurations produced by variations of the rules and checked for repeats using simple algorithms in *Mathematica*.)

As already explained in the previous section, the first basic consequence of the rule (i) above is that any even(odd) sequence of same-side crossing terms T_s can be extended repeatedly by a double T_s to an arbitrary degree. In this sense it is possible to use a compact notation for any sequence of terms in T_s and T_c by a prescription that indicated whether any two consecutive T_c's are separated by an even or an odd number of T_s terms. We utilise a notation that writes either no or one T_s and implies the extension of the rule (i) summation by eventually including the factor

$$1 + T_sT_s + T_sT_sT_sT_s + \ldots = (1 - T_sT_s)^{-1} . \tag{4.22}$$

In this sense the application of rule (i) is almost trivial except when it is combined with rule (ii). One can hence go ahead to introduce new terms by including all the possibilities for odd or even expansions of T_s and then complete the series above after all other configuration types have been introduced.

It is instructive to write down a hybrid composite of rules (i) and (ii):

(i'a) $T_c \to T_cT_sT_cT_sT_c$

(i'b) $T_c \to T_cT_cT_sT_cT_s$

(ii') $T_s \to T_cT_sT_c$.

We note here that the two parts rule (i') can be interpreted in two ways: either the sequence $T_sT_cT_sT_c$ is appended to the right of the original crossing T_c, or, the sequence $T_cT_sT_cT_s$ is added on the left of the original T_c. We choose the first of these two conventions since rules (i'a) and (i'b) produce equivalent configurations under the cyclic property – see Appendix B.2.

Consequently, the basic winding number expression can be expanded without repeating configurations under rule (i'a)

$$\begin{aligned} Z^{(w)}_{\text{basic}} &= (T_c T_c)^w \\ &\to T_c \left(1 + T_c T_s T_c T_s + T_c T_s T_c T_s T_c T_s T_c T_s + \ldots\right) \times \ldots \\ &= \left(T_c \left(1 - T_c T_s T_c T_s\right)^{-1} T_c \left(1 - T_c T_s T_c T_s\right)^{-1}\right)^w . \end{aligned} \tag{4.23}$$

However, this clearly does not represent a sum over all possible configurations, since rule (ii') has not been completely applied. In principle, all configurations should be given by repeated applications of the rules to all newly introduced parts of terms. The partition function using rule (i'a) as depicted above clearly does not repeat any configurations, yet does not produce all permissible configurations. We use this to calculate an *approximate* partition function

$$Z^{(w)}_{\text{appx1}} = \left\{ \frac{T_c}{\left(1 - T_s T_s\right)\left[1 - T_s T_c \left(1 - T_s T_s\right)^{-1} T_s T_c \left(1 - T_s T_s\right)^{-1}\right]} \right\}^{2w} . \tag{4.24}$$

Integration over relevant degrees of freedom of this expression is implied. Since the weight of each configuration in eq. (4.24) is the same as in the complete sum for the partition function the complete partition function for winding number w given by $Z^{(w)}$ is related to the approximation as follows,

$$Z^{(w)}_{\text{appx1}} \leq Z^{(w)}. \tag{4.25}$$

(We note that careful implementation of rule (ii') on a subset of T_s terms above will lead to an ever better lower bound than $Z^{(w)}_{\text{appx1}}$.)

Another interpretation of iterative application of rules (i') and (ii') is given by the definition of two coupled effective terms

$$T_c^{\text{eff}} = T_c \left(1 - T_s T_s\right)^{-1} + T_c T_s^{\text{eff}} T_c T_s^{\text{eff}} T_c^{\text{eff}} \tag{4.26}$$

$$T_s^{\text{eff}} = T_s + T_c^{\text{eff}} T_s^{\text{eff}} T_c^{\text{eff}}. \tag{4.27}$$

Here explicit evaluation shows that the systems eventually does lead to repetition of some configurations, but all configurations are produced when combined with (4.22) at the last

step. The partition function calculated using the recipe in (4.26–4.27) is defined by

$$Z^{(w)}_{\text{appx2}} = \left[T_c^{\text{eff}} T_c^{\text{eff}}\right]^w. \tag{4.28}$$

Now since eq. (4.23) leads to a partition function $Z^{(w)}_{\text{appx1}}$ with correctly weighted, yet fewer configurations, and equations (4.26–4.27) yield a partition function $Z^{(w)}_{\text{appx2}}$ with all yet some multiply occurring configurations we know how the true partition function is bounded

$$Z^{(w)}_{\text{appx1}} \leq Z^{(w)} \leq Z^{(w)}_{\text{appx2}}. \tag{4.29}$$

In principle these two approximations are calculable in the scenario of a polymer loop winding around certain obstacles in the plane, as described in sections 4.4 and 4.5, and can be used to understand upper and lower bounds for free energy associated with a particular winding number. We calculate only the lower bound $Z^{(w)}_{\text{appx1}}$ here, as the nonlinear coupled equations (4.26) and (4.27) pose formidable challenges. As stated, the approximations still need to be integrated over the relevant degrees of freedom, as will be set out in section 4.3.4.

4.3.2 Counting the number of crossing or same-side terms

In either of the suggested approximations for the partition function (see (4.24) and (4.28)) it is possible to include generating terms that may be used to calculate the number of T_s or T_c terms. If in these summations we simply replace $T_s \to e^{g_s} T_s$ and $T_c \to e^{g_c} T_c$, then we may calculate the average number of crossing terms as

$$\langle N_c \rangle = \left[\frac{\partial}{\partial g_c} \log Z^{(w)}(g_c, g_s)\right]_{g_c=g_s=0}, \tag{4.30}$$

and the average number of same-side terms as

$$\langle N_s \rangle = \left[\frac{\partial}{\partial g_s} \log Z^{(w)}(g_c, g_s)\right]_{g_c=g_s=0}. \tag{4.31}$$

4.3.3 Probability distribution of a flexible polymer in half-space

We still have to assign a statistical weight to each string in the summation over all diagrams. We proceed to do this for a flexible polymer. In principle other polymer variants

could be described by the formalism up to this point, but the form of the probability distribution would be different.

For a flexible polymer we treat the sub-arcs (labelled by the various Ts) as random walks confined to half-spaces. In polymer systems with suitable solubility and flexibility conditions this is, of course, a reasonable assumption [56]. The notion of confined random walks is certainly not a new one. In a 1943 review Chandrasekhar [57] pointed out how one-dimensional random walks with reflecting and absorbing boundary conditions may be treated. Naturally boundaries change the probability distribution for random walks. A reflection off such a boundary implies that a walker must necessarily retrace its last step. An absorbing boundary, in contrast, would prevent any further displacements. Consequently the probability distribution of a walker confined by a reflecting boundary is obtained by adding an "image distribution" to that of an unconfined walker. This accounts for additional possible paths to a given end point, stemming from the reflecting boundary (these paths may be viewed as mirrored paths in the excluded region). On the other hand, the distribution of a walker confined by an absorbing boundary is obtained by subtracting a similar mirror distribution. This, in turn, accounts for the exclusion of trajectories that terminate on the absorbing boundary.

This discussion may be extended to a random walker restricted to a half-space in three dimensions (see, for instance, the article of Slutsky [58] where a similar "method of images" is used). We shall draw on these notions in order to assign appropriate statistical weights to the sub-arcs mentioned in the previous section. To this end we make the following assumptions (as illustrated in Figure 4.6):

1. there exists a finite minimal length-scale (such as a bond length or Kuhn length) in this polymer system,

2. for every (sub)sequence $T_{xy}T_{yz}$ (for any $x, y, z \in \{+, -\}$), there exists a trans-plane polymer segment of length 2ϵ that is normal to the plane and connects the two sub-arcs between the $z > 0$ or the $z < 0$ half-spaces,

3. thus any given sub-arc begins and ends at a distance ϵ from the xy-plane (see Figure 4.6),

4. each polymer sub-arc is modelled as a random walk constrained by an absorbing

boundary plane to either the $z > 0$ or the $z < 0$ half-spaces,

5. such a random walk begins and ends at $\vec{r}_0 = (x_0, y_0, \eta\epsilon)$ and $\vec{r} = (x, y, \eta\epsilon)$ respectively (here $\eta = +1$ for the $z > 0$ half-space or $\eta = -1$ for $z < 0$),

6. the random walks are fully flexible, and each has a variable arc-length s_i.

The assumption of an absorbing boundary is based on the fact that we are interested in the two piercings that a sub-arc makes with the plane, since it is there that one particular sub-arc ends and another one begins. In reality, the trans-plane connecting segment should

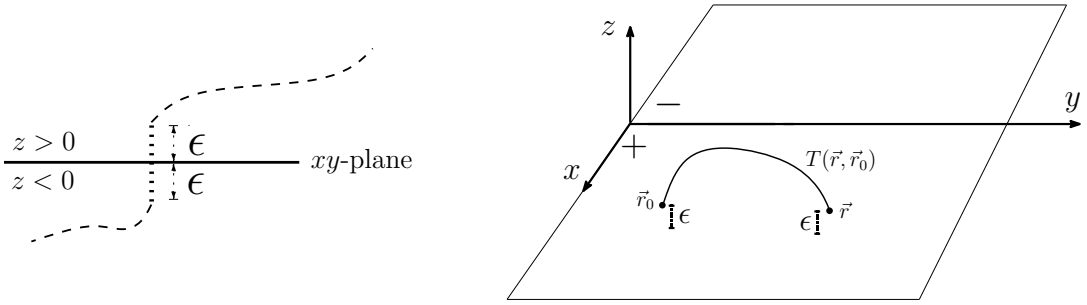

(a) Side view of trans-plane segment. (b) Polymer in the half plane $z > 0$.

Figure 4.6: Sub-arcs as random walks that begin and end at a distance ϵ from the plane.

be free to take on any orientation. Our approximation that it is normal to the plane should be a small correction for a sufficiently long arc-segment. It is clear from Figure 4.6 that, barring constraints due to the total length of the polymer, the y components of the beginning and end vectors of a random walk could take any value. The x components, however, are restricted either to the interval $(0, \infty)$ or to the interval $(0, -\infty)$, depending on whether they fall on the $+$ or $-$ sides of the rod. Naturally this will constrain the integration bounds for x in the partition function accordingly.

Therefore, for a Gaussian chain with all lengths expressed in terms of the Kuhn length, we may now assign the corresponding probability distribution to a typical sub-arc as set out in [58],

$$\begin{aligned} T(\vec{r}, \vec{r}_0, s, \epsilon) &= (2\pi s)^{-3/2} e^{-[(x-x_0)^2+(y-y_0)^2]/2s} \left[e^{-(z-z_0)^2/2s} - e^{-(z+z_0)^2/2s} \right] \\ &= (2\pi s)^{-3/2} e^{-[(x-x_0)^2+(y-y_0)^2]/2s} \left[1 - e^{-\epsilon^2/s} \right], \end{aligned} \tag{4.32}$$

where s is the arc length of the polymer sub-arc between $\vec{r}_0$ and $\vec{r}$. The z dependence

vanishes due to assumptions (2) and (3) above. Here we have interchanged the discrete number of steps N for the arc-length variable s through appropriate re-scaling. Finally, if we take ϵ as the Kuhn length, and assume that the polymer system has a sufficiently small Kuhn length, we may Taylor expand the exponential in Equation (4.32) to obtain

$$T_p(\vec{r}, \vec{r}_0, s, \epsilon) = \frac{\epsilon^2}{\sqrt{(2\pi)^3 s^5}} e^{-[(x-x_0)^2+(y-y_0)^2]/2s}. \tag{4.33}$$

The subscript p here simply refers to the "parity" of the particular T under consideration, as described in Section 4.2.4. This merely indicates whether the x co-ordinates are on equal sides of the rod or not, which will determine the integration domains for the x co-ordinates in the partition function.

4.3.4 Partition function for $w = 1$

Using Section 4.2.5 we constructed a symbolic summation of all possible configurations for $w = 1$ in two possible approximations, (4.24) and (4.28). We now proceed to use this summation in order to write the partition function for this system. Let us denote the set of all valid configurations as Λ. Supposing that the total length of the polymer loop is L, we note that

$$\mathbf{Z}_{\text{total}}^{(w=1)}(L) = \sum_{\chi \in \Lambda} Z_{\chi}^{(w=1)}(L), \tag{4.34}$$

i.e., the total partition function is simply the sum of the partition functions for all valid configurations for $w = 1$. A typical valid configuration χ which has N piercings of the xy-plane is represented by some sequence (of length N) of Ts that adheres to the conditions in Section 4.2.6, and simply corresponds to one of the terms in the summation. Let us make the notation in equations (4.3) and (4.5) more concrete: the partition function corresponding such a generic sequence would be

$$\begin{aligned} Z_{\chi}^{(w=1)}(L) \quad = \quad & \int_0^{\infty} dX \int_{-\infty}^{\infty} dY \int_{\epsilon}^{\infty} dS \;\; \delta(x_0 - x_N)\delta(y_0 - y_N) \\ & \prod_{j=1}^{N} T_{p_j}(x_{j-1}, x_j; y_{j-1} - y_j; s_j; \epsilon)\delta(\sum_{k=1}^{N} s_k - L). \end{aligned} \tag{4.35}$$

The condensed notation implies

$$\begin{aligned} dX &= dx_0\, dx_1 \dots dx_N, \\ dY &= dy_0\, dy_1 \dots dy_N, \\ dS &= ds_1\, ds_2 \dots ds_N, \end{aligned} \tag{4.36}$$

and the functions T_p in the integrand are each of the form (4.33). Naturally there is one less s integral than for x or y, since one arc-segment connects two planar points. The first two delta functions ensure that the strand is closed: the first and last x and y co-ordinates must be equal. The length s_i of each of the N sub-arcs is bounded from below by the minimal length ϵ - hence the integration bounds on the s integrals. It is, however, necessary that these lengths add up to the total length L of the entire polymer. This constraint is enforced by the third delta function. As set out in Section 4.3.3, the y co-ordinates of each strand are not constrained. For this reason they are integrated over the whole axis. From (4.32) it is clear that the Ts are symmetric under the exchanges $(x_{i-1} - x_i) \to -(x_{i-1} - x_i)$ and $(y_{i-1} - y_i) \to -(y_{i-1} - y_i)$. Since the x co-ordinates are constrained to one half of their axis (as set out after Equation (4.33)), we need to distinguish between the terms that cross over the rod (T_c) and those that remain on the same side of the rod (T_s). For T_s, the two x argument have the same sign and the function depends on $\pm(x_{i-1} - x_i)$. For T_c, the two x arguments have opposite signs and the function depends on $\pm(x_{i-1} + x_i)$. We may thus change all x integrals to run over $(0, \infty)$ under the condition that

$$\begin{aligned} T_s(x_{i-1}, x_i) &= T(x_{i-1} - x_i) = \frac{\epsilon^2}{\sqrt{(2\pi)^3 s_i^5}} e^{-[(x_{i-1}-x_i)^2 + (y_i - y_{i-1})^2]/2s_i}, \\ T_c(x_{i-1}, x_i) &= T(x_{i-1} + x_i) = \frac{\epsilon^2}{\sqrt{(2\pi)^3 s_i^5}} e^{-[(x_{i-1}+x_i)^2 + (y_i - y_{i-1})^2]/2s_i}, \end{aligned} \tag{4.37}$$

i.e., with these integration bounds the same-side contributions depend on the difference between their x co-ordinates, whereas the crossing contributions depend on the sum (compare to (4.33)). For the reasons set out above, it is clear that translational invariance holds for the y co-ordinates but not for the x co-ordinates. In Appendix B.3 we outline how some integrals in (4.35) may be diagonalised using a Laplace transformation in the length of the polymer and Fourier transformations of the y co-ordinates. The result is the Laplace

transformed partition function for some configuration χ,

$$\tilde{Z}_{\chi}^{(w=1)}(t) = \int_0^{\infty} dX\ \delta(x_0 - x_N) \int_{-\infty}^{\infty} dk\ \prod_{i=1}^{N} T_{p_i}^{L,F}(x_{i-1}, x_i; k; t), \tag{4.38}$$

where the superscript "L, F" implies that the Ts from (4.37) have been Laplace transformed and Fourier transformed in y. We have thus obtained a diagonalisation for the s and y co-ordinates. What remains are the integrals over the positive (real) x axis, and the integral over the Fourier variable k. We shall deal with these integrals for two cases. First we consider restricting the x integrals to a narrow slit, thereby effectively constraining the polymer to be wound through two slits in the plane. In this case no x integration is necessary, and only the k integral remains. Secondly we shall outline possible approximation schemes to deal with the general case.

As stated, the complete partition function $Z^{(w=1)}$ is found by the summation over various diagrams. This summation is approximated by (4.24) or (4.28). The integrand in this partition function may then be repeated w times to obtain the approximated partition function for higher winding numbers $w > 1$.

4.4 Specific case: polymer wound through two slits

Let us consider a polymer looping around two slits, the inner edges of the slits separated by the distance d and each slit with a width Δ, as shown in Figure 4.7. We note that similar scenarios of confined wound polymers have been considered in [52].

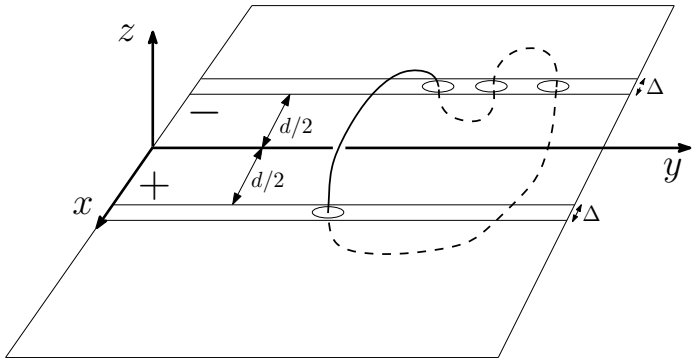

Figure 4.7: Constraining the polymer to two narrow slits in the plane.

We can compute the average number of the types of arc elements in this scenario using

the formalism developed in Section 4.3.2. By winding the polymer around a double slit geometry, the combinatorics clearly remain unaltered. The partition function for the chain now has integration restricted over the domain $x_i \in [d/2, d/2+\Delta]$. This means that equation (4.38) takes the integral form

$$\tilde{Z}_{\chi}^{(w=1)}(t,\Delta,d) = \int_{\frac{d}{2}}^{\frac{d}{2}+\Delta} dX\ \delta\left(x_0 - x_N\right) \int_{-\infty}^{\infty} dk\ \prod_{i=1}^{N} T_{p_i}^{L,F}(x_{i-1}, x_i; k; t). \tag{4.39}$$

We begin by considering the case of zero slit-width.

4.4.1 Zero slit width: $\Delta = 0$

In the limiting case where $\Delta \to 0$ such that each T has exactly the same x–value $x_i = d/2,\ \forall i \in \{0,\ldots,N\}$, the partition function becomes especially simple as the operator sums of eq. (4.24) or (4.28) now become simple algebraic sums. (This is the scenario where no integration is necessary, and conformations are simply summed because the problem is "diagonal" already in the simplest terms. The next section will deal with the extension of this to narrow and easily integrable slits configurations.) Choosing the first approximation (4.24) we obtain

$$\tilde{Z}_{\text{appx1}}^{(w=1)}(t,d) \quad = \quad \int_{-\infty}^{\infty} dk\ \frac{(T_c^{L,F})^2[1-(T_s^{L,F})^2]^2}{\left[1-[2+(T_c^{L,F})^2](T_s^{L,F})^2+(T_s^{L,F})^4\right]^2}, \tag{4.40}$$

since the operations of summing over various configurations and integration over k may be exchanged.

Turning to equation (4.37) we see that Fourier transformation in y leads us to the following two cases,

$$T_s^F(d;k;s_i) = \frac{\sqrt{3}\epsilon^2 e^{-\frac{k^2 s_i}{6}}}{2s_i^2} \tag{4.41}$$

and

$$T_c^F(d;k;s_i) = \frac{\sqrt{3}\epsilon^2 e^{-\frac{3d^2}{2s_i}-\frac{k^2 s_i}{6}}}{2s_i^2}. \tag{4.42}$$

Since ϵ is non-zero and finite, these expressions are well-defined. We now need to perform

the Laplace transforms of each of these,

$$\begin{aligned} T_s^{L,F}(d;k;t) &= \int_\epsilon^\infty ds_i \;\; e^{-s_i t}\frac{\sqrt{3}\epsilon^2 e^{-\frac{k^2 s_i}{6}}}{2s_i^2} \\ &= \frac{\sqrt{3}\epsilon^2}{2}\left[\frac{e^{-\frac{1}{6}\epsilon\left(k^2+6t\right)}}{\epsilon} - \frac{1}{6}\left(k^2+6t\right)\Gamma\left(0,\frac{1}{6}\left(k^2+6t\right)\epsilon\right)\right] \end{aligned} \tag{4.43}$$

and

$$T_c^{L,F}(d;k;t) \approx \int_{d^2}^\infty ds_i \;\; e^{-s_i t}\frac{\sqrt{3}\epsilon^2 e^{-\frac{3d^2}{2s_i}-\frac{k^2 s_i}{6}}}{2s_i^2}. \tag{4.44}$$

In (4.43) the answer contains an incomplete gamma function. The integral in (4.44) has an approximated lower bound of d^2 (recall that s_i and d are dimensionless). In principle this bound should be ϵ (i.e., of the order of the Kuhn length). If the polymer were inextensible, the minimum arc-length for $T_c^{L,F}$ should be d. Although we deal with a Gaussian chain here, this approximation is reasonable since the integrand is dominated by $s_i \geq d^2$. We approximate

$$T_c^{L,F}(d;k;t) \approx \frac{1}{2}e^{-\frac{3d^2}{2s^*}}\int_{d^2}^\infty ds_i \;\; e^{-s_i t}\frac{\sqrt{3}\epsilon^2 e^{-\frac{k^2 s_i}{6}}}{2s_i^2}, \tag{4.45}$$

where $s^* = (\int_{d^2}^\infty ds \;\; s\, e^{-\frac{k^2 s}{6}})/(\int_{d^2}^\infty ds \;\; e^{-\frac{k^2 s}{6}}) = \frac{6+d^2k^2}{k^2}$ is a constant value that captures some of the k scaling of the answer. Numerical verification shows this approximation to perform very well for various ranges of t and k. The integral in (4.45) may now be evaluated explicitly,

$$\begin{aligned} T_c^{L,F}(d;k;t) &= \frac{\sqrt{3}\epsilon^2}{2}e^{-\frac{3d^2k^2}{2(6+d^2k^2)}} \\ &\quad\times\left[\frac{e^{-\frac{1}{6}d^2\left(k^2+6t\right)}}{d^2} - \frac{1}{6}\left(k^2+6t\right)\Gamma\left(0,\frac{1}{6}d^2\left(k^2+6t\right)\right)\right]. \end{aligned} \tag{4.46}$$

We may now insert the answers (4.43) and (4.46) into (4.40) to obtain two approximations for the partition function. Naturally the integrand above is some very complicated function of k. As is verifiable numerically, however, a saddle point approximation is reliable for various ranges of t and d. We omit the cumbersome explicit form of the result.

The average length of the loop for $w = 1$ may be calculated from (4.40),

$$\langle L\rangle(t) = -\frac{\partial}{\partial t}\log\left[\tilde{Z}^{(w=1)}_{\text{appx1}}(t,d)\right]. \tag{4.47}$$

In Figure 4.8 we see that $\langle L\rangle(t)$ is a concave function for various values of the slit separation d. Here we have set $\epsilon = 1$ for convenience; this convention is used henceforth. It is also clear that small Laplace parameters correspond to longer length-scales, particularly for small d. As we increase the size of d, we note that $\langle L\rangle$ seems to strive asymptotically to increasingly large values. This is simply a manifestation of the fact that the non-zero slit-separation implies a minimal length-scale for the polymer loop.

We thus have a "lookup table" that allows us to associate an average length of the polymer to a particular Laplace parameter (of course this is not the inverse Laplace transform, as would ideally be the case).

Figure 4.8: Average length of the loop as function of the Laplace parameter t, calculated according to equation (4.47). Parameters: $d = 1$ (solid), $d = 3$ (dashed), $d = 5$ (dashdotted).

It is further interesting to ask what is the relative weight of the undressed term / basic loop T_cT_c (see Figure 4.1) in the summation over all valid diagrams for $w = 1$. To this end we simply look at the probability for this configuration,

$$P(T_c^2) = \frac{\int_{-\infty}^{\infty} dk\ \ (T_c^{L,F})^2}{\tilde{Z}^{(w=1)}_{\text{appx1}}(t,d)}. \tag{4.48}$$

We see in Figure 4.9 that, for various values of d, this probability is unity for sufficiently large Laplace parameters. Through Figure 4.8 we may thus identify length-scales (for various slit separations) at which the basic (undressed) loop provides the dominant contribution to the partition function. This makes sense physically, since large Laplace parameters correspond to short length-scales. Naturally the afore-mentioned minimal length-scale set by the slit separation implies that as soon as the length of the loop becomes small enough, it is clear that the basic configuration consisting of two crossing terms will be the dominant configuration in the partition function.

Figure 4.9: Probability for the configuration T_c^2 as a function of the Laplace parameter t (calculated according to equation (4.48)). Parameters: $d = 1$ (solid), $d = 3$ (dashed), $d = 10$ (dashdotted).

The average number of crossing terms and same-side terms may also be calculated as a function of the Laplace parameter according to equations (4.30) and (4.31). From Figure 4.10 we note that as soon as the Laplace parameter is sufficiently large (i.e., the polymer is typically short), there are exactly two T_c terms and zero T_s terms present. This agrees with the previous conclusion: at short polymer lengths, the undressed basic term T_cT_c dominates the summation over valid diagrams. We note that as the slit separation d is increased, this undressed configuration dominates at decreasing t, i.e., at longer polymer lengths. This can be related to Figure 4.8, where we observe the minimal length of the polymer increasing with increases in slit separation.

As is to be expected for sufficiently small polymer length-scales, the results are not

particularly sensitive to which approximation is used to approximate the summation. Indeed, for short or stiff polymers it should be sufficient to generate the first few terms (valid sequences) explicitly as an approximation to the complete partition function.

(a) Average number of crossing terms (b) Average number of same-side terms

Figure 4.10: The average number of crossing and same-side terms as functions of Laplace parameter, calculated numerically from (4.30) and (4.31). Parameters: $d = 1$ (solid), $d = 2$ (dashed), $d = 3$ (dashdotted).

Lastly we consider the free energy of the system for various values of slit separation. This quantity is simply the negative logarithm of the partition function, and is plotted parametrically as a function of the average polymer length in Figure 4.11. It is clear that as the polymer is made shorter and approaches the minimal length-scale set by the slit separation, the free energy increases sharply which is compatible with the sharp decrease of entropy experienced by the Gaussian chain.

Figure 4.11: Parametric plot of free energy dependence on average polymer length. Parameters: $d = 1$ (solid), $d = 2$ (dashed), $d = 3$ (dashdotted).

4.4.2 Finite slit width: $\Delta \neq 0$

We shall briefly outline a possible approach to solving the case for non-zero slit width in (4.39). As a first order approach it would be sensible to decouple consecutive Ts completely and to replace the various x integrals ($\int_{\frac{d}{2}}^{\frac{d}{2}+\Delta} dx_i$) with a localisation approximation,

$$\int_{-\infty}^{\infty} dx \int_{-\infty}^{\infty} dx' \frac{\mathcal{N}}{\Delta} \exp\left[-\frac{(x-\frac{d}{2})^2}{\Delta} - \frac{(x'-\frac{d}{2})^2}{\Delta} - \frac{(x-x')^2}{s}\right] \tag{4.49}$$

and

$$\int_{-\infty}^{\infty} dx \int_{-\infty}^{\infty} dx' \frac{\mathcal{N}}{\Delta} \exp\left[-\frac{(x-\frac{d}{2})^2}{\Delta} - \frac{(x'-\frac{d}{2})^2}{\Delta} - \frac{(x+x')^2}{s}\right] \tag{4.50}$$

for T_s and T_c respectively. The analogues of equations (4.41) and (4.42) now become

$$T_s^F(d;k;s_i) = \frac{\sqrt{3}\epsilon^2 e^{-\frac{k^2 s_i}{6}}}{2s_i^2}\sqrt{\frac{s_i}{s_i+2\Delta}} \tag{4.51}$$

and

$$T_c^F(d;k;s_i) = \frac{\sqrt{3}\epsilon^2 e^{-\frac{3d^2}{2s_i}-\frac{k^2 s_i}{6}}}{2s_i^2}\sqrt{\frac{s_i}{s_i+2\Delta}}e^{-\frac{3d^2}{2(2\Delta^2+s_i)}}. \tag{4.52}$$

Naturally these expressions reduce to the case of zero slit-width if $\Delta \to 0$. Again we require Laplace transformations in order to use (4.24), and we must do the k integral as

for (4.40). This may be approximated in various ways. A Taylor expansion of (4.51) and (4.52) to $\mathcal{O}(\Delta)$, for instance, allows us to repeat the analysis from Section 4.4.1 without many modifications, yielding an approximation for Laplace transformed partition function, $\tilde{Z}^{(w=1)}_{\text{appx1}}(t,d,\Delta)$. (We may recover (4.40) through $\lim_{\Delta\to 0}\tilde{Z}^{(w=1)}_{\text{appx1}}(t,d,\Delta) = \tilde{Z}^{(w=1)}_{\text{appx1}}(t,d)$.) One may now calculate, for instance, the force exerted by the slit as the derivative of the free energy,

$$f(t,d,\Delta) = -\frac{\partial}{\partial\Delta}\left(-\log\left[\tilde{Z}^{(w=1)}_{\text{appx1}}(t,d,\Delta)\right]\right). \tag{4.53}$$

With the aid of *Mathematica* we may "invert" the Laplace transformation numerically to obtain the Laplace parameter as a function of the average length, $t = t(\langle L\rangle, d, \Delta)$. This allows us to plot, for instance, the force as a function of slit separation for a fixed $\langle L\rangle$, see Figure 4.12.

(a) Force dependence on d.

(b) $\frac{\langle N_s\rangle}{\langle N_c\rangle}$ as function of d.

Figure 4.12: Force exerted by the slit as a function of slit separation d, for $\Delta = 0$ and a fixed $\langle L\rangle = 20$. The ratio $\frac{\langle N_s\rangle}{\langle N_c\rangle}$ exhibits a peak corresponding to the minimum of the force. Compare to Figure 4.8 to see why $d > 3.1$ is excluded.

Despite the somewhat crude simplifying assumptions made (using independent localisation of each arc), expected physical aspects are well captured. For a fixed average polymer length, there is a sign change in the force at some slit separation. This makes sense: for sufficiently small d the slit has a "compressing" effect on the polymer, and for sufficiently large d the polymer is "stretched". Again the competition of the two length-scales d and $\langle L\rangle$ is manifest. In Figure 4.12b we plot the ratio $\frac{\langle N_s\rangle}{\langle N_c\rangle}$ as defined in (4.30) and (4.31) for a fixed $\langle L\rangle$. Consider the trend in this plot as we decrease the slit-separation d. For large d

all of the polymer is in the crossing terms and $\langle N_s \rangle \approx 0$. As we decrease d the fraction of same-side terms increases: more of the polymer's length is free to occupy the slits. As d is decreased even further, the ratio begins decreasing again: at some stage sufficiently much polymer length is free so that additional crossing terms may arise, thereby decreasing $\langle N_s \rangle$ and increasing $\langle N_c \rangle$. Corresponding behaviour of the force is evident in Figure 4.12a (also compare to Figure 4.10).

4.5 General case: outline of solution strategy

Suppose we return to the general form of the partition function in equation (4.38). For the general case of an infinitesimally thin rod in the plane, the remaining integrals over x are not as easy to diagonalize. Instead of such a rod we shall consider a flat slab of width d lying along the y axis in the xy plane; see Figure 4.13. This amounts to modifying the two-slit scenario of previous section by removing the "outer barrier" of each slit, thereby changing the x integration domains to $(\frac{d}{2}, \infty)$. The limit $d \to 0$ represents the original scenario of Edwards' rod in the plane.

Recall that the terms in the partition function consist of multiples of T_c with even or odd geometric series of T_s, i.e., $T_c(1 - T_s^2)^{-1}$ or $T_c T_s (1 - T_s^2)^{-1}$. We approximate these contributions to the partition function in two steps:

- address the sub-sequences of single-side contributions that originate from augmentations of the type (4.12), i.e.,
  $T_c(x + x_0) \underbrace{T_s(x_0 - x_1) \dots T_s(x_{m-1} - x_m)}_{m \text{ single-side terms}} T_c(x_m + x')$, and then
- approximate the crossing terms T_c.

4.5.1 Approximation of T_s sequences

Let us begin by considering a sub-sequence of m single-side contributions in the integral (4.38) between x_0 and x_m, say. For notational convenience we omit k and t dependence (which is the same in all terms), but recall that the k integral still remains. Let us consider the case where we have *not yet* performed the Laplace transformation w.r.t. L, and define

$$T^F_{\text{eff.}}(x_0, x_m; k; \{s_i\}) = \int_{d/2}^{\infty} dx_1 \dots \int_{d/2}^{\infty} dx_{m-1} \; T^F_s(x_0 - x_1; k; s_1) \dots T^F_s(x_{m-1} - x_m; k; s_m). \quad (4.54)$$

Here each T_s^F has been Fourier transformed in its ys but not yet Laplace transformed, i.e.,

$$T_s^F(x_i, x_{i+1}; k; s_i) = \frac{\mathcal{N}}{s_i^2} e^{-3(x_i - x_{i+1})^2/2s_i - k^2 s_i/6}, \tag{4.55}$$

as is easily seen from (4.33). This implies that we may write

$$\prod_{i=1}^{m-1} T_s^F(x_i, x_{i+1}; k; s_i) = \left(\prod_{i=1}^{m-1} \frac{\mathcal{N}}{s_i^{3/2}} e^{-k^2 s_i/6} \right) \left(\prod_{j=1}^{m-1} \frac{1}{s_j^{1/2}} e^{-\frac{3(x_j - x_{j+1})^2}{2s_j}} \right). \tag{4.56}$$

We note that second product is simply one of Green functions for a one-dimensional polymer chain,

$$G_x(x_i, x_{i+1}; s_i) = \frac{\mathcal{N}'}{s_i^{1/2}} e^{-3(x_i - x_{i+1})^2/2s_i}. \tag{4.57}$$

The restriction imposed by the integration bound on each intermediate x_i (where the polymer pierces the plane) implies that none of the piercings may enter the excluded region of the bar in the region $x \in (-\frac{d}{2}, \frac{d}{2})$. This however does *not* preclude any other part of the polymer arc to cross over this region, as illustrated in Figure 4.13.

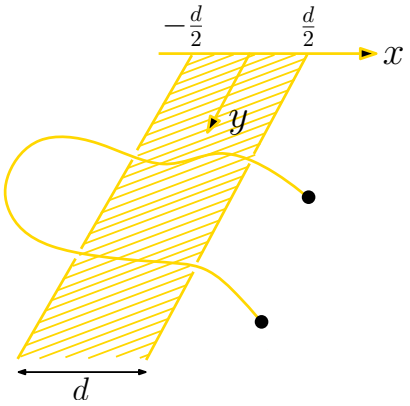

Figure 4.13: Piercings are excluded from a slab region on the y axis, but the remainder of a polymer arc could still cross over this region.

We proceed with our approximation by assuming that indeed *none* of the segments in an arc may cross the excluded region, i.e., all x co-ordinates of an arc (and not just those of its piercings) must lie in the region $(\frac{d}{2}, \infty)$. Naturally this approximation would exclude several possible configurations, and we are significantly under-estimating the true entropy

of the polymer arc. As such this would provide a sensible upper bound for the free energy of the system. This case should be adaptable to the scenario of a polymer in a cavity from [52] through a similar argument in a cylindrically symmetric setting.

Under this assumption the product $\prod_{i=1}^{m-1} G_x(x_i, x_{i+1}; s_i)$ reduces to a single chain of length $\sum_{i=1}^{m-1} s_i$ that *nowhere* crosses into the forbidden x domain, i.e., the polymer arc is effectively restricted to a quadrant around the forbidden region. For such a restricted random walk we may once more use Chandrasekhar's argument of mirror images to construct an effective Green function,

$$\begin{aligned}\prod_{i=1}^{m-1} G_x^{(x\geq d/2)}(x_i, x_{i+1}; s_i) &= G_x^{(x\geq d/2)}(x_0, x_m; \sum_{i=1}^{m-1} s_i) \\ &= G_x^{(x\in\mathbf{R})}((x_0 - \frac{d}{2}) - (x_m - \frac{d}{2}); \sum_{i=1}^{m-1} s_i) \\ &\quad - G_x^{(x\in\mathbf{R})}((x_0 - \frac{d}{2}) + (x_m - \frac{d}{2}); \sum_{i=1}^{m-1} s_i). \qquad (4.58)\end{aligned}$$

Here the superscripts on the Green functions refer to the respective x integration domains. We have thus replaced the sequence of G_xs with an effective Green function by making use of the Markov property of random walks after having extended the x integration to all space by making use of Chandrasekhar's argument. This is manifest in the last line above of equation (4.58) where the Green function with the reflected end co-ordinate has been subtracted. This means that all intermediate x integrals have vanished, and only the integrals over the beginning and end x co-ordinates of $G_x^{(x\geq d/2)}(x_0, x_m; \sum_{i=1}^{m} s_i)$ remain. In this approximation the dependence on m has completely disappeared out of one part of the expression in equation (4.56) yielding

$$\prod_{i=1}^{m-1} T_s^F(x_i - x_{i+1}; k; s_i) \approx \left(\prod_{i=1}^{m-1} \frac{\mathcal{N}}{s_i^{3/2}} e^{-k^2 s_i/6}\right) G_x^{(x\geq d/2)}(x_0, x_m; \sum_{i=1}^{m-1} s_i). \qquad (4.59)$$

What remains is to perform the integrals over the s co-ordinates, with the relevant cuttoff

on the lower integration bound,

$$\hat{T}^{F}_{\text{eff.}}(x_0, x_m; t) = \int_{-\infty}^{\infty} dx_0\, dx_m \int_{\epsilon}^{\infty} \prod_{j=1}^{m-1} ds_j \; e^{-\sum_i s_i t} \prod_{i=1}^{m-1} \frac{\mathcal{N}}{s_i^{3/2}} e^{-k^2 s_i/6}\, G_x^{(x \geq d/2)}(x_0, x_m; \sum_{i=1}^{m-1} s_i). \tag{4.60}$$

This effective quantity depends only on the first and last co-ordinates, x and x', and on the number m of same-side steps in the sub-sequence. A summation over m will lead to a geometric series $G^{\text{odd/even}}_{\text{eff.}}(x, x')$ that may now be included between T_c terms in a chosen approximation scheme for the summation over valid sequences.

4.5.2 Approximating the T_c terms

The second step is to deal with rod-crossing terms of the form $T_c(x, x')$. These terms are responsible for the localisation of the polymer around the rod at these points. We propose an approximation that decouples x and x',

$$T_c(x, x') \approx f(x) f(x'). \tag{4.61}$$

This could be done in several ways, and would lead to a complete diagonalisation of the integral. For a short polymer one may assume that the crossing terms will be localised close to the boundary of the slab, i.e., $\langle x \rangle \approx \frac{d}{2}$. For other length-scale regimes this average localisation could also be guessed as a function of the Laplace parameter t or solved in some self-consistent manner.

A slightly more general approach would be to assume that the piercings of the crossing terms are localised by Gaussians around $x, x' = \frac{d}{2}$. Naturally one would expect a T_c term to show a corresponding decline if $x \in (\frac{d}{2}, \infty)$ and $x' \in (\frac{d}{2}, \infty)$ are moved further from the origin, since it is a Gaussian in $x + x'$. The Laplace parameter t is related to the inverse of the arc-length of the crossing segment, and should be indicative of this localization. A sensible approximation for the x dependent part would thus be to say that T_c localises x and x' independently (i.e., we decouple the function into two independent Gaussians),

$$T_c^L(x + x') \approx \mathcal{N}_q e^{-\frac{qt}{2}(x - \frac{d}{2})^2 - \frac{qt}{2}(x' - \frac{d}{2})^2}, \tag{4.62}$$

where the localisation parameter q is treated as a guess to the localisation length-scale. Here $\mathcal{N}_q$ is the normalisation such that

$$\int_0^\infty dx \int_0^\infty dx' \, \mathcal{N}_q e^{-\frac{qt}{2}(x-\frac{d}{2})^2 - \frac{qt}{2}(x'-\frac{d}{2})^2} = 1. \tag{4.63}$$

One could also determine the strength of the localisation using, for instance, a variational calculation. The result could now be combined with those of Section 4.5.1 and Section 4.3.1 in some approximation for the partition function.

4.6 Summary and outlook

The problem of winding a polymer around an infinitely long obstacle was addressed by labelling configurations according to sequences of sub-arcs constrained to a half-space. By considering arcs that cross the obstacle or remain on the same side thereof, combinatoric rules were derived that allow winding number conserving augmentations of these sequences. These augmentations rely on topology conservation through type 2 Reidemeister moves. Properties of valid sequences were identified and an algorithm was presented for discriminating whether a given sequence is valid.

Two possible approximations for the partition function were found by considering summations over valid configurations, one bounding the true partition function from above and the other from below. Given a particular choice of polymer variant (Gaussian, semiflexible etc.) a statistical weight may be attached to each sub-arc. Through a series of diagonalising transformations the lower bound approximation for the partition function was written as an integral of these statistical weights.

For the case of a Gaussian chain a specific statistical weight was assigned, and the partition function for $w = 1$ was approximated for the case of windings through two slits in a plane. For a zero slit-width it was found that the basic undressed loop dominates the partition function when the polymer is short, as expected. Various expectation values were calculated and the free energy was plotted for different slit separations. The results make good physical sense for various average polymer length-scales, lending credibility to our approximations.

The case of non-zero slit width was treated in a localising approximation. The force of the slits on the polymer shows an expected sign change as slit separation is varied for

a fixed average polymer length. Correspondingly different length-scale regimes arise that determine what fraction of the polymer is in crossing terms or in same-side terms.

Only the case $w = 1$ was treated in detail. Since the partition function arises from summing integrals of products of functions, the partition function for higher winding numbers may in principle be constructed from higher order basic loops by our rules. This implies that some statistical quantities calculated from logarithms of $Z^{(w)}_{\text{appx1}}$ (e.g., $\langle L\rangle(t)$, $\langle N_s\rangle$, $\langle N_c\rangle\ldots$) scale with the winding number of the system. In our lower bound approximation scheme, at least, higher windings entail repeats of the integrand a corresponding number of times. The upper bound approximation scheme could also be useful in some regimes since the first few terms in the summation over configurations dominate the partition function for certain length-scales.

Lastly suggested approximations were sketched for a slab-like obstacle in the plane. It was observed that the latter case should be relatable to other confined geometries studied in existing literature. Our approach allows different and intuitive calculation strategies for partition functions of wound polymers.

CHAPTER 5
OPERATOR FORMALISM FOR CROSSING DYNAMICS

In previous chapters we set out dynamical rules that encode the topology conservation of the Reidemeister moves on bow diagrams. The aim is now to consider some form of stochastic dynamics subject to these rules, in order to study relevant dynamical quantities. In Section 5.1 we shall provide an overview of how master equations may be analysed in terms of an operator formalism. A few physical applications (chosen for their relevance to later work) will be considered.

In Section 5.2 we then derive a formalism to describe the dynamics on bow diagrams, drawing on these examples. The purpose there is to explore how the topological constraints affect dynamical quantities and correlations. In particular we shall address the behaviour of densities and correlators of crossings in bow diagrams under the Reidemeister moves.

5.1 Doi's formalism for reaction-diffusion systems: mapping master equations onto operators

Theoretical physics often entails descriptions of systems involving processes such as creation, annihilation, diffusion and reactions of particles on a lattice. We shall refer to such systems under the umbrella-term of "reaction-diffusion" systems. The natural language to represent the various states of a lattice system with particles is that of occupation numbers for lattice sites. In statistical physics the aforementioned processes may then be described in terms of stochastic differential equations, such as master equations or Fokker-Planck equations; standard references include the books of Gardiner [59] and Risken [60]. Such differential equations govern the time-evolution of the probability that the system occupies each state, subject to the physical processes (e.g., reaction-diffusion) occurring in the system.

In 1976 Doi presented an elegant formalism for translating master equations (describing the rate of change of probability in bosonic occupation number systems) into a field theoretical description [61]. Peliti later expanded on this work in an extensive article [62] where descriptions of birth and decay processes on a lattice are discussed. This formalism stemming from Doi's work has become a broadly-used tool in the study of reaction-diffusion

systems. Such systems could thus be analysed in the context of powerful field theoretic tools such as renormalisation techniques [63, 64]. Typically the systems considered in this setting are bosonic systems where the occupation number of the lattice sites or states is not restricted in any way. There exist, however, prescriptions for systems with restricted occupation numbers [65, 66]. One may expect that the extension to this formalism simply involves replacing bosonic degrees of freedom with fermionic ones. This is indeed not the case, since fermions encode an anti-symmetry under exchange of particles which is not desired in this setting: we are considering dynamic processes on lattice sites and simply want the occupation number of each site to be restricted. The solution to this involves the introduction of so-called "paulions" which have both fermionic attributes (restricted occupation number) and bosonic attributes (symmetry under exchange of particles). Such systems with occupation number restrictions were studied in the context of aggregation reactions [65, 67] and frameworks were suggested for finding their classical actions in terms of modified Grassmann variables [66]. It may be of interest that master equations for some one-dimensional non-equilibrium systems can be written as Schrödinger equations describing certain quantum chains; this connection is investigated, for instance, in [68] and references therein.

In the following sections we shall provide a brief outline of Doi's formalism and some basic extensions thereof. This illustration will be made at the hand of some standard examples. We shall point out in particular how one may arrive at differential equations for the time-evolution of densities and correlators under stochastic dynamics. This mathematical toolbox will later be useful in the context of recasting the rules for crossing dynamics into master equations and an associated operator formalism.

5.1.1 Mapping master equations onto an operator formalism

Here we present a brief overview of the techniques alluded to above. The discussion is an amalgamate of the early ideas of Doi [61], and the later extensions thereof by Peliti [62], Mattis and Glasser [63] and Täuber *et al.* [64]. In Section 5.1.2 we discuss systems with restricted occupation numbers. Here we begin by considering a bosonic system whose states are labeled completely by a vector of occupation numbers on N lattice sites (n_i is

the occupation number at site $i = 1, \ldots, N$),

$$\mathbf{n} = (n_1, n_2, \ldots, n_i, \ldots, n_N), \quad n_i = 0, 1, 2, \ldots. \tag{5.1}$$

The dynamics of such systems may be understood in terms of master equations that describe the rate of change of the probability for certain configurations,

$$\partial_t P(\mathbf{n}|t) = \sum_{\mathbf{n}'} \omega_{(\mathbf{n}' \to \mathbf{n})} P(\mathbf{n}'|t) - \sum_{\mathbf{n}''} \omega_{(\mathbf{n} \to \mathbf{n}'')} P(\mathbf{n}|t). \tag{5.2}$$

Master equations must be probability conserving, as is seen by summing both sides under the assumption that probabilities are initially normalised. It is further clear that for any choice of non-negative initial probabilities, equation (5.2) cannot generate negative probabilities since the only negative contribution to a given $P(\mathbf{n}|t)$ is proportional to $P(\mathbf{n}|t)$ itself. The first summation in (5.2) runs over all states $\mathbf{n}'$ that could precede the sate $\mathbf{n}$ (henceforth termed "precursor states") and the second over all states $\mathbf{n}''$ that could result from the state $\mathbf{n}$ (henceforth termed "descendant states"). The transition rates between states are encoded in the rate constants ω. These rates need not be simple constant linear quantities, but typically depend on the configurations $\mathbf{n}$, $\mathbf{n}'$ and $\mathbf{n}''$. The right side of equation (5.2) can, of course, be written as $\sum_{\mathbf{n}'} \left\{ \omega_{(\mathbf{n}' \to \mathbf{n})} P(\mathbf{n}'|t) - \omega_{(\mathbf{n} \to \mathbf{n}')} P(\mathbf{n}|t) \right\}$, which immediately implies that the condition of detailed balance is met if each term in this summation vanishes at equilibrium,

$$\omega_{(\mathbf{n}' \to \mathbf{n})} P(\mathbf{n}'|t) = \omega_{(\mathbf{n} \to \mathbf{n}')} P(\mathbf{n}|t). \tag{5.3}$$

It is the specific dynamical processes of the system (diffusion, creation, annihilation, aggregation, etc.) that relate the states $\mathbf{n}$, $\mathbf{n}'$ and $\mathbf{n}''$. As a basic example, we consider diffusion of a particle from site i to site j. A possible precursor state to $\mathbf{n}$ under this process is the state

$$\mathbf{n}' = (n_1, n_2, \ldots, n_i + 1, \ldots, n_j - 1, \ldots, n_N), \tag{5.4}$$

which has one more particle at site i and one less particle at site j than the current sate $\mathbf{n}$. A possible descendant state is

$$\mathbf{n}'' = (n_1, n_2, \ldots, n_i - 1, \ldots, n_j + 1, \ldots, n_N). \tag{5.5}$$

Following the aforementioned references, we now introduce for each site a set of creation and annihilation operators obeying standard bosonic commutation relations,

$$[a_i, a_j^\dagger] = \delta_{i,j} \quad \text{and} \quad [a_i, a_j] = [a_i^\dagger, a_j^\dagger] = 0. \tag{5.6}$$

Here $[A, B] = AB - BA$ is the standard commutator. We introduce the N-site vacuum state as the tensor product of vacua for all sites,

$$\begin{aligned} |\mathbf{0}\rangle &= |0\rangle \otimes |0\rangle \otimes \ldots \otimes |0\rangle \\ &\equiv |n_1 = 0, \ldots, n_N = 0\rangle . \end{aligned} \tag{5.7}$$

This state vanishes under the action of any a_i. A general occupation number state is written as

$$|\mathbf{n}\rangle = \prod_{i=1}^{N} (a_i^\dagger)^{n_i} |\mathbf{0}\rangle = |n_1, \ldots, n_N\rangle . \tag{5.8}$$

The normalisation here differs from that usually considered in a quantum mechanical setting: pre-factors of $\frac{1}{\sqrt{n_i!}}$ have been omitted. This convention has been adopted ubiquitously in the literature pertaining to this method since it simplifies later steps. The states in equation (5.8) are orthogonal with respect to the following inner product,

$$\langle \mathbf{n} | \mathbf{n}' \rangle = \prod_{i=1}^{N} (n_i!)\, \delta_{n_i, n_i'}, \tag{5.9}$$

where the factorials are due to the choice of normalisation. The action of the operators in (5.6) on the occupation number state (5.8) is

$$a_i |\mathbf{n}\rangle = n_i |n_1, \ldots, n_i - 1, \ldots, n_N\rangle \quad \text{and} \quad a_i^\dagger |\mathbf{n}\rangle = |n_1, \ldots, n_i + 1, \ldots, n_N\rangle , \tag{5.10}$$

where the departure from standard normalisation should again be noted. In order to connect the operator formalism and the master equation (5.2) we define a so-called state vector

$$|\phi(t)\rangle \equiv \sum_{\mathbf{n}} P(\mathbf{n}|t)\, |\mathbf{n}\rangle . \tag{5.11}$$

This vector is just a sum over all states of the system, appropriately weighted by the respective (time-dependent) probabilities of the states. The probability of a particular state $\tilde{\mathbf{n}}$ may be recovered through the overlap

$$P(\tilde{\mathbf{n}}|t) = \frac{1}{\prod_i \tilde{n}_i!} \langle \tilde{\mathbf{n}}|\phi(t)\rangle \,. \tag{5.12}$$

As stated, the particular dynamics of a system (i.e., diffusion, reaction or aggregation processes) are captured in the master equation (5.2). Through equation (5.12) it is now, in principle, possible to identify an operator $\hat{L}$ (the Liouvillian) that governs the time-evolution of the state vector,

$$\partial_t \,|\phi(t)\rangle = \hat{L}\,|\phi(t)\rangle \,, \tag{5.13}$$

where $\hat{L}$ encodes the physical processes that relate current, precursor and descendant states in a master equation of the form (5.2). In Section 5.1.3 we shall discuss some basic examples of applications; the reader is also referred once again to references [63, 64] for discussions of pair annihilation / creation, diffusion, aggregation, multi-species processes and higher-order decay processes. It should be noted that the Liouvillian need not be Hermitian in general. Indeed, probability conservation is not encoded through unitary time-evolution as would be the case in a quantum mechanical setting. Instead we define a "sum" state

$$|s\rangle \equiv e^{\sum_{i=1}^{N} a_i^\dagger}\,|\mathbf{0}\rangle = \sum_{\mathbf{n}} |\mathbf{n}\rangle \,. \tag{5.14}$$

This state is a uniform superposition of all possible combinations of occupation numbers, as can be seen by Taylor expansion of the exponential, subject to the commutation relations in (5.6). (Equation (5.14) is a coherent state, and an eigenstate with an eigenvalue of unity of all a_i.) Consequently, due to the orthogonality condition (5.9), $|s\rangle$ has an overlap of unity with any other state of the form (5.8). Supposing the operator $\hat{L}$ is known, the formal solution to (5.13) is

$$|\phi(t)\rangle = e^{\hat{L}t}\,|\phi(0)\rangle \tag{5.15}$$

for some initial state $|\phi(0)\rangle$. We see that

$$1 = \langle s|\phi(t)\rangle = \langle s|\, e^{\hat{L}t}\,|\phi(0)\rangle \,. \tag{5.16}$$

Since this must hold for any choice of initial state, probability conservation is thus enforced by the requirement

$$\langle s|\,\hat{L} = 0, \tag{5.17}$$

which is automatically satisfied by Liouvillians derived from probability-conserving master equation; see [64]. The condition (5.17) on the Liouvillian may be viewed as the analogue of hermiticity in quantum mechanics. The sum state (5.14) allows us to express time-averages of observable quantities $A(\mathbf{n},t)$ that depend on the occupation numbers in the system through the identification

$$\begin{aligned}\langle A(t)\rangle &= \sum_{\mathbf{n}} P(\mathbf{n}|t)A(\mathbf{n}) \\ &= \sum_{\mathbf{n}} P(\mathbf{n}|t)\,\langle s|\,\hat{A}\,|\mathbf{n}\rangle \\ &= \langle s|\,\hat{A}\,|\phi(t)\rangle\,. \end{aligned} \tag{5.18}$$

Here the operator $\hat{A}$ is obtained by the association

$$n_i \leftrightarrow \hat{n}_i \equiv a_i^\dagger a_i. \tag{5.19}$$

The average $\langle\cdot\rangle$ here refers to an average over all realisations of the stochastic dynamics encoded in the master equation. It further follows from (5.13) and (5.17) that

$$\begin{aligned}\partial_t\langle A(t)\rangle &= \langle s|\,\hat{A}\hat{L}\,|\phi(t)\rangle \\ &= \langle s|\,[\hat{A},\hat{L}]\,|\phi(t)\rangle\,. \end{aligned} \tag{5.20}$$

This allows us to calculate the rate of change of averages and correlators of various quantities [65, 66]. In particular we point out for the single-site occupancy ($\hat{n}_I$) that

$$\partial_t\langle\hat{n}_I\rangle(t) = \langle s|\,[a_i^\dagger a_i,\hat{L}]\,|\phi(t)\rangle\,. \tag{5.21}$$

Using this one may further study the time-evolution of the two-site correlator

$$C_{I,J} = \langle n_I n_J\rangle - \langle n_I\rangle\langle n_J\rangle. \tag{5.22}$$

The formalism set out here thus establishes a mapping between master equations and a time-evolution equation formulated in terms of creation and annihilation operators. Not only may we calculate average quantities through (5.20), but the mapping also opens the door to techniques such as time-slicing to obtain a field theoretical representation of equation (5.15) [62, 63, 64, 66] which may be addressed, for instance, through renormalisation methods [64]. It is further possible to calculate the corresponding action through a coherent state path integral. A fairly generic discussion of this procedure for bosonic systems is found in [64].

In this dissertation we wish to express the Reidemeister moves as represented on bow diagrams (see Section 2.7) in terms of Liouvillians that are obtained from the corresponding master equations. As stated, the occupation numbers in bow diagrams are subject to certain restrictions that will need to be encoded into this description. To this end the bosonic commutation relations (5.6) will need to be modified. We briefly discuss these modifications in a general setting in Section 5.1.2.

5.1.2 Doi's formalism for restricted occupation numbers: the paulionic case

Suppose we repeat the analysis of the preceding section, but for systems described by a vector of restricted occupation numbers $\mathbf{n} = (n_1, \ldots, n_N)$ with

$$n_i \in \{0, 1\}, \quad i = 1, \ldots, N. \tag{5.23}$$

We shall now summarise briefly the consequences of this restriction, following the discussions in [63, 64, 65]. It is clear that the bosonic commutation relations (5.6) should be replaced with fermionic ones. We do not, however, require the anti-symmetry associated with standard fermionic states, since we are not interested in the order of particle creation / annihilation. We simply desire the restriction of occupation number and wish to retain symmetry under exchange of particles. Consequently we define operators that commute at different lattice sites but obey fermionic anti-commutation relations on-site. Such species are referred to as paulions in [63], since they may be represented in terms of a set Pauli

matrices that commute off-site. Explicitly we require

$$\begin{aligned} \{a_i, a_j^\dagger\} &= \delta_{i,j}, \\ [a_i, a_j] &= [a_i^\dagger, a_j^\dagger] = 0, \\ a_i^2 &= (a_i^\dagger)^2 = 0, \\ [a_i, a_j^\dagger] &= \delta_{i,j}(1 - 2a_i^\dagger a_i). \end{aligned} \tag{5.24}$$

Here $\{A, B\} = AB + BA$ is used to denote the standard anti-commutator. The last line of equation (5.24) is easily seen to be a consequence of the first three, and will be useful in further calculations. These mixed commutation relations preclude the undesired anti-symmetry that results from standard fermionic anti-commutators. Paulions a may be related to standard fermions b through the Jordan-Wigner transformation,

$$a_k = b_k \, e^{i\pi \sum_{m<k} a_m^\dagger a_m}, \tag{5.25}$$

although we shall not use this fact explicitly — see [63] for more details. The exponential factor in (5.25) simply introduces a $(-1)^n$ prefactor that cancels out the corresponding sign change which would arise from permuting one fermion past n other fermions.

Barring the modifications in (5.24), the remainder of the formalism set out in Section 5.1.1 is not altered. In this way states are still labelled by an occupation number vector $|\mathbf{n}\rangle$, constructed as in equation (5.8), except that $n_i \in \{0, 1\}$. The mathematical definition of the sum state $|s\rangle$ from equation (5.14) is unchanged. However, the modified commutation relations (5.24) imply that this state is no longer an infinite superposition. Instead, $|s\rangle$ is a superposition (of 2^N terms for N lattice sites) of all possible combinations of occupation numbers that are either 0 or 1 at each site.

The definition of the state vector (5.11), the time-evolution equation (5.13) and the calculation of stochastic averages in equations (5.18) and (5.20) are all unchanged. Any expansions of exponentials of the operators from (5.24) will truncate after the first order term, since all operators square to zero. Conveniently the occupation number restriction further implies that all factorials that arise in the inner product (5.9) for the bosonic case need not be considered explicitly for paulions; this also holds for the mapping from the state vector to the probabilities in equation (5.12). The specific dynamics of such a system (and

the corresponding Liouvillian) would have to include the restriction of occupation numbers; see, for instance, [65]. To illustrate the differences between bosonic and paulionic systems in this setting, we shall consider a few examples of dynamical processes in the next section.

5.1.3 Examples of Doi's formalism applied to dynamical processes

Here we briefly illustrate the concepts of Section 5.1.1 through applications to specific physical processes. In particular, we point out the differences between the bosonic and paulionic descriptions. Throughout we shall assume that we are dealing with a single species (described in terms of operators a_i and $a_i^\dagger$) living on a lattice with N sites. The following ideas will be developed for the application to crossing dynamics later.

5.1.3.1 Diffusion

Diffusion on a lattice may be viewed as hopping of particles between nearest-neighbouring sites i and j. We base the following discussion loosely on references [64] and [66].

Bosonic case

For a bosonic system, the master equation that describes this process would be

$$\partial_t P(\mathbf{n}|t) = D \sum_{<i,j>} \{(n_i+1)P(\ldots, n_i+1, n_j-1, \ldots|t) - n_i P(\mathbf{n}|t)\}\,. \tag{5.26}$$

The summation is implied to be over nearest-neighbour sites, and could also be written as $\sum_i \sum_{j(i)}$ where $j(i)$ are nearest neighbouring sites of i. Above, D is some diffusion constant. The first term on the right indicates probability flux *into* state $|\mathbf{n}\rangle$. This term captures the possible precursor states of the state $|\mathbf{n}\rangle$ (see (5.4)), since diffusion from i to j can only happen from a precursor state where there is one more particle at i and one less at j; the (n_i+1) encodes that any one of the particles could undergo this diffusion process. The second term on the right indicates probability flux *out of* state $|\mathbf{n}\rangle$ through this process, which clearly only depends on the number of particles at site i: in the bosonic case there is no restriction on the descendant state. By considering the mapping in equation (5.12), one may deduce that the Liouvillian corresponding to the bosonic diffusion master equation (5.26) is

$$\hat{L}_{\text{diff., bos.}} = D \sum_{<i,j>} \{a_j^\dagger a_i - a_i^\dagger a_i\}, \tag{5.27}$$

where the ladder operators obey the bosonic relations (5.6). Note that it is the *backward* action of $\hat{L}$ and the factorials in (5.12) that generate the appropriate prefactors in equation (5.26). It is easy to verify that this Liouvillian is probability conserving through equation (5.17) since

$$\langle s|\, a_j^\dagger a_i = \langle s|\, a_i = \langle s|\, a_i^\dagger a_i. \tag{5.28}$$

This follows from the fact that $\langle s|$ is an infinite superposition of (bosonic) occupation numbers which is unaffected by laddering down once at any site k through $\langle s|\, a_k^\dagger$. We may now calculate, for instance, the average occupation number at site I subject to (5.27) through equation (5.20). We explain here explicitly the steps omitted in the results of [66],

$$\begin{aligned}
\partial_t \langle \hat{n}_I \rangle &= \langle s|\, [\hat{n}_I, \hat{L}_{\text{diff., bos.}}]\, |\phi(t)\rangle \\
&= D \sum_{i(I)} \langle s|\, a_I^\dagger a_i - a_i^\dagger a_I\, |\phi(t)\rangle \\
&= D \sum_{i(I)} \langle s|\, a_i^\dagger a_i - a_I^\dagger a_I\, |\phi(t)\rangle \\
&= D \sum_{i(I)} \{\langle \hat{n}_i \rangle - \langle \hat{n}_I \rangle\}\,.
\end{aligned} \tag{5.29}$$

Here the summation is over sites i that are nearest neighbours to I. The result is a standard discrete diffusion equation where a positive contribution to $\langle \hat{n}_I \rangle$ can only occur if neighbouring sites $i(I)$ are occupied, and a negative contribution to $\langle \hat{n}_I \rangle$ can only occur if there are particles present at site I.

A similar calculation may be performed for the two-site correlator (5.22); we cite the result of [66],

$$\begin{aligned}
\partial_t C_{I,J}(t) &= D \sum_{k(I)} (C_{I,k} - C_{I,J}) + D \sum_{k(J)} (C_{k,J} - C_{I,J}) \\
&\quad - D\, \delta_{<I,J>}\, (\langle n_I \rangle + \langle n_J \rangle - 2\langle n_I n_J \rangle) \\
&\quad + D\, \delta_{I,J} \sum_{k(I)} (\langle n_I \rangle + \langle n_k \rangle - 2\langle n_I n_k \rangle).
\end{aligned} \tag{5.30}$$

Here $\delta_{<I,J>}$ is the Kronecker delta function for nearest-neighbouring sites I and J.

Paulionic case

For the paulionic case the diffusion master equation reads

$$\partial_t P(\mathbf{n}|t) = D \sum_{<i,j>} \{(n_i+1)P(\ldots,n_i+1,n_j-1,\ldots|t) - (1-n_j)n_i P(\mathbf{n}|t)\}\,. \tag{5.31}$$

In contrast to the bosonic case (5.26) there is a pre-factor $(1-n_j)$ in the second term. This enforces diffusion from i to j can only occur *if site j is unoccupied*. By implication, the descendant state undergoes a selection that is absent in the bosonic case. Correspondingly, the Liouvillian needs to be modified,

$$\hat{L}_{\text{diff., paul.}} = D \sum_{<i,j>} \{a_j^\dagger a_i - a_j a_j^\dagger a_i^\dagger a_i\}, \tag{5.32}$$

where the operators now obey the paulionic commutation relations (5.24). The inclusion of the operator $a_j a_j^\dagger$ to the second term generates the aforementioned pre-factor $(1-n_j)$. The selection of descendant states in the master equation is thus modified through the occupation number restriction. We note that the other pre-factors in the master equation are unchanged, but now subject to the constraint $n_i \in \{0,1\}\ \forall i$.

Formally, average quantities may be computed as for the bosonic case but while using the paulionic relations (5.24) instead of the bosonic relations (5.6). This implies that the calculation of commutators with the Liouvillian (see (5.20)) requires more care. Furthermore, for paulions it is no longer true that $\langle s|\, a_k^\dagger = \langle s|\ \forall k$. Instead we note for paulions that

$$\langle s|\, a_k^\dagger = \langle s|\, a_k a_k^\dagger \quad \text{and} \quad \langle s|\, a_k = \langle s|\, a_k^\dagger a_k. \tag{5.33}$$

This is easily proven by considering a single paulion for which $|s\rangle = |0\rangle + |1\rangle$. Here

$$a^\dagger a\,|s\rangle = a^\dagger\,|0\rangle = |1\rangle = a^\dagger\,|s\rangle\,. \tag{5.34}$$

The paulionic diffusion Liouvillian (5.32) is also probability conserving, since

$$\begin{aligned}\langle s|\,\hat{L}_{\text{diff., paul.}} &= D\sum_{<i,j>}\langle s|\,\{a_j^\dagger a_i - a_j a_j^\dagger a_i^\dagger a_i\}\\ &= D\sum_{<i,j>}\langle s|\,\{a_j^\dagger a_i - a_j^\dagger a_i\}\\ &= 0,\end{aligned} \tag{5.35}$$

where we have used (5.33). Despite the departures from the bosonic case, it is easy to verify that the equation for the density at site I is unchanged,

$$\begin{aligned}\partial_t\langle\hat{n}_I\rangle &= \langle s|\,[\hat{n}_I,\hat{L}_{\text{diff., paul.}}]\,|\phi(t)\rangle\\ &= D\sum_{i(I)}\langle s|\,a_I^\dagger a_i - a_i^\dagger a_I\,|\phi(t)\rangle\\ &= D\sum_{i(I)}\langle s|\,a_I a_I^\dagger a_i^\dagger a_i - a_i a_i^\dagger a_I^\dagger a_I\,|\phi(t)\rangle\\ &= D\sum_{i(I)}\{\langle\hat{n}_i\rangle - \langle\hat{n}_I\rangle\}\,,\end{aligned} \tag{5.36}$$

where we first used (5.33) and then identified $a_i a_i^\dagger = 1 - a_i^\dagger a_i = 1 - \hat{n}_i$. Indeed, for a non-interacting diffusion system the differences between restricted and unrestricted occupation numbers is only seen on the level of correlators [66]. We omit this result.

5.1.3.2 Particle creation and annihilation

In Section 5.1.3.1 we discussed both the master equations and Liouvillians for particle diffusion. Here we shall only present the Liouvillians that are involved in creation and annihilation processes, and indicate how they select possible precursor and descendant states for the process of creating or annihilating a particle at site i. Again we shall contrast the bosonic and paulionic cases.

Bosonic case

The master equation encoding the process of creation of a boson at site i is

$$\partial_t P(\mathbf{n}|t) = g\sum_i\{P(\ldots,n_i-1,\ldots|t) - P(\mathbf{n}|t)\}\,, \tag{5.37}$$

where g determines the rate of creation. The first term indicates that the precursor state to

creating a particle at i must have one less particle at that site. The second term indicates that system can exit the current state through creation of a particle at site i without any restrictions, since we are dealing with bosons. These conditions are encoded in the following Liouvillian,

$$\hat{L}_{\text{cr.,bos.}} = g \sum_{i=1}^{N} \left(a_i^\dagger - 1 \right), \tag{5.38}$$

as found in [64]. This mapping is easily established through (5.10) and (5.12).

For boson annihilation at site i the master equation is

$$\partial_t P(\mathbf{n}|t) = h \sum_i \left\{ (n_i + 1) P(\ldots, n_i + 1, \ldots |t) - n_i P(\mathbf{n}|t) \right\}, \tag{5.39}$$

where h is a rate constant. The first term in the summation ensures that the precursor state to annihilating a particle at i must have one more particle at that site. Any of the $n_i + 1$ particles could be annihilated, hence the prefactor. The second term shows that the system can only leave the current state through annihilation at site i if there is indeed a particle at this site; this can happen in n_i ways. Again we may map this equation onto a corresponding Liouvillian through (5.10) and (5.12),

$$\hat{L}_{\text{an.,bos.}} = h \sum_{i=1}^{N} \left(a_i - a_i^\dagger a_i \right). \tag{5.40}$$

Paulionic case

In the paulionic case we need to consider how occupation number restrictions affect the form of the Liouvillians. We present here some extensions to the results of [64]. If $n_i \in \{0, 1\}\ \forall i$, it is clear that a particle can only be created at site i if this site is previously unoccupied. The paulionic Liouvillian (analogous to (5.38) for this process is

$$\hat{L}_{\text{cr.,paul.}} = g \sum_{i=1}^{N} \left(a_i^\dagger - a_i a_i^\dagger \right). \tag{5.41}$$

The first term in the summation remains unchanged: we still require a precursor state that has one less particle at site i. Since $(a_i^\dagger)^2 = 0$ (see (5.24)), it is clear that the precursor state must indeed be unoccupied at i, as required. The second term, however is altered: a paulion can only be created at site i if this site is unoccupied. This is ensured by the

operator $a_i a_i^\dagger = 1 - a_i^\dagger a_i$.

For the annihilation to occur at site i, the only requirement is that some particle must be at this site. Consequently the paulionic Liouvillian for this process is the same as the bosonic operator in (5.40),

$$\hat{L}_{\text{an.,paul.}} = h \sum_{i=1}^{N} \left(a_i - a_i^\dagger a_i \right). \tag{5.42}$$

As with bosons, the precursor state to annihilation of a particle at i must have one more particle at this site. This is ensured by the first term in (5.42), and the occupation number restriction is enforced by $a_i^2 = 0$; again, see (5.24). The second term again indicates that the system can only depart from the current state through creation of a particle at i if indeed there is a particle at this site; this is enforced by the number operator $a_i^\dagger a_i$ which has eigenvalues of 0 or 1 for paulions.

5.1.3.3 Other processes

For the purposes of this dissertation, the illustrative examples of diffusion and creation / annihilation suffice. The formalism of Doi may however be applied to a multitude of other processes, including (but not limited to) aggregation ($A + A \to A$) and multi-particle birth and decay processes ($0 \leftrightarrow A^m$, $m \geq 2$). For detailed discussions, see [63, 64] and the references therein.

5.1.3.4 Multiple species

It is further possible to generalise the above discussions to processes involving multiple species. Examples include multi-species reactions ($A + B \to 0$ or $A + B \to C$) and "harvesting"-type reactions ($A + B \to A$). The latter are studied, for instance, in the context of aggregation-limited diffusion in [65].

The extension of the framework set out in Sections 5.1.1 and 5.1.2 is easy. For two species, A and B we define independent creation and annihilation operators a_i, $a_i^\dagger$, b_i and $b_i^\dagger$. These operators are independent in that all operators for species A commute with all operators for species B, but operators for each species individually obey the on-site bosonic or paulionic commutation relations, as in (5.6) and (5.24), respectively. Corresponding Liouvillians can now be defined in terms of these operators, allowing the calculation of

various quantities as set out above.

5.2 Reidemeister moves viewed as stochastic dynamics: Occupation numbers, master equations and Liouvillians for bow diagrams

In Section 2.7 we illustrated how the crossings of a particular knot may be captured in a bow diagram, and derived rules on these diagrams that encode topology conservation through the Reidemeister moves. In this section we show that bow diagrams can be labelled in terms of occupation numbers, and translate aforementioned dynamical rules into a form of stochastic dynamics through Doi's formalism.

We begin by noting that a given bow diagram can be represented by a set of occupation numbers,

$$\Lambda = \{N_{i,j,\sigma}\}, \tag{5.43}$$

where

- $i, j = 1, 2, \ldots, N$ label two positions on the line of a bow diagram that has been discretised into N sites,
- $i \neq j$ and $i < j$ are assumed (ordering convention),
- $\sigma \in \{+, -\}$ represents the sign of a particular bow,
- $N_{i,j,\sigma} = 1$ if there exists a bow of species σ between sites i and j.

Here Λ is the analogue of the vector of occupation numbers $\mathbf{n}$ from (5.1). The restrictions on occupation numbers for bow diagrams, as discussed in Section 2.7, imply that, for some $i < j$,

$$\begin{aligned} &N_{i,j,\sigma} \in \{0, 1\}, \\ &N_{i,j,\sigma} = 1 \implies N_{i,k,\sigma'} = 0 \;\forall\; k \neq j,\; \forall \sigma', \quad \text{and} \\ &\sum_{k(<i)} \sum_{\sigma} N_{k,i,\sigma} + \sum_{k(>i)} \sum_{\sigma} N_{i,k,\sigma} \leq 1. \end{aligned} \tag{5.44}$$

(In the second line it is implied that the same conditions hold on $N_{k,i,\sigma'}$ if $k < i$.)

The aim now is to formulate a master equation that determines the rate of change of

the probability for a configuration Λ,

$$\partial_t P(\Lambda|t) = \sum_{\Lambda'} \omega_{(\Lambda' \to \Lambda)} P(\Lambda'|t) - \sum_{\Lambda''} \omega_{(\Lambda \to \Lambda'')} P(\Lambda|t). \tag{5.45}$$

As for the examples discussed in Section 5.1, the first term on the right is a summation over all possible "precursor" states Λ', which could evolve *into* the state Λ. The second term is a summation over all possible "descendant" states Λ'', which could evolve *from* the state Λ. The ωs are transition rates between these various states, and may depend in a non-trivial way on the Λ, Λ' and Λ''. It is clear that the precursor and descendant states must be related to Λ through the Reidemeister moves on bow diagrams, as set out in Chapter 2.

In the next section we explicate how occupation number states corresponding to (5.43) may be defined, how the restriction on occupation numbers may be encoded through appropriate operator relations, and how we may define Liouvillians to represent the various Reidemeister moves.

5.2.1 Operator representation of bow diagrams as occupation number states

In order to encode the occupation number restrictions for bow diagrams, as in (5.44), we shall require two species of paulions; see Section 5.1.3.4. Accordingly, we choose the host space for our states as a tensor product of the state spaces for these two species,

$$\mathcal{H} = \mathcal{S} \otimes \mathcal{B}. \tag{5.46}$$

The space $\mathcal{S}$ is spanned by states $|\mathbf{n}_s\rangle$ that are labelled by a vector $\mathbf{n}_s = (n_1, n_2 \ldots, n_N)$ which contains the individual occupation occupation numbers for bow feet at single sites on the line of the bow diagram, as with the vector (5.1). Since we restrict $n_i \in \{0, 1\}$ in bow diagrams, $\dim(\mathcal{S}) = 2^N$. The space $\mathcal{B}$ is spanned by states $|\mathbf{n}_b\rangle$ that are labelled by the numbers $\{n_{i,j,\sigma}\}$ ($i, j = 1, \ldots, N$ and $\sigma = \pm 1$), which indicate the bows between sites and their species. Unless otherwise stated, it is implied that $i < j$ for a given $n_{i,j,\sigma}$. Since there are two possible species and we want to choose two of N sites for each bow, $\dim(\mathcal{B}) = 2\binom{N}{2} = N(N-1)$.

These states are defined in terms of paulionic creation operators $a_i^\dagger$ and $b_{i,j,\sigma}^\dagger$ akin to

those in equation (5.24), such that

$$|\mathbf{n}_s\rangle = \prod_i (a_i^\dagger)^{n_i} |\mathbf{0}\rangle_{\mathcal{S}} \tag{5.47}$$

and

$$|\mathbf{n}_b\rangle = \prod_{i,j,\sigma} (b_{i,j,\sigma}^\dagger)^{n_{i,j,\sigma}} |\mathbf{0}\rangle_{\mathcal{B}}\,. \tag{5.48}$$

Here the vaccum states are the vacuua of the spaces $\mathcal{S}$ and $\mathcal{B}$, respectively. The states in equation (5.47) are orthogonal with respect to the usual inner product (5.9) — naturally subject to the occupation number restriction. The states in equation (5.48) are orthogonal with respect to the inner product

$$\langle \mathbf{n}_b | \mathbf{n}_b' \rangle = \prod_{i,j=1}^{N} \prod_{\sigma=\pm} \delta_{n_{i,j,\sigma}, n'_{i,j,\sigma}}. \tag{5.49}$$

The creation operators and the corresponding annihilation operators obey paulionic commutation relations, i.e., if *all* indices on two operators are equal they anti-commute, otherwise they commute. For the operators on $\mathcal{S}$ this is simply given by (5.24). For the operators on $\mathcal{B}$ we have

$$\begin{aligned}
\{b_{i,j,\sigma}, b_{i',j',\sigma'}^\dagger\} &= \delta_{i,i'}\,\delta_{j,j'}\,\delta_{\sigma,\sigma'}, \\
[b_{i,j,\sigma}, b_{i',j',\sigma'}] &= [b_{i,j,\sigma}^\dagger, b_{i',j',\sigma'}^\dagger] = 0, \\
(b_{i,j,\sigma})^2 &= (b_{i,j,\sigma}^\dagger)^2 = 0, \\
[b_{i,j,\sigma}, b_{i',j',\sigma'}^\dagger] &= \delta_{i,i'}\,\delta_{j,j'}\,\delta_{\sigma,\sigma'}\,(1 - 2b_{i,j,\sigma}^\dagger b_{i,j,\sigma}).
\end{aligned} \tag{5.50}$$

This may be interpreted as the three-index version of paulions, i.e., on-site fermions that commute off-site which ensures that each site has a restricted occupancy of 0 or 1, but that the order of creation of particles does not affect the symmetry of a particular state. It is further implied that any operator on $\mathcal{S}$ commutes with any operator on $\mathcal{B}$.

From (5.46) it is evident that any state in $\mathcal{H}$ may be written as

$$|\mathbf{n}_s\rangle \otimes |\mathbf{n}_b\rangle \in \mathcal{H}, \quad \text{with} \quad |\mathbf{0}\rangle_{\mathcal{H}} \equiv |\mathbf{0}\rangle = |\mathbf{0}\rangle_{\mathcal{S}} \otimes |\mathbf{0}\rangle_{\mathcal{B}}\,. \tag{5.51}$$

We note that the operator relations in (5.50) alone are not sufficient to encode the required exclusion statistics for bow diagrams. We require that a given site on the bow diagram cannot be occupied by more than one bow foot. In order to encode these conditions (see equation (5.44)) fully, we further need to restrict ourselves to a particular subspace of $\mathcal{H}$. To this end we define the composite operators

$$c_{i,j,\sigma} = a_i a_j b_{i,j,\sigma} \tag{5.52}$$

and their adjoints

$$c^\dagger_{i,j,\sigma} = a^\dagger_i a^\dagger_j b^\dagger_{i,j,\sigma}. \tag{5.53}$$

The action on the vacuum of $\mathcal{H}$ is defined as

$$c^\dagger_{i,j,\sigma} |\mathbf{0}\rangle = |0, \ldots, n_i = 1, 0, \ldots, n_j = 1, \ldots, 0\rangle \otimes |0, \ldots, n_{i,j,\sigma} = 1, 0, \ldots, 0\rangle . \tag{5.54}$$

Clearly the operators in equations (5.52) and (5.53) are only non-zero if $i \neq j$, due to the paulionic nature of the as. For the same reason it is further evident that for $k, j > i$, $k \neq j$,

$$c^\dagger_{i,j,\sigma} c^\dagger_{i,k,\sigma} = 0, \tag{5.55}$$

with a corresponding condition holding for the annihilation operators. Avoiding explicit ordering of indices, one could make the more general statement that

the product of any two $c^\dagger$s that share a position label is zero; similarly for the cs.

It is this property of the compound operators (5.52) and (5.53) that captures the important restrictions on occupation numbers for bow diagrams, as in (5.44) — we reiterate that the operator relations (5.50) alone would not be sufficient to achieve this. To see this we define super-occupation numbers,

$$N_{i,j,\sigma} = n_i \, n_j \, n_{i,j,\sigma}, \tag{5.56}$$

which count the compound species created by the operators in (5.53): there must be an a-particle at *each* site i and j, *and* there must be a bow of species σ between i and j in order for $N_{i,j,\sigma} = 1$. It is not difficult to see that this set of super-occupation numbers obeys the conditions (5.44). The physical interpretation of the single-site occupation numbers n_i

pertains to the presence of *some* bow-foot at site i on the bow diagram, where the other end of the bow could be at *any other* site. The bow occupation numbers $n_{i,j,\sigma}$ pertain to the presence of a bow of species σ between sites i and j. Thus if $N_{i,j,\sigma} = 1$, three conditions must hold:

- there must be a bow-foot at site i,
- there must be a bow-foot at site j, and
- there must be a bow (of species σ) connecting sites i and j.

To the occupation number label Λ of a given bow diagram (as in equation (5.43)), we now associate the occupation number state

$$|\Lambda\rangle = \prod_{i,j,\sigma} (c^{\dagger}_{i,j,\sigma})^{N_{i,j,\sigma}} \, |\mathbf{0}\rangle \, . \tag{5.57}$$

This is in analogy with (5.8). We further define a time-dependent state vector as in (5.11),

$$|\phi(t)\rangle \equiv \sum_{\Lambda} P(\Lambda|t) \, |\Lambda\rangle \, , \tag{5.58}$$

from which the probabilty of a particular configuration Λ' may be obtained through

$$P(\Lambda'|t) = \langle \Lambda'|\phi(t)\rangle \, . \tag{5.59}$$

Equation (5.59) again provides the link between the master equation and the operator representation thereof, as set out in Section 5.1.1. This enables us to write down the Liouvillian $\hat{L}$ for a given physical process so that formally

$$|\phi(t)\rangle = e^{\hat{L}t} \, |\phi(0)\rangle \tag{5.60}$$

for some initial state $|\phi(0)\rangle$ of the system. Lastly we need to define a sum state on the space $\mathcal{H}$. In analogy to equation (5.14) this is simply a uniform superposition of all possible occupation number states that span $\mathcal{H}$,

$$|s\rangle = e^{\sum_i a^{\dagger}_i + \sum_{i,j,\sigma} b^{\dagger}_{i,j,\sigma}} \, |\mathbf{0}\rangle \, . \tag{5.61}$$

Given a Liouvillian, we can describe the time-evolution of quantities $\hat{A}$ as in equation (5.20),

$$\partial_t \langle A(t) \rangle = \langle s | \, [\hat{A}, \hat{L}] \, | \phi(t) \rangle \, . \tag{5.62}$$

Here the quantity A could be some function of the super-occupation numbers $N_{i,j,\sigma}$, the bow-occupation numbers $n_{i,j,\sigma}$ or the single-site occupation numbers n_i. Correspondingly the operator $\hat{A}$ would then be a function of the respective number operators

$$\hat{N}_{i,j,\sigma} \equiv c^\dagger_{i,j,\sigma} c_{i,j,\sigma}, \quad \hat{n}_{i,j,\sigma} \equiv b^\dagger_{i,j,\sigma} b_{i,j,\sigma}, \quad \text{and} \quad \hat{n}_i \equiv a^\dagger_i a_i. \tag{5.63}$$

This allows us to investigate the dynamical behaviour of densities and correlators of crossings on arc-segments.

5.2.2 The physical subspace $\mathcal{P} \subset \mathcal{H}$ and physical sum state

The "creation of bows" on the vacuum state of $\mathcal{H}$ with the compound operators $c^\dagger_{i,j,\sigma}$ — see (5.53) and (5.57) — ensures that the requirements for valid bow diagrams, as set out in equation (5.44), are encoded into the physical states as required. Accordingly, we define the subspace $\mathcal{P} \subset \mathcal{H}$ of "physical" states as the span of all possible states of the form (5.57) (i.e., states created by the action of the composite operators (5.53) on the vacuum in $\mathcal{H}$). The state $a^\dagger_i b^\dagger_{i,j,\sigma} |\mathbf{0}\rangle$ would, for instance, not lie in $\mathcal{P}$, since the j index on the $b^\dagger$ is not paired with a corresponding $a^\dagger_j$.

If we assume that $|\phi(0)\rangle \in \mathcal{P}$, and that the Liouvillian leaves $\mathcal{P}$ invariant, then (5.60) implies $|\phi(t)\rangle \in \mathcal{P}$. It is thus sufficient to restrict our sum state (5.61) to physical states,

$$|s_{\mathcal{P}}\rangle = e^{\sum_{i,j,\sigma} c^\dagger_{i,j,\sigma}} |\mathbf{0}\rangle \, . \tag{5.64}$$

Instead of (5.62) we may thus write

$$\partial_t \langle A(t) \rangle = \langle s_{\mathcal{P}} | \, [\hat{A}, \hat{L}] \, | \phi(t) \rangle \, . \tag{5.65}$$

Note that the set theoretic complement of $\mathcal{P}$, denoted as $\bar{\mathcal{P}}$ is *not* a vector space. To see this, take states $\phi_1 \in \mathcal{P}$ and $\phi_2 \in \bar{\mathcal{P}}$. It is clear that the states $\phi_\pm = \phi_1 \pm \phi_2$ lie in $\bar{\mathcal{P}}$, but that $\phi_+ + \phi_-$ lies in $\mathcal{P}$. Thus $\bar{\mathcal{P}}$ is not a vector space. Instead, consider the orthogonal

complement of $\mathcal{P}$, denoted as $\mathcal{P}_\perp$, containing all states in $\mathcal{H}$ that are orthogonal to those in $\mathcal{P}$. $\mathcal{P}_\perp$ is indeed a vector space. This distinction is important when considering the form of the identity operator on $\mathcal{H}$ which may be written as the sum of projectors onto $\mathcal{P}$ and $\mathcal{P}_\perp$,

$$\hat{\mathbb{I}}_{\mathcal{H}} = \hat{\mathbb{P}}_{\mathcal{P}} + \hat{\mathbb{P}}_{\mathcal{P}_\perp}. \tag{5.66}$$

The requirement that a given $\hat{L}$ should leave $\mathcal{P}$ invariant thus implies that

$$[\hat{L}, \hat{\mathbb{P}}_{\mathcal{P}}] = 0. \tag{5.67}$$

It is, however, not trivial to write down the projector $\mathbb{P}_{\mathcal{P}}$ explicitly. In the sections to follow, we shall thus simply test the analogous condition that all Liouvillians obey

$$\hat{L}\,|\phi\rangle \in \mathcal{P} \quad \forall\, |\phi\rangle \in \mathcal{P} \tag{5.68}$$

so that equation (5.65) may be used instead of (5.62). Lastly, all Liouvillians must be probability conserving. Assuming that condition (5.68) is met, and the initial state of the system is in $\mathcal{P}$, probability conservation is encoded through the requirement that

$$\langle s_{\mathcal{P}}|\,\hat{L} = 0, \tag{5.69}$$

where it is only necessary to consider the backwards action of $\hat{L}$ on the *physical* sum state (5.64) — compare to equation (5.17).

5.2.3 Important relations of occupation numbers and properties of the physical subspace

We have defined the physical subspace $\mathcal{P}$ as the span of all states created by the action of the compound paulionic creation operators in (5.53) on the vacuum in $\mathcal{H}$. States of this form — see (5.57) — are labelled with super-occupation numbers $N_{i,j,\sigma}$ as defined in (5.56). We consider now some properties for relating super-occupation numbers, bow-occupation numbers and single site occupation numbers of any physical state, thereby encoding properties of bow diagrams.

- $N_{i,j,\sigma} = n_i\, n_j\, n_{i,j,\sigma}$ with n_i, n_j, $n_{i,j,\sigma} \in \{0, 1\}$,

- $n_{i,j,\sigma} = 1 \implies n_i = n_j = 1$ since if $\exists$ a bow between i and j there must be bow feet at these sites,
- $n_{i,j,\sigma} = 0 \not\implies n_i = 0$ or $n_j = 0$ since the absence of a bow between i and j does not imply that feet of other bows may not be at these sites,
- $n_i = 0$ and / or $n_j = 0 \implies n_{i,j,\sigma} = 0$ since the absence of bow feet at sites i and / or j implies that there also cannot be a bow between them, and
- $n_i = 1$ and / or $n_j = 1 \not\implies n_{i,j,\sigma} = 1$ since the presence of bow feet at sites i and j does not imply that there is a bow between them.

Consequently it is clear that $N_{i,j,\sigma} = n_{i,j,\sigma}$. By considering the possible different combinations, one may also conclude that, for instance,

$$n_i \, n_{i,j,\sigma} = n_{i,j,\sigma}. \tag{5.70}$$

This equivalence also holds on the level of the corresponding number operators (5.63), and will aid simplification of later results. This implies that some operators are equivalent on this sub-space. For instance, instead of checking whether there exists some bow that has a foot at site i, one could simply check whether site i is occupied by *some* bow foot, i.e.,

$$\begin{aligned} a_i^\dagger a_i &= \sum_\sigma \left\{ \sum_{k(<i)} b_{k,i,\sigma}^\dagger \, b_{i,k,\sigma} + \sum_{k(>i)} b_{i,k,\sigma}^\dagger \, b_{i,k,\sigma} \right\} \\ &= \sum_\sigma \left\{ \sum_{k(<i)} c_{k,i,\sigma}^\dagger \, c_{i,k,\sigma} + \sum_{k(>i)} c_{i,k,\sigma}^\dagger \, c_{i,k,\sigma} \right\}. \end{aligned} \tag{5.71}$$

Several other examples exist, but all are based on the above properties.

It is further useful to note the following properties of expectation values of the form $\langle \cdot \rangle = \langle s_\mathcal{P} | \cdot | \phi(t) \rangle$:

- $\langle c_{i,k,\sigma} \rangle = \langle c_{i,k,\sigma}^\dagger c_{i,k,\sigma} \rangle = \langle \hat{N}_{i,k,\sigma} \rangle$ since $\langle s_\mathcal{P} | \, c_{i,k,\sigma} = \langle s_\mathcal{P} | \, c_{i,k,\sigma}^\dagger c_{i,k,\sigma}$ (in analogy to (5.28)),
- similarly $\langle c_{i,k,\sigma}^\dagger \rangle = \langle c_{i,k,\sigma} c_{i,k,\sigma}^\dagger \rangle$,
- $\langle a_i \rangle \neq \langle a_i^\dagger a_i \rangle$ since $\langle s_\mathcal{P} | \, a_i \neq \langle s_\mathcal{P} | \, a_i^\dagger a_i$,

- $\langle \hat{N}_{i,k,\sigma} c_{i,j,\sigma'} \rangle = \langle a_i^\dagger a_i a_k^\dagger a_k b_{i,k,\sigma}^\dagger b_{i,k,\sigma} a_i a_j b_{i,j,\sigma'} \rangle = 0 \ \forall j,k,\sigma,\sigma'$ since $a_i^2 = 0$,
- similarly $\langle c_{i,j,\sigma'} \hat{N}_{i,k,\sigma} \rangle = \langle \hat{N}_{i,k,\sigma} c_{i,j,\sigma'}^\dagger \rangle = \langle c_{i,j,\sigma'}^\dagger \hat{N}_{i,k,\sigma} \rangle = 0$, due to the states that the number operators select and the cs and $c^\dagger$s annihilate or create when acting on $\langle s_{\mathcal{P}}|$,
- $\langle c_{i,j,\sigma} c_{i,j,\sigma}^\dagger \rangle = \langle a_i a_i^\dagger a_j a_j^\dagger b_{i,j,\sigma} b_{i,j,\sigma}^\dagger \rangle = \langle (1-\hat{n}_i)(1-\hat{n}_j)(1-\hat{n}_{i,j,\sigma}) \rangle \neq \langle 1 - \hat{N}_{i,j,\sigma} \rangle$, and
- $\langle (1-\hat{n}_i)(1-\hat{n}_j)(1-\hat{n}_{i,j,\sigma}) \rangle = \langle (1-\hat{n}_i)(1-\hat{n}_j) \rangle$ due to equation (5.70).

The above properties will be needed for calculations involving equation (5.65).

5.2.4 Reidemeister 0: Liouvillian and dynamical quantities

Here we shall describe the move **R0** on bow diagrams in terms of the operator formalism set out Section 5.2. In Section 2.7.1 this process was explained (see Figure 2.25). We now construct the Liouvillian corresponding to this process, drawing on the example of single-species paulionic diffusion set out in equation (5.32) in Section 5.1.3.1. There the diffusion of a particle from site i to site j was considered. In the context of bow diagrams, we have in mind a bow whose one foot is at site i, and then "diffuses" to site j. The other foot of the bow, at site k, is not involved in this process and remains stationary. The Liouvillian that encodes this is

$$\begin{aligned} \hat{L}_{\mathrm{R0}} \quad = \quad D \sum_{<i,j>} \sum_{\sigma} \Bigg\{ & \sum_{k=1}^{\min(i,j)} \left[c_{k,j,\sigma}^\dagger c_{k,i,\sigma} - a_j a_j^\dagger \, c_{k,i,\sigma}^\dagger c_{k,i,\sigma} \right] \\ & + \sum_{k=\max(i,j)}^{N} \left[c_{j,k,\sigma}^\dagger c_{i,k,\sigma} - a_j a_j^\dagger \, c_{i,k,\sigma}^\dagger c_{i,k,\sigma} \right] \Bigg\}, \end{aligned} \tag{5.72}$$

where D is some diffusion constant. The outer summation runs over nearest neighbours i and j, and the two summations over k account for the two cases $k < i,j$ and $k > i,j$. The latter summations encode that the *same* bow undergoes diffusion of its one foot, and includes all possible bows that could undergo this step. In both cases the operator

$$a_j a_j^\dagger = 1 - a_j^\dagger a_j \tag{5.73}$$

allows diffusion to occur only if the "target site" is unoccupied, as with equation (5.32). It is indeed sufficient to perform this check on the single-site occupancy number n_j, since

$n_j = 0 \implies N_{k,j,\sigma} = 0\ \forall k$ (see (5.44) and Section 5.2.3). The interpretation of the other terms is clear: the positive term "picks out" a pre-cursor state where a bow, whose one foot is based at site k, has its other bow foot at site i, but not at site j. The negative term indicates that the diffusion step out of the current state may only occur if j is unoccupied and there is some bow with a foot at site i. It is further evident that the Liouvillian in equation (5.72) leaves the physical subspace $\mathcal{P}$ invariant: any physical state of the form (5.57) will not be made "unphysical" through the action of $\hat{L}_{\mathrm{R0}}$ since all contributions that add or remove particles (bow feet) are written in terms of cs and $c^\dagger$s. It remains to check that $\hat{L}_{\mathrm{R0}}$ is probability conserving, i.e., that $\langle s_{\mathcal{P}}|\,\hat{L}_{\mathrm{R0}} = 0$ or equivalently $\hat{L}^\dagger_{\mathrm{R0}}\,|s_{\mathcal{P}}\rangle = 0$. Consider the action of the adjoint of the operators in the first line of (5.72) on the physical sum state,

$$\big[\underbrace{c^\dagger_{k,i,\sigma}c_{k,j,\sigma}}_{\equiv\hat{A}} - \underbrace{a_j a^\dagger_j\, c^\dagger_{k,i,\sigma}c_{k,i,\sigma}}_{\equiv\hat{B}}\big]\,|s_{\mathcal{P}}\rangle\,. \tag{5.74}$$

The operator $\hat{A}$ annihilates all terms in $|s_{\mathcal{P}}\rangle$ except the ones for which $N_{k,j,\sigma} = 1$, setting $N_{k,j,\sigma} = 0$ in these terms. Of the remaining terms, all are annihilated except those where $N_{k,i,\sigma} = 0$, and then $N_{k,i,\sigma} = 1$ is enforced. What remains are all terms where $N_{k,j,\sigma} = 0$ and $N_{k,i,\sigma} = 1$. The operator $\hat{B}$ annihilates all terms in $|s_{\mathcal{P}}\rangle$ where $n_j = 1$ and also all terms where $N_{k,i,\sigma} = 0$. What remains are all terms where $n_j = 0$ and $N_{k,i,\sigma} = 1$. However, if $N_{k,i,\sigma} = 1$, the two statements $n_j = 0$ and $N_{k,j,\sigma} = 0$ are equivalent for any state in $\mathcal{P}$ since $N_{k,j,\sigma} = 0 \implies n_j = 0$, and conversely ($N_{k,i,\sigma} = 1$ and $n_j = 0$) $\implies N_{k,j,\sigma} = 0$; see again (5.44). Consequently (5.74) is just zero. Similar reasoning applies to the other terms in (5.72), and thus this Liouvillian is indeed probability conserving, as required.

We now calculate some dynamical quantities using the machinery set out in Section 5.1. In particular, we will be interested in occupation numbers, i.e., the eigenvalues of the number operators in (5.63). We repeat here the time-evolution equation for dynamical quantities (5.65),

$$\partial_t\langle A(t)\rangle = \langle s_{\mathcal{P}}|\,[\hat{A},\hat{L}]\,|\phi(t)\rangle = \langle[\hat{A},\hat{L}]\rangle. \tag{5.75}$$

We begin with the single-site number operator $\hat{n}_I = a^\dagger_I a_I$ for a particular site I. This operator clearly commutes with the negative terms of the Liouvillian for **R0** in (5.72). For

$k < i, j$, for instance, we have

$$[\hat{n}_I, a_j a_j^\dagger\, c^\dagger_{k,i,\sigma} c_{k,i,\sigma}] = 0. \tag{5.76}$$

The non-trivial commutators are with the positive terms in (5.72), e.g.,

$$\begin{aligned}[\hat{n}_I, c^\dagger_{k,j,\sigma} c_{k,i,\sigma}] &= a^\dagger_k a_k b^\dagger_{k,j,\sigma} b_{k,i,\sigma}\, [a^\dagger_I a_I, a^\dagger_j a_i] \\ &= a^\dagger_k a_k b^\dagger_{k,j,\sigma} b_{k,i,\sigma}\, \{a^\dagger_j [a^\dagger_I a_I, a_i] + [a^\dagger_I a_I, a^\dagger_j] a_i\}. \end{aligned} \tag{5.77}$$

For the case $k > i, j$ the position labels on the b and $b^\dagger$ would be exchanged. Using the paulionic commutation relations in equation (5.24) we find that

$$\begin{aligned}[a^\dagger_\alpha a_\alpha, a_\beta] &= \delta_{\alpha,\beta}\,(2a^\dagger_\alpha a_\alpha - 1)\, a_\alpha = -\delta_{\alpha,\beta}\, a_\alpha, \quad \text{and} \\ [a^\dagger_\alpha a_\alpha, a^\dagger_\beta] &= a^\dagger_\alpha\, \delta_{\alpha,\beta}\,(1 - 2a^\dagger_\alpha a_\alpha) = \delta_{\alpha,\beta}\, a^\dagger_\alpha. \end{aligned} \tag{5.78}$$

Inserting this into (5.77) and then performing cancellations and relabellings in the summations of the Liouvillian (5.72) in the time-evolution equation yields

$$\begin{aligned}\partial_t \langle \hat{n}_I \rangle_{\mathrm{R0}} = D \sum_\sigma \sum_{i(I)} \Bigg\{ &\sum_{k=1}^{\min(i,I)} \left(\langle c^\dagger_{k,I,\sigma} c_{k,i,\sigma} \rangle - \langle c^\dagger_{k,i,\sigma} c_{k,I,\sigma} \rangle \right) \\ &+ \sum_{k=\max(i,I)}^{N} \left(\langle c^\dagger_{I,k,\sigma} c_{i,k,\sigma} \rangle - \langle c^\dagger_{i,k,\sigma} c_{I,k,\sigma} \rangle \right) \Bigg\}. \end{aligned} \tag{5.79}$$

Here $i(I)$ are again sites i that are nearest neighbours of I. Let us consider a generic term in this expression,

$$\begin{aligned}\langle c^\dagger_{k,I,\sigma} c_{k,i,\sigma} \rangle &= \langle (1 - \hat{n}_k)(1 - \hat{n}_I)(1 - \hat{n}_{k,I,\sigma}) c_{k,i,\sigma} \rangle \\ &= \underbrace{\langle c_{k,i,\sigma} \rangle}_{\langle \hat{N}_{k,i,\sigma} \rangle} - \underbrace{\langle \hat{n}_k c_{k,i,\sigma} \rangle}_{0} - \langle \hat{n}_I c_{k,i,\sigma} \rangle - \langle \hat{n}_{k,I,\sigma} c_{k,i,\sigma} \rangle \\ &\quad + \underbrace{\langle \hat{n}_k \hat{n}_I c_{k,i,\sigma} \rangle}_{0} + \underbrace{\langle \hat{n}_k \hat{n}_{k,I,\sigma} c_{k,i,\sigma} \rangle}_{0} + \langle c_{k,i,\sigma} \underbrace{\hat{n}_I \hat{n}_{k,I,\sigma}}_{\hat{n}_{k,I,\sigma}} \rangle - \underbrace{\langle \hat{N}_{k,I,\sigma} c_{k,i,\sigma} \rangle}_{0} \\ &= \langle \hat{N}_{k,i,\sigma} (1 - \hat{n}_I) \rangle \\ &= \langle \hat{n}_{k,i,\sigma} (1 - \hat{n}_I) \rangle \end{aligned} \tag{5.80}$$

where we have used the fact that $i \neq I$ and also the properties set out in Section 5.2.3. We can now do the summations over k and σ explicitly in (5.79), since we know that $\sum_\sigma(\sum_{k(<i)} \hat{n}_{k,i,\sigma} + \sum_{k(>i)} \hat{n}_{i,k,\sigma}) = \hat{n}_i$. We obtain the simple relation

$$\partial_t \langle \hat{n}_I \rangle_{\mathrm{R0}} = D \sum_{i(I)} \left[\langle \hat{n}_i \rangle - \langle \hat{n}_I \rangle \right], \tag{5.81}$$

which is exactly the same discrete diffusion equation obtained in equation (5.36) for diffusion of a single species of paulions. (The right side above is simply the discrete version of the second order spatial derivative of the density.) We conclude the following important result: the diffusion of bow-feet is a local process, which is insensitive to the location of the non-diffusing bow-feet.

We now calculate the single-site correlator,

$$\partial_t \langle \hat{n}_I \hat{n}_J \rangle_{\mathrm{R0}} = \langle [\hat{n}_I \hat{n}_J, \hat{L}_{\mathrm{R0}}] \rangle. \tag{5.82}$$

Consequently we require commutators of the following type,

$$\begin{aligned}
[\hat{n}_I \hat{n}_J, c^\dagger_{k,j,\sigma} c_{k,i,\sigma}] &= a^\dagger_k a_k b^\dagger_{k,j,\sigma} b_{k,i,\sigma} \, [a^\dagger_I a_I \, a^\dagger_J a_J, a^\dagger_j a_i] \\
&= a^\dagger_k a_k b^\dagger_{k,j,\sigma} b_{k,i,\sigma} \, \{ - \delta_{i,J} a^\dagger_j \hat{n}_I a_i - \delta_{i,I} a^\dagger_j a_i \hat{n}_J + \delta_{j,J} \hat{n}_I a^\dagger_j a_i + \delta_{j,I} a^\dagger_j \hat{n}_J a_i \} \\
&= c^\dagger_{k,j,\sigma} c_{k,i,\sigma} \Big\{ \delta_{i,J} \, \delta_{i,I} + \delta_{j,J} \, \delta_{j,I} - \delta_{j,J} \, \delta_{i,I} - \delta_{j,I} \, \delta_{i,J} \\
&\qquad + \hat{n}_I \, (\delta_{j,J} - \delta_{i,J}) + \hat{n}_J \, (\delta_{j,I} - \delta_{i,I}) \Big\}.
\end{aligned} \tag{5.83}$$

We note that, since $I \neq J$, terms such as $\delta_{i,J} \, \delta_{i,I}$ vanish. Using equation (5.80) we conclude that

$$\begin{aligned}
\partial_t \langle \hat{n}_I \hat{n}_J \rangle_{\mathrm{R0}} &= D \sum_{k \neq i,j} \sum_\sigma \Big\{ - \delta_{<I,J>} \left(\langle \hat{n}_{k,I,\sigma} (1 - \hat{n}_J) \rangle + \langle \hat{n}_{k,J,\sigma} (1 - \hat{n}_I) \rangle \right) \\
&\quad + \sum_{i(J)} \langle \hat{n}_{k,i,\sigma} (1 - \hat{n}_J) \hat{n}_I \rangle + \sum_{j(J)} \langle \hat{n}_{k,J,\sigma} (1 - \hat{n}_j) \hat{n}_I \rangle \\
&\quad + \sum_{i(I)} \langle \hat{n}_{k,i,\sigma} (1 - \hat{n}_I) \hat{n}_J \rangle + \sum_{j(I)} \langle \hat{n}_{k,I,\sigma} (1 - \hat{n}_j) \hat{n}_J \rangle \Big\}.
\end{aligned} \tag{5.84}$$

In the summation over k we have implied the correct ordering of indices on the $\hat{n}$s according

to $k < i, j$ or $k > i, j$. Using the properties from Section 5.2.3 this summation and that over σ may be done explicitly, yielding

$$\begin{aligned}\partial_t \langle \hat{n}_I \hat{n}_J \rangle_{\mathrm{R0}} &= D \Big\{ -\delta_{<I,J>} \left(\langle \hat{n}_I \rangle + \langle \hat{n_J} \rangle \right) \\ &\quad + \sum_{i(J)} \left(\langle \hat{n}_i \hat{n}_I \rangle - \langle \hat{n}_J \hat{n}_I \rangle \right) \\ &\quad + \sum_{i(I)} \left(\langle \hat{n}_i \hat{n}_J \rangle - \langle \hat{n}_I \hat{n}_J \rangle \right) \Big\}. \end{aligned} \tag{5.85}$$

For the case that I and J are not nearest neighbours, a continuum version of this equation would could be written as $\partial_t\, c(x,y) = D'(\frac{\partial^2}{\partial x^2} c + \frac{\partial^2}{\partial y^2} c)$ where D' is some rescaled diffusion constant arising from the continuum limit. If I and J are nearest neighbours, one simply obtains discrete versions of the gradient.

Next we turn to the number operator for bows, $\hat{n}_{I,J,\tilde{\sigma}} = b^\dagger_{I,J,\tilde{\sigma}} b_{I,J\tilde{\sigma}}$. This operator also commutes with the negative terms in Liouvillian (5.72). In analogy to equation (5.77), non-trivial commutators of the following type remain,

$$\begin{aligned}[\hat{n}_{I,J,\tilde{\sigma}}, c^\dagger_{k,j,\sigma} c_{k,i,\sigma}] &= a^\dagger_k a_k a^\dagger_j a_i \, [b^\dagger_{I,J,\tilde{\sigma}} b_{I,J\tilde{\sigma}}, b^\dagger_{k,j,\sigma} b_{k,i,\sigma}] \\ &= a^\dagger_k a_k a^\dagger_j a_i \, \left\{ b^\dagger_{k,j,\sigma} [\hat{n}_{I,J,\tilde{\sigma}}, b_{k,i,\sigma}] + [\hat{n}_{I,J,\tilde{\sigma}}, b^\dagger_{k,j,\sigma}] b_{k,i,\sigma} \right\}. \end{aligned} \tag{5.86}$$

We may now use the relations (5.50) to derive the following condition,

$$\begin{aligned}[\hat{n}_{\alpha,\beta,\sigma}, b_{\gamma,\delta,\sigma'}] &= -\delta_{\alpha,\gamma}\, \delta_{\beta,\delta}\, \delta_{\sigma,\sigma'}\, b_{\alpha,\beta,\sigma}, \quad \text{and} \\ [\hat{n}_{\alpha,\beta,\sigma}, b^\dagger_{\gamma,\delta,\sigma'}] &= \delta_{\alpha,\gamma}\, \delta_{\beta,\delta}\, \delta_{\sigma,\sigma'}\, b^\dagger_{\alpha,\beta,\sigma}. \end{aligned} \tag{5.87}$$

This may be re-inserted into the time-evolution equation for $\hat{n}_{I,J,\tilde{\sigma}}$, and simplified through equation (5.80) to obtain

$$\begin{aligned}\partial_t \langle \hat{n}_{I,J,\tilde{\sigma}} \rangle_{\mathrm{R0}} &= D \sum_\sigma \sum_{<i,j>} \Big\{ \sum_{k=1}^{\min(i,j)} (\delta_{I,k}\, \delta_{\sigma,\tilde{\sigma}}) \, (\delta_{K,j} - \delta_{K,i}) \, \langle \hat{N}_{k,i,\sigma} (1 - \hat{n}_j) \rangle \\ &\quad + \sum_{k=\max(i,I)}^{N} (\delta_{I,k}\, \delta_{\sigma,\tilde{\sigma}}) \, (\delta_{K,j} - \delta_{K,i}) \, \langle \hat{N}_{i,k,\sigma} (1 - \hat{n}_j) \rangle \Big\}. \end{aligned} \tag{5.88}$$

The first line of this equation (the case where $k < i, j$) could be simplified as follows,

$$\begin{aligned}
&\sum_{\sigma}\sum_{<i,j>}\sum_{k(<i,j)} \delta_{I,k}\,\delta_{\sigma,\tilde{\sigma}}\,(\delta_{J,j}-\delta_{J,i})\,\langle \hat{N}_{k,i,\sigma}(1-\hat{n}_j)\rangle \\
&= \sum_{<i,j>}(\delta_{J,j}-\delta_{J,i})\,\langle \hat{N}_{I,i,\tilde{\sigma}}(1-\hat{n}_j)\rangle \\
&= \sum_{i(J)}\langle \hat{N}_{I,i,\tilde{\sigma}}(1-\hat{n}_J)\rangle - \sum_{j(J)}\langle \hat{N}_{I,J,\tilde{\sigma}}(1-\hat{n}_j)\rangle \\
&= \sum_{i(J)}\Big(\langle \hat{N}_{I,i,\tilde{\sigma}}(1-\hat{n}_J)\rangle - \langle \hat{N}_{I,J,\tilde{\sigma}}(1-\hat{n}_i)\rangle\Big). \qquad (5.89)
\end{aligned}$$

Again recalling that $N_{i,j,\sigma} = n_{i,j,\sigma}$ and multiplying out the terms above, we conclude that for the case $k < i, j$

$$\partial_t\langle \hat{n}_{I,J,\tilde{\sigma}}\rangle_{\mathrm{R0}} = D\sum_{i(J)}\Big(\langle \hat{n}_{I,i,\tilde{\sigma}}\rangle - \langle \hat{n}_{I,J,\tilde{\sigma}}\rangle\Big) + D\sum_{i(J)}\Big(\langle \hat{n}_{I,J,\tilde{\sigma}}\hat{n}_i\rangle - \langle \hat{n}_{I,i,\tilde{\sigma}}\hat{n}_J\rangle\Big). \qquad (5.90)$$

The first summation is simply a discrete diffusion equation for the right foot of a bow where the left one is kept fixed — compare to the single-site diffusion equation (5.81). The second summation shows that bow diffusion also involves a correlation between the diffusing bows and the single-site occupancies. The result for $k > i, j$ is trivially obtainable in a similar manner.

Lastly we calculate the correlator for bow occupancies. We shall require the following commutator,

$$\begin{aligned}
[\hat{n}_{I,J,\sigma_1}\,\hat{n}_{K,L,\sigma_2}\,,\,c^{\dagger}_{k,j,\sigma}c_{k,i,\sigma}] &= a^{\dagger}_k a_k a^{\dagger}_j a_i\,[\hat{n}_{I,J,\sigma_1}\,\hat{n}_{K,L,\sigma_2}\,,\,b^{\dagger}_{k,j,\sigma}b_{k,i,\sigma}] \\
&= c^{\dagger}_{k,j,\sigma}c_{k,i,\sigma}\Big\{\big(\delta_{k,K}\,\delta_{j,L}\,\delta_{\sigma,\sigma_2}-\delta_{k,K}\,\delta_{i,L}\,\delta_{\sigma,\sigma_2}\big)\hat{n}_{I,J,\sigma_1} \\
&\quad + \big(\delta_{k,I}\,\delta_{j,J}\,\delta_{\sigma,\sigma_1}-\delta_{k,I}\,\delta_{i,J}\,\delta_{\sigma,\sigma_1}\big)\hat{n}_{K,L,\sigma_2}\Big\}. \qquad (5.91)
\end{aligned}$$

Inserting this into the time-evolution equation (5.75) with the Liouvillian (5.72) we obtain

$$\begin{aligned}
\frac{\partial_t\langle \hat{n}_{I,J,\sigma_1}\hat{n}_{K,L,\sigma_2}\rangle_{\mathrm{R0}}}{D} &= \sum_{i(L)}\Big[\langle \hat{n}_{K,i,\sigma_2}(1-\hat{n}_L)\hat{n}_{I,J,\sigma_1}\rangle - \langle \hat{n}_{K,L,\sigma_2}(1-\hat{n}_i)\hat{n}_{I,J,\sigma_1}\rangle\Big] + \\
&\quad \sum_{i(J)}\Big[\langle \hat{n}_{I,i,\sigma_1}(1-\hat{n}_J)\hat{n}_{K,L,\sigma_2}\rangle - \langle \hat{n}_{I,J,\sigma_1}(1-\hat{n}_i)\hat{n}_{K,L,\sigma_2}\rangle\Big]. \qquad (5.92)
\end{aligned}$$

Comparing this with the bow-diffusion equation (5.89), we note that $\hat{n}_{I,J,\sigma_1}$ is only correlated with $\hat{n}_{K,L,\sigma_2}$ if the bow between sites K and L is undergoing diffusion (and vice versa). Since we are considering only the **R0**-move in this correlator, the expected encoding of the diffusive behaviour is manifest here. This result would lend itself well to a mean field approximation wherein one may decouple bow diffusion terms of the type (5.89) and bow densities.

5.2.5 Boundary conditions on bow diagrams

As set out in Section 2.7 (see Figure 2.24), bow diagrams have periodic boundary conditions subject to a sign change at the boundary. This means that the diffusion of a bow foot across this boundary must result in a sign change of the bow. By implication the Liouvillian for **R0** should technically be augmented with a sign-changing term at the boundary. We shall not do this explicitly here; instead we shall calculate quantities "in the bulk" (i.e., away from this boundary). A corresponding boundary current term could always be included by hand at a later stage.

5.2.6 Reidemeister 1: Liouvillian and dynamical quantities

Reidemeister 1 involves the creation and annihilation of a single bow at nearest-neighbour sites on the line, as stated in Section 2.7.2 (see, in particular, Figure 2.26). The Liouvillian for the bow-creation process is

$$\hat{L}_{\mathrm{R1,cr.}} = g \sum_{i=1}^{N} \sum_{\sigma} \left\{ c^{\dagger}_{i,i+1,\sigma} - c_{i,i+1,\sigma} c^{\dagger}_{i,i+1,\sigma} \right\}, \tag{5.93}$$

where g is some rate constant. The analogies to the paulionic Liouvillian for single-species particle creation (5.41) are clear. The positive term selects all precursor states which do not have a bow at nearest-neighbouring sites i and $i+1$. The negative term ensures that flux out of the current state through creation of a bow may only happen if the current state has no bows at these nearest neighbouring sites. The operator $\hat{L}_{\mathrm{R1,cr.}}$ leaves $\mathcal{P}$ invariant. Now, as for (5.74), we consider the action of the adjoint of the operators in (5.93) on the physical sum state,

$$\big[\underbrace{c_{i,i+1,\sigma}}_{\equiv \hat{A}} - \underbrace{c_{i,i+1,\sigma} c^{\dagger}_{i,i+1,\sigma}}_{\equiv \hat{B}} \big] \, |s_{\mathcal{P}}\rangle \, . \tag{5.94}$$

The operator $\hat{A}$ only retains terms in $|s_{\mathcal{P}}\rangle$ where $N_{i,i+1,\sigma} = 0$, and the same applies to the operator $\hat{B}$. We conclude that the Liouvillian (5.93) is probability conserving.

The Liouvillian for the bow-annihilation process is

$$\hat{L}_{\text{R1,an.}} = h \sum_{i=1}^{N} \sum_{\sigma} \left\{ c_{i,i+1,\sigma} - c^{\dagger}_{i,i+1,\sigma} c_{i,i+1,\sigma} \right\}, \tag{5.95}$$

where h is some rate constant. Here, too, the analogies to the corresponding paulionic Liouvillian for single-species particle annihilation (5.42) are evident. The positive term selects a precursor state with one more bow between sites i and $i+1$ than the current state. The negative term enforces that the current state may only be exited through annihilation of a bow between these sites if indeed such a bow exists. It is easy to verify that the Liouvillian for bow-annihilation (5.95) also leaves the physical subspace $\mathcal{P}$ invariant and is probability conserving, as required.

Next we calculate dynamical quantities for the **R1** Liouvillians (5.93) and(5.95). As for **R0**, all number operators commute with the negative parts of both of these Liouvillians. Again we require the several commutators, obtained from the paulionic relations (5.24) and (5.50). For the single-site quantities we need the following,

$$\begin{aligned}
[\hat{n}_I, c^{\dagger}_{i,i+1,\sigma}] &= (\delta_{I,i} + \delta_{I,i+1})\, c^{\dagger}_{i,i+1,\sigma}, \\
[\hat{n}_I, c_{i,i+1,\sigma}] &= -(\delta_{I,i} + \delta_{I,i+1})\, c_{i,i+1,\sigma}, \\
[\hat{n}_I \hat{n}_J, c^{\dagger}_{i,i+1,\sigma}] &= c^{\dagger}_{i,i+1,\sigma} \Big\{ \delta_{i+1,J} \left(\hat{n}_I + \delta_{i+1,I} + \delta_{i,I}\right) + \delta_{i,J} \left(\hat{n}_I + \delta_{i+1,I} + \delta_{i,I}\right) \\
&\qquad + \delta_{i+1,I}\, \hat{n}_J + \delta_{i,I}\, \hat{n}_J \Big\}, \\
[\hat{n}_I \hat{n}_J, c_{i,i+1,\sigma}] &= c_{i,i+1,\sigma} \Big\{ -\delta_{i+1,J} \left(\hat{n}_I + \delta_{i+1,I} - \delta_{i,I}\right) - \delta_{i,J} \left(\hat{n}_I - \delta_{i+1,I} - \delta_{i,I}\right) \\
&\qquad - \delta_{i+1,I}\, \hat{n}_J - \delta_{i,I}\, \hat{n}_J \Big\}.
\end{aligned} \tag{5.96}$$

For the bow quantities we will need the following additional commutators,

$$\begin{aligned}
[\hat{n}_{I,J,\tilde{\sigma}}\,,\,c^{\dagger}_{i,i+1,\sigma}] &= \delta_{I,i}\,\delta_{J,i+1}\,\delta_{\sigma,\tilde{\sigma}}\,c^{\dagger}_{i,i+1,\sigma},\\
[\hat{n}_{I,J,\tilde{\sigma}}\,,\,c_{i,i+1,\sigma}] &= -\delta_{I,i}\,\delta_{J,i+1}\,\delta_{\sigma,\tilde{\sigma}}\,c_{i,i+1,\sigma},\\
[\hat{n}_{I,J,\sigma_1}\,\hat{n}_{K,L,\sigma_2}\,,\,c^{\dagger}_{i,i+1,\sigma}] &= c^{\dagger}_{i,i+1,\sigma}\Big\{\delta_{I,i}\,\delta_{J,i+1}\,\delta_{\sigma_1,\sigma}\,\hat{n}_{K,L,\sigma_2}\\
&\quad +\delta_{K,i}\,\delta_{L,i+1}\,\delta_{\sigma_2,\sigma}\,\hat{n}_{I,J,\sigma_1}\Big\},\\
[\hat{n}_{I,J,\sigma_1}\,\hat{n}_{K,L,\sigma_2}\,,\,c_{i,i+1,\sigma}] &= c_{i,i+1,\sigma}\Big\{-\delta_{I,i}\,\delta_{J,i+1}\,\delta_{\sigma_1,\sigma}\,\hat{n}_{K,L,\sigma_2}\\
&\quad -\delta_{K,i}\,\delta_{L,i+1}\,\delta_{\sigma_2,\sigma}\,\hat{n}_{I,J,\sigma_1}\Big\}. \qquad (5.97)
\end{aligned}$$

Furthermore we know that $\langle c_{i,i+1,\sigma}\rangle = \langle \hat{N}_{i,i+1,\sigma}\rangle = \langle \hat{n}_{i,i+1,\sigma}\rangle$ and $\langle c^{\dagger}_{i,i+1,\sigma}\rangle = \langle (1-\hat{n}_i)(1-\hat{n}_{i+1})\rangle$. These results, together with the commutators (5.96) and (5.97), allow us to calculate the time-evolution of several average densities.

We begin with the single-site density. For the creation of a bow we obtain

$$\partial_t\langle \hat{n}_I\rangle_{\mathrm{R1,cr.}} = g\sum_{\sigma}\big[\langle (1-\hat{n}_I)(1-\hat{n}_{I+1})\rangle + \langle (1-\hat{n}_{I-1})(1-\hat{n}_I)\rangle\big]. \qquad (5.98)$$

The interpretation here is clear: the creation of a bow can only increase the single-site density $\hat{n}_I$, and this can only happen if both the site I and one of its neighbours are unoccupied. Saturation effects of the restricted occupancy are evident.

The single-site correlator for the **R1** creation process is found to be

$$\begin{aligned}
\partial_t\langle \hat{n}_I\hat{n}_J\rangle_{\mathrm{R1,cr.}} &= g\sum_{\sigma}\Big\{\delta_{<I,J>}\big[\langle (1-\hat{n}_I)(1-\hat{n}_J)\rangle + \langle (1-\hat{n}_I)(1-\hat{n}_I)\rangle\big]\\
&\quad +\big[\langle (1-\hat{n}_{J-1})(1-\hat{n}_J)\hat{n}_I\rangle + \langle (1-\hat{n}_J)(1-\hat{n}_{J+1})\hat{n}_I\rangle\big]\\
&\quad +\big[\langle (1-\hat{n}_{I-1})(1-\hat{n}_I)\hat{n}_J\rangle + \langle (1-\hat{n}_I)(1-\hat{n}_{I+1})\hat{n}_J\rangle\big]\Big\}. \qquad (5.99)
\end{aligned}$$

This correlator is a complicated function of higher orders of single-site correlators. The first term on the right indicates correlation if I and J are nearest neighbours. The remaining terms show that site occupancy at site I is correlated with an unoccupied site J and one of its unoccupied nearest neighbours, and vice-versa. This makes sense, since the process under consideration here is the creation of bows, which happens at empty nearest-neighbouring sites. Again the saturation brought about by occupancy restrictions is evident. In equation

(5.99) one could, in principle, multiply out the various terms. A continuum version would then include gradient terms and triplet correlator terms.

We now repeat this analysis for the bow-density, obtaining

$$\begin{aligned}\partial_t\langle\hat{n}_{I,J,\tilde{\sigma}}\rangle_{\text{R1,cr.}} &= g\sum_i\sum_\sigma \delta_{I,i}\,\delta_{J,i+1}\,\delta_{\sigma,\tilde{\sigma}}\,\langle c^\dagger_{i,i+1,\sigma}\rangle \\ &= g\,\delta_{<I,J>}\langle(1-\hat{n}_I)(1-\hat{n}_J)\rangle, \end{aligned} \tag{5.100}$$

where the $\delta_{<I,J>}$ ensures that the bow-density $\hat{n}_{I,J,\tilde{\sigma}}$ can only increase through the creation of a bow if indeed I and J are nearest neighbours. It is further clear from the term $\langle(1-\hat{n}_I)(1-\hat{n}_J)\rangle$ that the sites must be unoccupied in order for a bow to be created — the restriction of occupation numbers is manifest.

One may also calculate the correlator for bow quantities,

$$\begin{aligned}\partial_t\langle\hat{n}_{I,J,\sigma_1}\,\hat{n}_{K,L,\sigma_2}\rangle_{\text{R1,cr.}} &= g\Big\{\delta_{<I,J>}\langle(1-\hat{n}_{I,J,\sigma_1})\hat{n}_{K,L,\sigma_2}\rangle \\ &\quad + \delta_{<K,L>}\langle(1-\hat{n}_{K,L,\sigma_2})\hat{n}_{I,J,\sigma_1}\rangle\Big\}. \end{aligned} \tag{5.101}$$

This result may be interpreted as follows: under the **R1**-creation move, two bows are only correlated if the occupancy conditions for a creation move are met. This is ensured by the "$1-n$" terms and the Kronecker delta functions.

Turning to the Liouvillian for the annihilation process, we obtain for the single-site density

$$\partial_t\langle\hat{n}_I\rangle_{\text{R1,an.}} = -h\sum_\sigma\big[\langle\hat{n}_{I,I+1,\sigma}\rangle + \langle\hat{n}_{I-1,I,\sigma}\rangle\big]. \tag{5.102}$$

The implication is that the single-site density $\hat{n}_I$ can only be decreased by the annihilation of a bow if there exists a bow (of either species) that has one foot at site I and another foot at a nearest neighbouring site.

The single-site correlator for the **R1** annihilation process is found to be

$$\begin{aligned}\partial_t\langle\hat{n}_I\hat{n}_J\rangle_{\text{R1,an.}} &= h\sum_\sigma\Big\{\delta_{<I,J>}\big[\langle\hat{n}_{I,J,\sigma}\rangle+\langle\hat{n}_{J,I,\sigma}\rangle\big]\\ &\quad-\big[\langle\hat{n}_{J-1,J,\sigma}\hat{n}_I\rangle+\langle\hat{n}_{J,J+1,\sigma}\hat{n}_I\rangle\big]\\ &\quad-\big[\langle\hat{n}_{I-1,I,\sigma}\hat{n}_J\rangle+\langle\hat{n}_{I,I+1,\sigma}\hat{n}_J\rangle\big]\Big\}. \qquad (5.103)\end{aligned}$$

Unlike equation (5.99) for the creation process, this correlator for the annihilation process is not only a function of higher order single-site correlators. Indeed, the correlation of single sites with bows is evident. The first term on the right indicates correlation if I and J are nearest neighbours. The remaining terms show that site occupancy at site I is correlated with the presence of a bow between J and one of its nearest neighbours, and vice-versa. This makes sense, since the process under consideration here is the annihilation of bows, which can only occur if a bow is present between nearest-neighbouring sites. It is for this reason that correlation to bow number operators (and not just single-site operators) is observed.

For the annihilation process we obtain the following result for the bow density,

$$\begin{aligned}\partial_t\langle\hat{n}_{I,J,\tilde{\sigma}}\rangle_{\text{R1,an.}} &= -h\sum_i\sum_\sigma\,\delta_{I,i}\,\delta_{J,i+1}\,\delta_{\sigma,\tilde{\sigma}}\,\langle c_{i,i+1,\sigma}\rangle\\ &= -h\,\delta_{<I,J>}\langle\hat{n}_{I,J,\tilde{\sigma}}\rangle. \qquad (5.104)\end{aligned}$$

Here it is clear that there must be a bow species $\tilde{\sigma}$ present in order for the **R1** annihilation process to decrease the bow-density $\hat{n}_{I,J,\tilde{\sigma}}$, and this can only happen if I and J are nearest neighbouring sites.

Lastly we calculate the bow correlator for the annihilation process,

$$\begin{aligned}\partial_t\langle\hat{n}_{I,J,\sigma_1}\,\hat{n}_{K,L,\sigma_2}\rangle_{\text{R1,an.}} &= -h\Big\{\delta_{<I,J>}\langle\hat{n}_{I,J,\sigma_1}\,\hat{n}_{K,L,\sigma_2}\rangle\\ &\quad+\;\delta_{<K,L>}\langle\hat{n}_{K,L,\sigma_2}\,\hat{n}_{I,J,\sigma_1}\rangle\Big\}. \qquad (5.105)\end{aligned}$$

Since we are only considering the **R1**-annihilation move, it makes sense that two bows can only be correlated if one of them could be removed through **R1**. This is ensured by the Kronecker delta functions and the occupancy number combinations. In equations (5.104) and (5.105) we note an explicit dependence on the initial conditions: if the initial

configuration is such that two bow feet at sites I and J can never become nearest neighbours through **R0** bow diffusion, then this bow cannot be removed. Here it is instructive to consider the two cases in Figure 5.1.

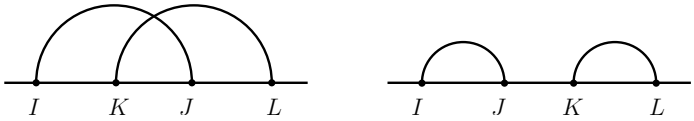

Figure 5.1: Two different initial conditions. In the first case, it is impossible that dynamics under **R0** and **R1** ever result in removal of either bow. In the second case this is not true.

It is thus clear that these dynamics encode the required topology conservation. This makes explicit the dependence on initial conditions (consider, for instance, stochastic evolution of different prime knots such as in Figure 2.29).

To obtain a comprehensive picture of the dynamics it would be instructive to combine the differential equations for the densities or correlators subject to *all* Reidemeister moves considered thus far. This would make explicit the competing effects of annihilation and creation, and may be of particular interest when investigating rate-limiting behaviour of the various dynamical processes.

5.2.7 Reidemeister 2 and 3: first steps and perspective

The Liouvillian for the **R2**-annihilation process is easy to write down,

$$\hat{L}_{\text{R2,an.}} = h \sum_{i=1}^{N} \sum_{j=i}^{N} \sum_{k(i)} \sum_{l(j)} \sum_{\sigma} \left\{ c_{i,j,\sigma} c_{k,l,\sigma} - \underbrace{c^{\dagger}_{i,j,\sigma} c_{i,j,\sigma}}_{\hat{N}_{i,j,\sigma}} \underbrace{c^{\dagger}_{k,l,\sigma} c_{k,l,\sigma}}_{\hat{N}_{k,l,\sigma}} \right\}. \tag{5.106}$$

As required, this Liouvillian leaves $\mathcal{P}$ invariant. Through similar reasoning as in previous sections, it may also be shown to be probability conserving. The first term checks that the precursor state has two neighbouring bows that that are not present in the "current" state. The second term ensures that the current state can only be "exited" if the correct configuration is present.

The creation Liouvillian is more difficult to write down, because we need to count the number of bow-feet between the sites where we are creating the bow pair. This is required in order to get the orientation of the two strands right — see Section 2.7.3. This counting procedure is, of course, extremely non-local. In a very rough approximation one could neglect this non-local counting to obtain

$$\hat{L}_{\mathrm{R2,cr.}} = g \sum_{i=1}^{N} \sum_{j=i}^{N} \sum_{k(i)} \sum_{l(j)} \sum_{\sigma} \left\{ c^{\dagger}_{k,l,\sigma} c^{\dagger}_{i,j,\sigma} - c_{i,j,\sigma} c^{\dagger}_{i,j,\sigma}\, c_{k,l,\sigma} c^{\dagger}_{k,l,\sigma} \right\}, \tag{5.107}$$

which is no more difficult to deal with than the **R2**-annihilation Liouvillian (5.106).

In principle it is now possible to derive a hierarchy of equations for densities and correlators under **R2**, as was done for **R0** and **R1**. The only complication is that various commutators would be more tricky to calculate. One could also write down the Liouvillian for the **R3** move, using the rules set out in Section 2.7.4. This operator would, however, require very many different case checks — recall the various configurations illustrated in Figures 2.20, 2.21 and 2.22.

In principle, it us thus possible to extend this discussion to the higher order Reidemeister moves. This would entail the pairwise nearest-neighbouring creation and annihilation processes set out above, and triplet nearest-neighbouring exchange operations subject to configuration checks.

5.3 Summary and outlook

In this chapter we demonstrated the usefulness of an operator formalism in the description of various dynamical processes. We established an occupation number formalism that captures the restrictions on bow diagrams, and showed explicitly how the moves **R0** and **R1** may be described in terms of operators. The Liouvillians for **R2** were presented, with a suggested approximation to handling the non-local aspects of the creation process. In principle the Liouvillian for **R3** is derivable. In this way, crossings on a single self-entangled loop were described as particles in a quasi-one-dimensional system, subject to motions mapped from the Reidemeister moves. Extension of this description to a complete knot would involve the inclusion of a "current term" that captures the boundary conditions on

bow diagrams.

We have set out here a complete systemisation from which densities and correlators are derivable. The dynamics encode rules that leave the knot topology (represented in terms of bow diagrams) invariant. This is manifest in that correlation functions for different (i.e., topologically distinct) knots are different. Some of the lower order equations are possibly derivable by hand, but this formalism allows (in principle) for computation of all orders of correlators. This could be used to study time-scales associated with rearrangements, alterations or simplifications of a given knot. Such analytical results may be useful for the determination of time-scales in a possible Monte Carlo-type simulation of these dynamics. The bow correlation functions, for instance, could yield (average) time-scales associated with the growth or shrinking of a particular bow. Coupled with appropriate initial conditions, this could be used to study simplification of knots to underlying simpler knots.

The investigation of these dynamics could allow for the identification of various dynamical regimes of the system and of steady-state solutions. In particular, it may be of interest whether these *purely topological* dynamics may exhibit some sort of glass transition in certain regimes. This would happen if there is some significant slowing in the dynamics, as is known for single-file dynamics. The role of topology in the relaxation or rate-limiting behaviour of crossings subject to Reidemeister moves could be investigated systematically in this manner. The dependence on initial conditions and sensitivity to the various rate constants could also be studied.

Our rules are derived from two-dimensional projections of the three-dimensional knot, but we propose that in future this might be an ansatz by which the topology conservation and polymer interaction might be separated. Since we have recast these rules in the setting of particle dynamics, a variety of other techniques is available for further study. In particular, it may be of interest to address a coherent path integral description (as has been done for other systems).

The descriptions here could be refined in several ways. One could, for instance, make the rate constants for various processes dependent on length-scales to mimic bending energies or to penalise great curvatures. One may also ask whether a particular prime knot underlies some more complex knot. Naturally the discretisation length is relevant in this context, since at most N crossings are possible for N discrete sites on a bow diagram.

In the next chapter we present a brief outlook on a possible computational scheme for

simulated annealing of knots. This scheme draws on the rules for dynamics of crossings that were derived and investigated in preceding sections. As stated, the analytical results of this chapter could be of use in estimating relevant time-scales for the different dynamical processes in such an algorithm.

CHAPTER 6
THOUGHTS TOWARDS SIMULATED ANNEALING OF KNOTS

In this chapter we shall sketch some ideas towards a non-detailed algorithm for simulated annealing of knots. The question of interest here is how one may reduce or simplify a given knot to its "simplest form". For instance, one may be presented with some complex knotted structure that could be untangled and simplified to yield the underlying topologically equivalent prime knot. To make these notions more explicit, we shall discuss some standard measures of knot complexity. We shall point out that the crossing number has been used extensively in this context, and address the relation of minimal knot energies and "simplest forms" of knots. Thereafter we discuss and review some existing algorithms for simulated annealing of knots. Lastly we shall present some suggestions for addressing this question, based on the themes of this dissertation.

6.1 Measures of knot complexity

Frequently various physical quantities are studied as a function of knot complexity. In an article on the topological effects of knots on polymers and their dynamics, Quake [36] considered (amongst other things) the relaxation time and radius of gyration of polymers in relation to knot complexity. In particular, the crossing number of knots was used there as a measure of knot complexity. Although the crossing number is a weak invariant (i.e., several topologically nonequivalent knots may have same crossing number in their simplest form), the notion of using crossing numbers as an indicator of knot complexity is well-accepted. Kholodenko *et al.* [69], for instance, studied the crossing number and average writhe as measures of knot complexity. These were included analytically into path integral descriptions for semiflexible polymers to calculate estimates for the number of knots with n crossings.

Shimamura *et al.* [70] have used the crossing number in computer simulations addressing the relation of knot complexity and knotting probability. Further, the study of complexity of polygonal lattice knots [71] has shown the ratio of polygon length to crossing number to be a relevant quantity in this setting.

There exist, of course, other measures of knot complexity than the crossing number. For

instance, Nechaev *et al.* considered the powers of some algebraic invariants as a measure of knot complexity, and investigated knot entropies in the setting of braids and locally free groups [53].

Further, the relation of knot complexity and knot energy has much bearing in this context. For instance, Moffat [72] employed techniques from fluid mechanics to define a new topological invariant based on flux tubes, obtaining an energy spectrum for knots. In that reference the lowest knot energy is associated with simplest form of a knot, and is viewed as a measure of knot complexity. Defining a different type of knot energy, Fukuhara consider equidistantly spaced charged particles along a knot, demonstrating that electrostatic repulsion causes simplification of the knot [73]. O'Hara then extended this description by including bending energies [74]. Freedman *et al.* [75] built on these ideas, using Möbius knot energies (defined in terms of integrals of curves) to establish, for instance, upper bounds on the crossing number given a certain knot energy. Buck and co-workers have investigated several energy functions for knots. For instance, energy functions based on the total curvature of the knot and on electrostatic-type interactions were demonstrated to yield a minimal configuration of knots for a corresponding global energy minimum that is an invariant of knot type [76]. A simple energy function that is scale invariant and encodes self-avoidance has also been formulated for smooth knots, and is intimately connected with the crossing number [77].

Various definitions of knot thickness (aimed at capturing both geometric and topological properties of knot curves) and their relative merits in classifying knots were considered by Diao *et al.* [78]. The relation of knot thickness to crossing number (and thus knot complexity) was studied by Buck and Simon in the setting of self-repelling knot energies [79]. This notion was also explored by Grosberg *et al.* [80] who developed a Flory-type theory for knotted ring polymers, suggesting inflation of the knot-tube to attain a minimal configuration of the knot. Lower bounds on the ropelength of knots (defined as the ratio of length and maximum thickness) have also been studied in this setting by Cantarella *et al.* [81].

Knot complexity is also of importance for the study of self-avoiding random walks. These walks may, for instance, be generated in simulations based on pivot algorithms [82]. Janse van Rensburg *et al.* have investigated the entanglement complexity of such self-avoiding random walks in dependence on crossing numbers [83] and properties of minimal length

knotted lattice polygons [84] in a simulation context.

It is clear that the computational / algorithmic simplification of a given knot thus requires two ingredients,

1. a measure of knot complexity (e.g., the crossing number), and

2. a driving process for the simplification / reduction (e.g., minimisation of knot energy).

In the next section we shall briefly outline how these concepts have been employed in simulations for knot simplification.

6.2 Untangling knots: a brief overview

In this section we concern ourselves with the reduction or simplification of a given knot to a simpler underlying knot. Motivations for this procedure include studying probability distributions of randomly generated knots (see, for instance, [70]) and testing for the equivalence of given knots. The latter is a question that would otherwise involve testing for the existence of some sequence of Reidemeister moves that relates two knots (computationally an open problem), or calculating some knot invariant (an incomplete test for knot equivalence) [13].

In a simulation context, this process is typically addressed through the improvement of some cost function related to the knot complexity. This may be approached in several ways. It has been suggested to evolve knots iteratively along the gradient of some chosen energy function deterministically (e.g. [73]) or stochastically (e.g. [85]) through the introduction of small perturbations that are accepted if they affect the cost function favourably. Such techniques, however, are sensitive to getting stuck in local minima (or maxima) [13]. To avoid this issue, the problem has been tackled through simulated annealing [13, 86]. The latter approach involves the occasional acceptance of configurational changes (or perturbations) that evolve the system *against* the gradient of the cost function, and not only those that evolve *with* the gradient. The acceptance of such "uphill" perturbations may be related to a temperature parameter that initially makes this likely, and is gradually "cooled off" with time, thereby making uphill perturbations less likely. The applicability of such Metropolis-type algorithms to annealing and optimisation problems in statistical physics has been demonstrated extensively; see, for instance, the highly-cited article of Kirkpatrick *et al.* [87].

We return now to the application of simulated annealing to the untangling of knots. Various perturbation methods have been used, and include placing point charges near the (charged) knot and allowing it to evolve under electrostatic forces, tightening or loosening various parts of the knot [13], and perturbing the vertices of a piecewise linear curve representation of the knot [86]. More recently, knot untangling has been addressed through algorithms that combine energy minimisation and tree-based probabilistic planning, yielding a considerable improvement in computation times [88].

The notion of local deformations and perturbations has also found applications elsewhere. For instance, such techniques have been used to investigate the equivalence of lattice polygons. Work on this topic has been done by Janse van Rensburg *et al.* [89] who showed that ergodic classes of the so-called BCACF algorithm for growing random walks [90, 91, 92] are knot types.

6.3 Suggestions towards an algorithm based on bow diagrams or the Gauss code

Here we outline a brief summary of a suggested algorithm for simulated annealing of knots. Relevant steps are discussed in order.

A. Generation of a random knot

A random knot can be generated using pivot-type algorithms [82] or closures of random walks (see [93] and references therein).

B. Projection of the knot

The random knot can now be projected to yield a bow diagram by the techniques mentioned in Chapter 2. Alternatively one could modify existing tools for finding the Gauss code of the random knot so that the distances between consecutive crossings (in the projection) are recorded. This is essentially the same information as is contained in a bow diagram. (A possible point of departure could be the *Mathematica* package `KnotTheory` [94, 95].)

C. Cost function

For the purpose of driving the evolution of the annealing algorithm, we suggested a cost function with two core attributes. Firstly, a large crossing number should be penalised so that simplification of the knot (i.e., reduction of the crossing number) is favoured. Secondly, free loops should be penalised. Such trivial or free loops on the random knot are any simple

loops that could be removed through **R1** annihilation — see Figure 5.1. This aspect of the cost function could depend on the arc-length of such a loop (obtainable from the bow diagram), so that small loops are heavily penalised.

The total cost function for the complete knot is then the sum of contributions of all trivial loops together with the part that depends on the crossing number.

D. Simulated annealing

We split the simulation processes into several classes.

D1. ***Random stochastic evolution of the knot***

This is done according to the Reidemeister moves **R0** and **R3** (these govern "diffusion-type" processes), and annihilation moves **R1** and **R2** (these govern "simplification-type" processes that reduce the crossing number). Explicitly this could be achieved by selecting an occupied site on the bow diagram and allowing that bow-foot to diffuse under the following provisos.

- **R0** allows the segments of the knot to "diffuse" relative to each other. Diffusion may only occur to *empty* nearest-neighbouring sites.
- If the selected bow foot is part of a primitive loop, then there is a probability of removing this loop through an **R1** annihilation step, related to the net reduction of the cost function.
- Should the selected bow foot be adjacent to an occupied site, test for the following:
  - If a valid **R3** configuration is present, allow execution of **R3**. If not, the particle may not diffuse.
  - If the configuration allows for an annihilation move of the **R2**-type, allow this move with a certain probability (depending on the improvement of the cost function through reduction of the crossing number).

Every diffusion step should be such that it either reduces the cost function or leaves it unaltered.

D2. ***Perturbations***

The second class of simulation processes involves the introduction of new crossings at empty sites on the bow diagram. This can be done in two ways

- Introduce new primitive loops into the bow diagram through an **R1** creation step. This is an "uphill" perturbation: both the crossing number aspect *and* the primitive loop aspect of the cost function are affected against the simplification gradient. The likelihood of such an uphill perturbation may be related to a temperature parameter in the system (see **D3**). If a new primitive loop has been introduced into the bow diagram, it has a chance of "diffusing" into the rest of the knot through the stochastic evolution; see **D1**.

- Introduce crossing pairs through an through an **R2** creation step. The cost function is affected through the resulting increase in crossing number, again against the simplification gradient. These crossings, too, may diffuse into the rest of the knot through the stochastic evolution; see **D1**.

D3. Cooling

The temperature parameter (i.e., the likelihood of uphill perturbations) can be reduced as simulation time progresses. This induces the system to settle to the desired minimal configuration.

6.4 Summary and outlook

After considering various measures of knot complexity and knot energies, we presented here some ideas towards an algorithm for simulated annealing of knots. In particular, this algorithm could be applied to projections of computationally generated knots, and the resulting Gauss codes or bow diagrams. Since the manipulations we suggest here are on a quasi-one-dimensional representation of the knot, the computational cost of this algorithm would be minimal.

The core ingredient is a cost function that penalises trivial loops of the knot and favours a smaller crossing number. Stochastic evolution and perturbations of the knot may be introduced, based on the Reidemeister moves.

Such an algorithm could also be used to investigate the importance of the individual Reidemeister moves in a purely topological dynamical setting. This could be done through relative weighting of the various probabilities / rates that govern the different processes. It may be interesting to study the rate-limiting effects of such dynamics, possibly as an indicator of topologically-induced glassy behaviour.

The relevance and usefulness of our algorithm remains to be tested. It is not clear whether the projection procedure is necessarily easy. Neither is it clear whether sufficiently much information about the real-space configuration of the knot is maintained after the projection; it is possible that other types of cost functions would have to be investigated.

CHAPTER 7
CONCLUSION AND OUTLOOK

In this dissertation we have addressed the topological equivalence of knots under sequences of Reidemeister moves. Various representations of knots were discussed, and the Reidemeister moves were recast in terms of dynamical rules on crossings.

Two "equilibrium-type" systems were considered. The first, serving as a primer, entailed a restricted system where only **R0** and **R1** are allowed. In order to find the partition function of this system, we presented a diagrammatic series over all topologically equivalent (constrained) bow diagrams. Under certain simplifying approximations, a general algebraic equation was derived for the Laplace transformation of the partition function for a given Boltzmann weight. Simple scaling arguments were then used to motivate the example of an inverse arc-length dependence, and various quantities were calculated in dependence on crossing number and knot length. The basic ansatz here could be generalised, for instance by including a dependence on torsion and / or tension in the strands.

The second system entailed a polymer loop that is wound around a rod and closed, thereby fixing the winding number. Augmentation rules that obey this constraint were presented in terms of the move **R2**. By considering combinatorics of strings of modified sequences, we found approximations for the sum over such equivalent configurations for $w = 1$. It was argued that despite similarities of the enumeration procedure to braid manipulations, the algebraic properties of braid groups alone are not sufficient to enumerate all distinct configurations when coupling polymer degrees of freedom. In particular, we assigned statistical weights to the various configurations in terms of polymer arcs restricted to half-space, and approximated the partition function through a diagonalisation scheme. Various confining geometries were then discussed in detail, and physical quantities such as ratios of arc-types and slit forces were calculated. Despite simplifying assumptions, these physical quantities were shown to capture the expected behaviour of the system well. A solution strategy was sketched for the general case of a slab-like obstacle in the plane. It should be reasonably straight forward to extend this strategy to various other confined geometries.

The remainder of the dissertation involved a dynamical description for the crossing rules.

This was addressed in the context of an operator formalism that captures the occupancy restrictions and topological rules on bow diagrams. We argued that compound paulionic operators are necessary to achieve this. Using ideas based on similar work for reaction-diffusion systems, we derived Liouvillians that encode some of the Reidemeister. Using these operators, differential equations for single-site and bow densities and correlators were calculated, subject to stochastic dynamics under **R0** and **R1** creation and annihilation. Suggestions were presented for dealing with the higher order Reidemeister moves. This part of the dissertation thus provides a framework for the systemised calculation of differential equations for densities and correlators of crossings of knots under the afore-mentioned topological dynamical rules. As stated, it would be interesting to consider various aspects of this formalism in more detail. One possibility would be to study the hierarchy of differential equations that could be obtained through mean field-type approximations. These equations could be investigated with regard to rate-limiting behaviour and slowing of dynamics — this could provide information regarding the role of topological constraints in various dynamical regimes. Another avenue for further investigation could be a coherent state path integral representation of these dynamics. This could possibly be addressed through modified Grassman fields. Although exploratory work in this direction led to ambiguities for continuum limits, we believe that this idea could shed further light on these interesting questions. It may even be instructive to investigate the non-locality that would arise in such a path integral description in relation to star products that occur in the setting of non-commutative geometries.

Lastly, various aspects of the dissertation were incorporated into suggestions toward an algorithm for simulated annealing of knots.

We believe the suggested approaches to the conservation of topological states as set out in this dissertation to be novel. As stated, this work departs significantly from the usual invariant-based path integral descriptions of these aspects of polymer systems. This applies both to the "equilibrium" and the dynamical aspects discussed in the dissertation. In particular, the latter ideas open the door to a variety of interesting questions that could be addressed through various solution and approximation schemes.

BIBLIOGRAPHY

[1] T.A. Vilgis. Polymer theory: path integrals and scaling. *Physics Reports*, 336(3):167–254, 2000.

[2] M. Rubinstein and R.H. Colby. *Polymer physics*. OUP Oxford, 2003.

[3] P.G. De Gennes. *Scaling concepts in polymer physics*. Cornell University Press, 1979.

[4] R.T. Deam and S.F. Edwards. The theory of rubber elasticity. *Philosophical Transactions of the Royal Society of London. Series A, Mathematical and Physical Sciences*, 280(1296):317–353, 1976.

[5] B. Duplantier. Polymer network of fixed topology: renormalization, exact critical exponent γ in two dimensions, and d= 4-ε. *Physical Review Letters*, 57(8):941, 1986.

[6] D. Shore, J. Langowski, and R.L. Baldwin. DNA flexibility studied by covalent closure of short fragments into circles. *Proceedings of the National Academy of Sciences*, 78(8):4833, 1981.

[7] L.S. De Witt and N.R. Cozzarelli. *New scientific applications of geometry and topology*, volume 45. Amer. Mathematical Society, 1992.

[8] J.M.T. Thompson. Cutting DNA: Mechanics of the topoisomerase. *The European Physical Journal Special Topics*, 165(1):175–182, 2008.

[9] O. Lukin and F. Vögtle. Knotting and threading of molecules: chemistry and chirality of molecular knots and their assemblies. *Angewandte Chemie International Edition*, 44(10):1456–1477, 2005.

[10] N.D. Gilbert and T. Porter. *Knots and surfaces*. Oxford University Press, USA, 1996.

[11] W.B.R. Lickorish. *An introduction to knot theory*, volume 175. Springer Verlag, 1997.

[12] L.H. Kauffman. *Knots and physics*, volume 1. World Scientific Publishing Company, 1991.

[13] M. Huang, R.P. Grzeszczuk, and L.H. Kauffman. Untangling knots by stochastic energy optimization. In *Proceedings of the 7th conference on Visualization'96*, pages 279–ff. IEEE Computer Society Press, 1996.

[14] A.L. Kholodenko and T.A. Vilgis. Some geometrical and topological problems in polymer physics. *Physics reports*, 298(5):251–370, 1998.

[15] S.F. Edwards. Statistical mechanics with topological constraints: I. *Proceedings of the Physical Society*, 91:513, 1967.

[16] K. Reidemeister. *Knotentheorie, von K. Reidemeister...* J. Springer, 1932.

[17] C.M. Rohwer, K.K. Müller-Nedebock, and F.E. Mpiana Mulamba. Conservation of polymer winding states: a combinatoric approach. *Journal of Physics A: Mathematical and Theoretical*, 47(6):065001, 2014.

[18] L.H. Kauffman and V.O. Manturov. Virtual knots and links. *Proceedings of the Steklov Institute of Mathematics*, 252(1):104–121, 2006.

[19] L.H. Kauffman. Virtual knot theory. *Europ. J. Combinatorics*, 20:663–691, 1999.

[20] M. Goussarov, M. Polyak, and O. Viro. Finite type invariants of classical and virtual knots. *arXiv preprint math/9810073*, 1998.

[21] H. Schubert. *Die eindeutige Zerlegbarkeit eines Knotens in Primknoten.* Springer, 1949.

[22] J. Hoste, M. Thistlethwaite, and J. Weeks. The first 1,701,936 knots. *The Mathematical Intelligencer*, 20(4):33–48, 1998.

[23] Y. Oono and K.F. Freed. Conformation space renormalization of polymers. I. Single chain equilibrium properties using Wilson-type renormalization. *The Journal of Chemical Physics*, 75:993, 1981.

[24] Y. Oono. Statistical physics of polymer solutions: conformation-space renormalization-group approach. *Advances in chemical physics*, 61:301, 2009.

[25] S. Stepanow. Field theoretic renormalization group and the scaling behaviour in polymer solutions. *Annalen der Physik*, 495(6):301–316, 1983.

[26] P.A. Pearce, J. Rasmussen, and S.P. Villani. Solvable critical dense polymers on the cylinder. *Journal of Statistical Mechanics: Theory and Experiment*, 2010(02):P02010, 2010.

[27] J. Vinograd, J. Lebowitz, R. Radloff, R. Watson, and P. Laipis. The twisted circular form of polyoma viral DNA. *Proceedings of the National Academy of Sciences of the United States of America*, 53(5):1104, 1965.

[28] J.F. Marko and E.D. Siggia. Fluctuations and supercoiling of DNA. *Science*, 265(5171):506–508, 1994.

[29] J.F. Marko and E.D. Siggia. Statistical mechanics of supercoiled DNA. *Physical Review E*, 52(3):2912, 1995.

[30] B. Fain, J. Rudnick, and S. Östlund. Conformations of linear DNA. *Physical Review E*, 55(6):7364, 1997.

[31] J.F. Marko. Torque and dynamics of linking number relaxation in stretched supercoiled DNA. *Physical Review E*, 76(2):021926, 2007.

[32] J.F. Marko and S. Neukirch. Competition between curls and plectonemes near the buckling transition of stretched supercoiled DNA. *Physical Review E*, 85(1):011908, 2012.

[33] M.T.J. Van Loenhout, M.V. de Grunt, and C. Dekker. Dynamics of DNA supercoils. *Science*, 338(6103):94–97, 2012.

[34] M. Emanuel, G. Lanzani, and H. Schiessel. Multiplectoneme phase of double-stranded DNA under torsion. *Phys. Rev. E*, 88:022706, 2013.

[35] M. Muthukumar. Localized structures of polymers with long-range interactions. *The Journal of chemical physics*, 104:691, 1996.

[36] S.R. Quake. Topological effects of knots in polymers. *Physical Review Letters*, 73(24):3317, 1994.

[37] E. Orlandini and S.G. Whittington. Statistical topology of closed curves: Some applications in polymer physics. *Reviews of Modern Physics*, 79(2):611–642, April 2007.

[38] A.Y. Grosberg. A few notes about polymer knots. *Polymer Science Series A*, 51(1):70–79, 2009.

[39] C. Micheletti, D. Marenduzzo, and E. Orlandini. Polymers with spatial or topological constraints: Theoretical and computational results. *Physics Reports*, 504(1):1–73, July 2011.

[40] J. Marko. Linking topology of tethered polymer rings with applications to chromosome segregation and estimation of the knotting length. *Physical Review E*, 79(5):051905, May 2009.

[41] J.F. Marko. Linking topology of large DNA molecules. *Physica A: Statistical Mechanics and its Applications*, 389(15):2997–3001, August 2010.

[42] M. Bohn, D.W. Heermann, O. Lourenço, and C. Cordeiro. On the Influence of Topological Catenation and Bonding Constraints on Ring Polymers. *Macromolecules*, 43(5):2564–2573, March 2010.

[43] D. Marenduzzo, C. Micheletti, and E. Orlandini. Biopolymer organization upon confinement. *Journal of Physics: Condensed Matter*, 22(28):283102, June 2010.

[44] H.L. Frisch and E. Wasserman. Chemical topology1. *Journal of the American Chemical Society*, 83(18):3789–3795, 1961.

[45] S. Prager and H.L. Frisch. Statistical mechanics of a simple entanglement. *The Journal of Chemical Physics*, 46:1475, 1967.

[46] F.W. Wiegel. *Introduction to path-integral methods in physics and polymer science*. World Scientific Publishing Company Incorporated, 1986.

[47] M.G. Brereton and S. Shah. A gauge description of topological entanglements in polymers. *Journal of Physics A: Mathematical General*, 13:2751–2762, 1980.

[48] M.G. Brereton. Topology, gauge fields and the statistical mechanics of a melt of polymer rings. *Journal of Molecular Structure: THEOCHEM*, 336(2):191–207, 1995.

[49] M.G. Brereton and T.A. Vilgis. The statistical mechanics of a melt of polymer rings. *Journal of Physics A: Mathematical and General*, 28(5):1149–1167, 1995.

[50] E. Witten. Quantum field theory and the Jones polynomial. *Communications in Mathematical Physics*, 121(3):351–399, 1989.

[51] J.F.W.H. Van de Wetering. Knot invariants and universal R-matrices from perturbative Chern-Simons theory in the almost axial gauge. *Nuclear Physics B*, 379(1):172–198, 1992.

[52] A. Grosberg and H. Frisch. Winding angle distribution for planar random walk, polymer ring entangled with an obstacle, and all that: Spitzer–Edwards–Prager–Frisch model revisited. *Journal of Physics A: Mathematical and General*, 36(34):8955, 2003.

[53] S.K. Nechaev, A. Yu. Grosberg, and A.M. Vershik. Random walks on braid groups: Brownian bridges, complexity and statistics. *Journal of Physics A: Mathematical and General*, 29(10):2411, 1996.

[54] S. Nechaev. *Statistics of knots and entangled random walks*. Springer, 1999.

[55] V. Manturov. *Knot theory*. CRC Press, 2004.

[56] S.F. Edwards. The size of a polymer molecule in a strong solution. *Journal of Physics A: Mathematical General*, 8:1670–1680, 1975.

[57] S. Chandrasekhar. Stochastic problems in physics and astronomy. *Rev. Mod. Phys.*, 15:1–89, Jan 1943.

[58] M. Slutsky. Diffusion in a half-space: From Lord Kelvin to path integrals. *American Journal of Physics*, 73:308, 2005.

[59] C.W. Gardiner et al. *Handbook of stochastic methods*, volume 3. Springer Berlin, 1985.

[60] H. Risken. *Fokker-Planck Equation*. Springer, 1984.

[61] M. Doi. Second quantization representation for classical many-particle system. *Journal of Physics A: Mathematical and General*, 9(9):1465, 1976.

[62] L. Peliti. Path integral approach to birth-death processes on a lattice. *Journal de Physique*, 46(9):1469–1483, 1985.

[63] D.C. Mattis and M.L. Glasser. The uses of quantum field theory in diffusion-limited reactions. *Reviews of Modern Physics*, 70(3):979, 1998.

[64] U.C. Täuber, M. Howard, and B.P. Vollmayr-Lee. Applications of field-theoretic renormalization group methods to reaction–diffusion problems. *Journal of Physics A: Mathematical and General*, 38(17):R79, 2005.

[65] S. Sandow and S. Trimper. Aggregation processes in a master-equation approach. *EPL (Europhysics Letters)*, 21(8):799, 1993.

[66] H. Patzlaff, S. Sandow, and S. Trimper. Diffusion and correlation in a coherent representation. *Zeitschrift für Physik B Condensed Matter*, 95(3):357–362, 1994.

[67] M.G. Rudavets. The phase transition for the aggregation model in the effective-medium approach. *Journal of Physics: Condensed Matter*, 5(8):1039, 1993.

[68] F.C. Alcaraz, M. Droz, M. Henkel, and V. Rittenberg. Reaction-diffusion processes, critical dynamics and quantum chains. *arXiv preprint hep-th/9302112*, 1993.

[69] A.L. Kholodenko and D.P. Rolfsen. Knot complexity and related observables from path integrals for semiflexible polymers. *Journal of Physics A: Mathematical and General*, 29(17):5677, 1996.

[70] M.K. Shimamura and T. Deguchi. Knot complexity and the probability of random knotting. *Physical Review E*, 66(4):040801, 2002.

[71] Y. Diao and C. Ernst. The complexity of lattice knots. *Topology and its Applications*, 90(1):1–9, 1998.

[72] H.K. Moffatt. The energy spectrum of knots and links. *Nature*, 347(6291):367–369, 1990.

[73] S. Fukuhara. Energy of a knot. *A fête of topology*, pages 443–451, 1988.

[74] H. Ohara. Energy of a knot. *Topology*, 30(2):241–247, 1991.

[75] M.H. Freedman, Z.-X. He, and Z. Wang. Mobius energy of knots and unknots. *Annals of mathematics*, pages 1–50, 1994.

[76] G. Buck and J. Simon. Knots as dynamical systems. *Topology and its Applications*, 51(3):229–246, 1993.

[77] G. Buck and J. Orloff. A simple energy function for knots. *Topology and its Applications*, 61(3):205–214, 1995.

[78] Y. Diao, C. Ernst, and E.J.J. Van Rensburg. Thicknesses of knots. In *Mathematical Proceedings of the Cambridge Philosophical Society*, volume 126, pages 293–310. Cambridge Univ Press, 1999.

[79] G. Buck and J. Simon. Thickness and crossing number of knots. *Topology and its Applications*, 91(3):245–257, 1999.

[80] A.Yu. Grosberg, A. Feigel, and Y. Rabin. Flory-type theory of a knotted ring polymer. *Physical Review E*, 54(6):6618, 1996.

[81] J. Cantarella, R.B. Kusner, and J.M. Sullivan. On the minimum ropelength of knots and links. *Inventiones mathematicae*, 150(2):257–286, 2002.

[82] N. Madras and A.D. Sokal. The pivot algorithm: a highly efficient Monte Carlo method for the self-avoiding walk. *Journal of Statistical Physics*, 50(1-2):109–186, 1988.

[83] E.J. Janse Van Rensburg, D.A.W. Sumners, E. Wasserman, and S.G. Whittington. Entanglement complexity of self-avoiding walks. *Journal of Physics A: Mathematical and General*, 25(24):6557, 1992.

[84] E.J. Janse van Rensburg and A. Rechnitzer. Minimal knotted polygons in cubic lattices. *Journal of Statistical Mechanics: Theory and Experiment*, 2011(09):P09008, 2011.

[85] J.K. Simon. Energy functions for polygonal knots. *Random Knotting and Linking*, pages 67–88, 1994.

[86] T.J. Ligocki and J.A. Sethian. Recognizing knots using simulated annealing. *Journal of Knot Theory and its Ramifications*, 3(04):477–495, 1994.

[87] S. Kirkpatrick, D. Gelatt Jr., and M.P. Vecchi. Optimization by simmulated annealing. *Science*, 220(4598):671–680, 1983.

[88] A.M. Ladd and L.E. Kavraki. Using motion planning for knot untangling. *The International Journal of Robotics Research*, 23(7-8):797–808, 2004.

[89] E.J. Janse Van Rensburg and S.G. Whittington. The BFACF algorithm and knotted polygons. *Journal of Physics A: Mathematical and General*, 24(23):5553, 1991.

[90] B. Berg and D. Foerster. Random paths and random surfaces on a digital computer. *Physics Letters B*, 106(4):323–326, 1981.

[91] C.A. De Carvalho and S. Caracciolo. A new Monte-Carlo approach to the critical properties of self-avoiding random walks. *Journal de Physique*, 44(3):323–331, 1983.

[92] C.A. De Carvalho, S. Caracciolo, and J. Fröhlich. Polymers and $g|\varphi|^4$ theory in four dimensions. *Nuclear Physics B*, 215(2):209–248, 1983.

[93] P. Virnau, L.A. Mirny, and M. Kardar. Intricate knots in proteins: Function and evolution. *PLoS Computational Biology*, 2(9):e122, 2006.

[94] N. Imafuji and M. Ochiai. Computer aided knot theory using Mathematica and Mathlink. *Journal of Knot Theory and Its Ramifications*, 11(06):945–954, 2002.

[95] D. Bar-Natan. The Mathematica package KnotTheory.

APPENDIX A
Appendix to Chapter 3

.

A.1 Approximation of the inverse Laplace transformation

Below we plot the negative logarithm of $\tilde{Z}(t_c, t')$ from equation (3.27), together with a fit of the square root of a linear function of the Laplace parameter.

Figure A.1: Plot of $-\log[\tilde{Z}(t_c, t')]$ and fit of a square root function $\sqrt{at' + b}$.

Good agreement between the fit and the Laplace transform is evident, particularly for larger values of t'. It would thus be sensible to check whether

$$\log[\tilde{Z}(t_c, t')] \sim e^{-\sqrt{p_n(t')}}, \tag{A.1}$$

where $p_n(t')$ is an n-th degree polynomial in t'. To confirm this we plot below the square of the logarithm of $\tilde{Z}(t_c, t')$ together with two polynomial fits.

(a) Linear fit: $at' + b$ (b) Quadratic fit: $at'^2 + bt' + c$

Figure A.2: Plots of two fits, plotted together with $\log[\tilde{Z}(t_c, t')]^2$.

We note good agreements of both fits.

A.2 Diagrammatic summation

We wish to prove the final step in the diagrammatic summation outlined in Figure 3.3. As before, we denote the whole series as follows,

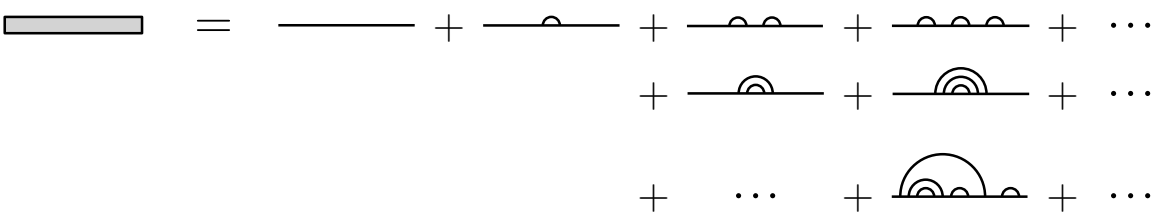

Now consider some diagram X that forms part of the superposition where the empty bow diagram has been removed,

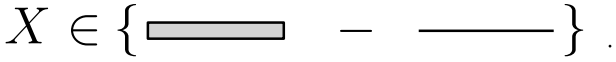

This diagram must be of the form

where A and B are some other diagrams in the series. It follows that a superposition of all X can be generated by summing over A and B,

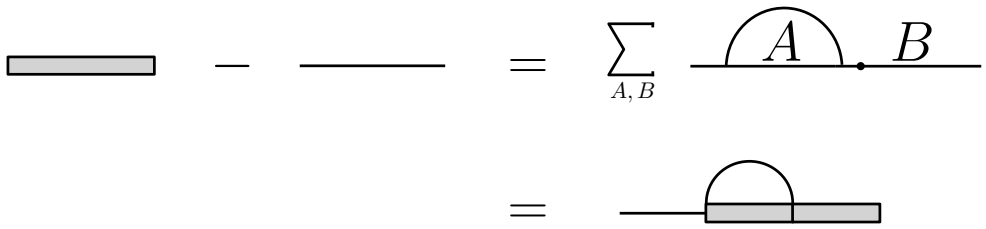

which proves the final step in Figure 3.3.

APPENDIX B
Appendix to Chapter 4

B.1 Comments on enumeration and braid groups

We explain here briefly the relation of our enumeration procedure of Section 4.2 to some properties of braid groups, and illustrate why braid group properties alone do not suffice to couple polymer degrees of freedom to a particular configuration.

A braid group B_n describes braids of n strings, and has $n-1$ group generators labelled $\{\sigma_1, \sigma_2, \ldots, \sigma_{n-1}\}$. The generators obey the relations

$$\begin{aligned} &\sigma_i\sigma_{i+1}\sigma_i = \sigma_{i+1}\sigma_i\sigma_{i+1}, && i = 1, 2, \ldots, n-1, \\ &\sigma_i\sigma_j = \sigma_j\sigma_i, && |i-j| \geq 2, \\ &\sigma_i\sigma_i^{-1} = \sigma_i^{-1}\sigma_i = e. \end{aligned} \tag{B.1}$$

Here e is the identity element. One may construct words from this set of generators and their inverses; these words correspond to braids of the n strands. (See, for instance, [12, 53, 54, 55] for further details.) For any given word the application of the braid group relations (B.1) may be used to obtain a minimal (irreducible) form of word.

The scenario of winding a strand around a rod could, of course, be viewed in terms of the braid group for two strands, B_2. This group is "trivial" in that it only has one generator σ, rendering the first two properties of (B.1) irrrelevant. In Figure B.1 we illustrate the B_2 words analogous to some sequences of Ts from Section 4.2. The braids shown there are projections of the winding scenarios along the plane in which the rod lies. Clearly the group properties thus encode similar conditions on reducibility as set out in Section 4.2. Since we consider words of even length, the winding number of a particular B_2 braid may be obtained by halving the number of σ generators remaining in the corresponding word that has been fully reduced. Alternatively, for a non-primitive word, the winding number is clearly the difference in number of σs and σ^{-1}s,

$$w = \frac{\#(\sigma) - \#(\sigma^{-1})}{2}. \tag{B.2}$$

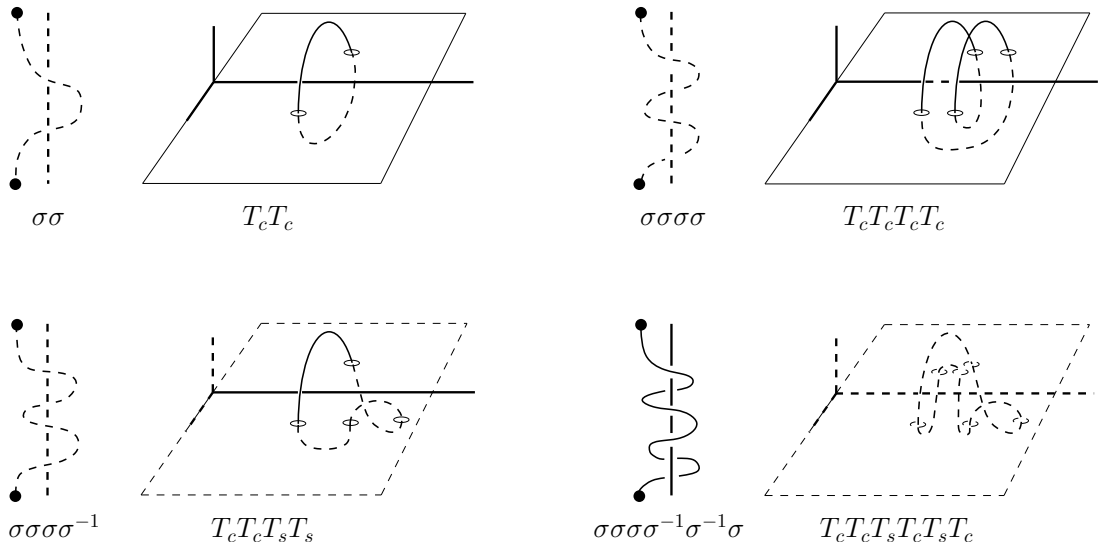

Figure B.1: Braids of two strands in analogy to winding scenarios from Section 4.2.

(Compare to the power of the Alexander invariant in equation (2.58) of [53].)

However, our aim is to couple polymer degrees of freedom (statistical weights) to these words. These weights are simply the probability distributions of connected arcs constrained to half-space, *viz.* the Ts. It is critical to identify the correct integration bounds on the beginning and end co-ordinates in these weights (see Sections 4.3.3 and 4.3.4) when stringing together these Ts for a given braid / winding scenario. Indeed, the group relation $\sigma\sigma^{-1} = \sigma^{-1}\sigma$ is problematic in that it alone does not, for instance, allow us distinguish between the sequences $T_sT_sT_s$ and $T_cT_sT_c$. Clearly, through (4.14) and (4.15) both of these sequences reduce to T_s. In our partition function, however, where the T_cs and T_ss do not have the same integration bounds, these two configurations would represent different statistical contributions.

Naturally it is possible to enumerate all unique (non-primitive) words in the "braids only" scenario, where the winding number constraint $w = 1$ may analogously be viewed as enumerating all words in B_2 that reduce to $\sigma\sigma$. One could do this by enumerating all possible words of even length, and then enforcing $w = 1$ through (B.2) and an appropriate Kronecker delta. However, the translation to arcs with position dependence must be made explicit to avoid the above-mentioned problem. The group relations alone (without position dependence) thus do not allow coupling to the polymer degrees of freedom. Our scheme has thus been developed to avoid the necessity of including the $\#(\sigma) - \#(\sigma^{-1})$ constraint in

terms of an additional integral for the Kronecker delta by enumerating the configurations (with position dependence) explicitly.

B.2 Redundancy of rule (i'b)

To see why rulle (i'b), for example, is not necessary when using rule (i'a), we consider how an initial knot configuration, given by a pure winding number such as

$$Z^{(w)}_{\text{basic}} = (T_c T_c)^w \tag{B.3}$$

is modified by the application of these two moves. Inserting rule (i') after the second T_c is equivalent to inserting $T_c T_s T_c T_s$ after the first T_c. Further equivalence can also be avoided by noting that the composite rules produce products of terms of the form

$$T_c \to (T_c T_s T_c T_s + T_s T_c T_s T_c)^m \,.$$

This can simplified by noting that the following cross product terms arise, but can be derived from from (ii') with the odd/even T_s convention

$$T_c T_s T_c T_s \times T_s T_c T_s T_c \leftarrow T_c T_s \qquad \underbrace{T_c \underbrace{T_s}_{(ii')}}_{\text{then even } T_s \text{ after 1st } T_c}$$

B.3 Various transformations in section 4.3.4

The general form of (4.35) may be simplified by performing a Laplace transformation. Suppressing all x and y dependences, we condense (4.35) to

$$\begin{aligned} Z^{(w=1)}_{\chi}(L) = \quad & \int_0^\infty dX \int_{-\infty}^\infty dY \int_\epsilon^\infty ds_1 \ldots \int_\epsilon^\infty ds_N \;\; \delta(x_0 - x_N)\delta(y_0 - y_N) \\ & T_{p_1}(s_1) \ldots T_{p_N}(s_N)\; \delta(\textstyle\sum_{k=1}^N s_k - L). \end{aligned} \tag{B.4}$$

Performing the Laplace transformation (indicated by the tilde below) yields

$$\begin{aligned} \tilde{Z}^{(w=1)}_{\chi}(t) \;\; &= \;\; \int_0^\infty dL \;\; Z^{(w=1)}_{\chi}(L)\, e^{-Lt} \\ &= \;\; \int_0^\infty dX \; \delta(x_0 - x_N) \int_{-\infty}^\infty dY \; \delta(y_0 - y_N)\; T^L_{p_1}(t) \ldots T^L_{p_N}(t), \end{aligned} \tag{B.5}$$

i.e., by performing all integrals over s we obtain the product of the Laplace transformations of the N individual Ts. The superscript Ls indicate the Laplace transform of (4.33). It is, however, understood that all s integrals are performed from the non-zero lower bound ϵ. The object (B.5) may further be simplified in terms of the y integrals. To this end we perform the linear and invertible co-ordinate transformation $\Delta y_i \equiv y_i - y_{i+1}$, $i = 0, 1, \ldots N-1$ and $R \equiv \sum_{i=0}^{N} y_k$. The Jacobian is $|J| = N+1$. Now suppressing the x and t dependences we may write (4.35) as

$$\begin{aligned}
\tilde{Z}_{\chi}^{(w=1)}(t) &= \int_0^\infty dX\ \delta(x_0 - x_N) \int_{-\infty}^{\infty} dy_0 \ldots \int_{-\infty}^{\infty} dy_N \\
&\qquad T_{p_1}^{L}(y_0 - y_1) \ldots T_{p_N}^{L}(y_{N-1} - y_N)\ \delta(y_0 - y_N) \\
&= |J| \int_0^\infty dX\ \delta(x_0 - x_N) \int_{-\infty}^{\infty} d\Delta y_1 \ldots \int_{-\infty}^{\infty} d\Delta y_N \int_{-\infty}^{\infty} dR \\
&\qquad T_{p_1}^{L}(\Delta y_1) \ldots T_{p_N}^{L}(\Delta y_N)\ \delta(\sum_{k=1}^{N} \Delta y_k) \\
&= \mathcal{N} \int_0^\infty dX\ \delta(x_0 - x_N) \int_{-\infty}^{\infty} dk\ \ T_{p_1}^{L,F}(k) \ldots T_{p_N}^{L,F}(k). \qquad \text{(B.6)}
\end{aligned}$$

where $\mathcal{N} = |J| \int_{-\infty}^{\infty} dR$ is a pre-factor related to the length of the rod. This pre-factor is, in principle, divergent, but its contribution to the free energy is additive and thus irrelevant. The superscripts in the final line above indicate Fourier transformations in y of the Laplace transformations of the Ts from (4.33). We used the Fourier representation of the delta function,

$$\delta(\sum_{k=1}^{N} \Delta y_k) = \int_{-\infty}^{\infty} dk\ \ e^{ik\,(\sum_{k=1}^{N} \Delta y_k)}, \qquad \text{(B.7)}$$

to do all the Δy integrals. Recalling that in (B.6) we suppressed dependence on the Laplace parameter t and on the various x co-ordinates, we write the Laplace transformation of $Z_{\chi}^{(w=1)}$ explicitly as

$$\tilde{Z}_{\chi}^{(w=1)}(t) = \int_0^\infty dX\ \delta(x_0 - x_N) \int_{-\infty}^{\infty} dk\ \ \prod_{i=1}^{N} T_{p_i}^{L,F}(x_{i-1}, x_i; k; t), \qquad \text{(B.8)}$$

as in (4.38).